TRANSFORMATION OF AN ALUMINIUM-IRON-MAGNESIUM-CHLORIDE SOLUTION DURING PYROHYDROLYSIS

By
Carlo Coscia

Department of Mining, Metals, & Materials Engineering,
McGill University, Montreal

February 2006

A thesis submitted to McGill University
in partial fulfilment of the requirements of the
degree of Doctor of Philosophy

Your file Votre référence
ISBN: 978-0-494-27766-9
Our file Notre référence
ISBN: 978-0-494-27766-9

ABSTRACT

Industrial experience has revealed that when used to treat multi-component metal chloride waste liquors, existing fluidized bed acid regeneration facilities are not as efficient as when employed for the pyrohydrolysis of conventional iron chloride solutions (i.e. waste pickle liquor). As a result, experimental studies and thermochemical modelling were performed to characterize the transformation of a saturated Al-Fe-Mg-Cl solution at 105°C, after it is injected into a reactor at 850°C. Efforts were geared toward defining the sequence of reactions that take place as the liquor gradually transforms into oxides.

Upon completing a comprehensive literature review, testwork was initially performed with a simplified experimental set-up to study the physical behaviour of the chloride solution as it is exposed to a static bed of oxides at 850°C, and ultimately identify the various phases of the transformation process. Subsequently, controlled evaporative crystallization experiments were conducted under pseudo-equilibrium conditions to define the $MeCl_x \cdot yH_2O$ precipitation path that takes place during the H_2O evaporation phase and to determine whether the chlorides precipitate independently or as complex compounds. Further experiments were performed in a fully instrumented tube furnace to elaborate on the nature of the reactions (dehydration and/or pyrohydrolysis) that take place after all of the water in the starting solution has evaporated (i.e. $T=300°C^+$).

In an effort to assist with the interpretation of the experimental results, thermochemical modelling was performed to predict the equilibrium phase assemblages that could occur during the transformation of the saturated Al-Fe-Mg-Cl solution, at reaction temperatures of $200°C^+$.

The research study at hand has shown that when the saturated Al-Fe-Mg-Cl solution at 105°C is exposed to fluidized bed pyrohydrolyzer operating conditions at 850°C, the following sequence of events take place:

- rapid solvent H_2O evaporation (i.e. vigorous boiling) and onset of solid metal chloride precipitation.

- slurry densification due to a gradual increase in crystal content (i.e. $AlCl_3 \cdot 6H_2O$, $FeCl_2 \cdot xH_2O$, and $MgCl_2 \cdot xH_2O$, where x = 2 or 4).
- hydrated crystal drying and onset of pyrohydrolysis (i.e. thermal decomposition of $MeCl_x \cdot yH_2O$).

The same holds true for the high temperature hydrolysis of typical waste pickle liquors (i.e. primarily $FeCl_2$ solution).

The crystallization studies revealed that when the Al-Fe-Mg-Cl solution is allowed to gradually evaporate at 105°C, $AlCl_3 \cdot 6H_2O$ precipitates when 15% of the solvent water evolves from the liquor, followed by $FeCl_2 \cdot xH_2O$ and $MgCl_2 \cdot xH_2O$ (where x = 2 or 4) at 26 and 41% evaporation, respectively. Ferric chloride remains in solution even after 54% of the water has been driven from the liquor. The latter result suggests that higher ferric concentrations in the reactor feed are more than likely to favour an increase in the quantity of liquor entrainment by the fluidizing gases and therefore lead to lower process efficiencies.

Dedicated pyrohydrolysis experiments, with a simulated reactor atmosphere (gaseous, not dynamic), have shown that excluding kinetic effects, the transformation of the Al-Fe-Mg-Cl solution occurs primarily over the 300 to 600°C temperature range.

Thermochemical modelling revealed that with the exception of $AlCl_3 \cdot 6H_2O$ hydrolysis, the majority of the reactions taking place as the saturated Al-Fe-Mg-Cl liquor is introduced into and eventually reaches 850°C are governed by either reaction kinetics or diffusion. Furthermore, the resulting phase assemblage at any given temperature was predicted to vary significantly with oxygen potential. A liquid chloride phase (including molten salt), other than the feed liquor, was not predicted to form at any temperature (i.e. 200°C or above) under the range of oxidizing or reducing conditions considered.

The findings of this research were quite useful in identifying the means for improving the performance of a commercial fluidized bed pyrohydrolyzer for a spent chloride liquor containing the said species.

RÉSUMÉ

L'expérience industrielle a démontré que quand la technologie de régénération d'acide en lit fluidisé est utilise pour traité une solution de chlorures métalliques multi-composé, le procédé n'est pas aussi efficace que pour la pyrohydrolyse des acides usés de décapage (c.à.d. solution de chlorure ferreux). Alors, une série d'expériences et de la modélisation thermochimique ont été effectuées pour caractériser la transformation d'une solution d'Al-Fe-Mg-Cl (saturé à 105°C), après avoir été injecté dans un réacteur à 850°C. L'étude visait à définir la séquence de réactions qui décrit la transformation graduelle de la solution en oxydes.

Après avoir complété une revue compréhensive de la littérature, des essais préliminaires ont été effectués avec un montage simplifié pour étudier le comportement physique de la solution de chlorures une fois exposée à un lit d'oxydes statique à 850°C. Le but était d'identifier les diverses phases de transformation. Par la suite, des expériences de cristallisation par évaporation ont été réalisées, sous des conditions « quasi-équilibre », pour définir la séquence dans la quel les $MeCl_x \cdot yH_2O$ précipite lors de la phase d'évolution d'eau. De plus, cette étude à servi à déterminer si les chlorures précipite sous forme de sels simples ou complexes. Finalement, une troisième série d'essais ont été effectuées dans un four à tube bien instrumenté pour élaborer la nature des réactions (déshydratation et/ou pyrohydrolyse) qui se produisent après que tout l'eau dans la solution de départ est évaporé (c.à.d. T=300°C$^+$).

La modélisation thermochimique a été entreprise pour prédire les assemblages de phase qui peuvent se produire en conditions d'équilibre lors de la transformation de la solution Al-Fe-Mg-Cl saturé, et ce a des températures de 200°C et plus. Ces résultats ont aidé à interpréter les résultats des expériences ci-haut mentionnées.

L'étude de recherche en question a illustré que quand la solution d'Al-Fe-Mg-Cl saturé à 105°C est exposé à un environnement de pyrohydrolyse à 850°C elle passe à :

- l'évaporation rapide de l'eau, suivi par la précipitation des chlorures métalliques en forme de sels solides.
- la formation d'une boue du à l'augmentation du contenu en cristaux (c.à.d. $AlCl \cdot 6H_2O$, $FeCl_2 \cdot xH_2O$ et $MgCl_2 \cdot xH_2O$, ou x = 2 or 4).

- le séchage des cristaux hydratés et le début de la pyrohydrolyse (c.à.d. décomposition thermique des $MeCl_x \cdot yH_2O$'s).

Les mécanismes d'hydrolyse à haute température des acides de décapage usé (solution de $FeCl_2$ en majorité) sont pareils.

L'étude de cristallisation a révélé que quand la solution d'Al-Fe-Mg-Cl est soumise à des conditions d'évaporation graduelle à 105°C, l'$AlCl_3 \cdot 6H_2O$ précipite quand 15% de l'eau de solution évolue de la liqueur, suivi par le $FeCl_2 \cdot xH_2O$ et $MgCl_2 \cdot xH_2O$ (ou x = 2 or 4) à 26 et 41% d'évaporation, respectivement. Le chlorure ferrique reste en solution même après l'évolution de 54% de l'eau de départ. Ceci suggère qu'une augmentation de la concentration de ferrique dans la solution alimenter à un réacteur de pyrohydrolyse, favorise plus d'entraînement de liqueur par les gazes de fluidisation et donc des efficacités inférieures.

Les expériences de pyrohydrolyse, dans une atmosphère de réacteur simulé (gazeux et non dynamique), ont illustré qu'en excluant les effets de cinétiques, la transformation de la solution Al-Fe-Mg-Cl est réalisée en gros parti entre 300 et 600°C.

La modélisation thermochimique a démontré qu'avec l'exception de l'hydrolyse d'$AlCl_3 \cdot 6H_2O$, la majorité des réactions qui se produisent une fois que la solution d'Al-Fe-Mg-Cl saturé est introduit dans le réacteur et approche 850°C sont contrôlés par les cinétiques ou la diffusion. De plus, les assemblages de phase à l'état d'équilibre varient de façon importante avec le potentiel d'oxygène et ce à tous les températures considérées. Selon l'étude, à part la solution de départ, les chlorures liquides (incluant des sels fondus) ne devraient pas former (à 200°C et plus), ni sous des conditions oxydantes ou réductrices considérées.

Avec les résultats de cette étude de recherche, il a été possible d'identifier les moyens pour améliorer la performance d'un réacteur de pyrohydrolyse commercial (lit fluidisé), utilisé pour le traitement d'une solution de chlorures d'aluminium, fer et magnésium.

ACKNOWLEGDEMENTS

I would like to express my gratitude to Professor Janusz A. Kozinski, for his time and support in this endeavour. This is particularly true since much of the experimental work was performed on a part-time basis under the constraints of my professional commitments. His patience and understanding were greatly appreciated and instrumental in the success of this project. Furthermore, his insights and advice were invaluable.

I would also like to extend special thanks to Professor George P. Demopoulos and Georgiana Moldoveanu for all of their contributions in the development of the experimental procedures, sampling techniques and analytical methods for the evaporative crystallization studies. Their input was priceless. Without the help of Dr. Arthur Pelton and Dr. Mike Wadsley of l'École Polytechnique de Montréal, the thermochemical modelling exercise would have been a much more difficult undertaking.

Clearly, the support provided by Rio Tinto – Iron & Titanium Inc, both financially and in the form of highly skilled technical personnel was also sincerely appreciated. In particular, I would like to single out Dr. Alfonso E. Grau, Mr. Pat Fiore, Mr. Jean-Francois Turgeon, Mr. Yves Pépin, Dr. John T. Chao, and Dr. Krzysztof Borowiec. There is no question that this project could not have been completed, or indeed undertaken, without their flexibility and generosity. Furthermore, their technical contributions and moral support were also extremely helpful.

I am also grateful of all the technicians and summer students that made a contribution to this project: Mr. Martin Rouette, Mr. Jean-Louis Leblanc, Mr. Frank Cantin, Mr. Benjamin Gagnon, Ms. Nathalie Lambert, Mr. Graeme Goodall. They were the key behind the success of the experimental and analytical work.

Finally, I would like to personally thank my wife Sarah and daughters Megan and Gillian for really making this possible. Sarah never questioned my choice to pursue graduate studies while simultaneously working full-time, despite the many evenings and weekends lost to the lab, the office or at my computer.

TABLE OF CONTENTS

LIST OF FIGURES

LIST OF TABLES

NOMENCLATURE

T	=	Temperature (°C)
T^*	=	Species saturation temperature (°C)
T_M	=	Species supersaturation labile zone temperature (°C)
R	=	Universal ideal gas constant (8.314 $J \cdot mol^{-1} \cdot K^{-1}$)
$\Delta G°$	=	Standard Gibbs Free Energy ($kcal \cdot mol^{-1}$)
ΔG	=	Gibbs energy change ($J \cdot mol^{-1}$)
ΔH	=	Change in enthalpy ($J \cdot mol^{-1}$)
ΔS	=	Change in entropy ($J \cdot K^{-1}$)
c_p	=	heat capacity at constant pressure ($J \cdot mol^{-1} \cdot K^{-1}$)
k	=	Kinetic rate constant ($mol \cdot min^{-1}$)
Re	=	Reynolds number
Sc	=	Schmidt number
Pr	=	Prandlt number
Sh	=	Sherwood number
Nu	=	Nusselt number
δ	=	Thickness of polystyrene disk (mm)
N_A	=	Mass flux of component A ($kg \cdot m^2 \cdot s$)
A	=	Surface area of drop (m^2)
A_e	=	Effective surface area of drop (m^2)
A_t	=	Cross section of supporting tube (m^2)
q	=	Heat flux ($W \cdot m^{-2}$)
λ	=	Latent heat of vaporization ($J \cdot kg^{-1}$)
Q_c	=	Heat transfer rate (W)
c_L	=	Heat capacity of liquid ($J \cdot kg^{-1} \cdot K^{-1}$)
W	=	Weight of drop (kg)
κ_t	=	Thermal conductivity of thermocouple ($W \cdot m^{-1} \cdot K^{-1}$)
l_t	=	Length of thermocouple (m)
ω	=	Mass fraction
D_A	=	Drop diameter (m)

D_s	=	Diameter of supporting polystyrene disk (m)
h	=	Distance designated in Figure 17 (m)
C	=	Concentration of salt (wt%)
ρ_{sc}	=	Density of aqueous salt solution (kg/m^3)
DOE	=	Degree of solvent H_2O evaporation (wt%)
P_i	=	Partial pressure of species i (kPa)
$V_{Initial}$	=	Initial solution volume (L)

1.0 INTRODUCTION:

1.1 Background:

Based on a review of the literature (see Section 2.1), it appears as though the majority of the technical developments in the area of fluidized bed pyrohydrolysis, for the regeneration of hydrochloric acid, have been limited to physical aspects of the process (i.e. alternative offgas cyclone design, feed lance orientation, seed additions, etc...). This may be attributed to the fact that most of the existing installations involve the thermal decomposition of an iron chloride solution: a relatively simple single component system. As a result, after having successfully operated commercial scale facilities for a number of years, the concerned fluidized bed technology suppliers did not see much reason to further their understanding of the process fundamentals. The users of these pyrohydrolysis units have never really been inclined to study the fundamentals either, as the technology has been until very recently, used almost exclusively for the regeneration of waste acid from steel pickling plants (a relatively small unit operation within the overall steelmaking process).[1]

As for the nonferrous industry, the recovery of hydrochloric acid from waste liquors makes up a much more noteworthy portion of the overall production costs. Given this, as well as the fact that spent liquors generated by a nonferrous chloride leach process typically contain a number of metal species, the incentives for developing an improved understanding of multi-component metal chloride pyrohydrolysis are much more significant. This is further supported by the fact that the use of hydrochloric acid as lixiviant, by the nonferrous metals extraction industry, has become increasingly more popular during the last 20-30 years.[2-7]

In light of the above-mentioned considerations, fundamental studies were initiated to develop an improved technical understanding of the mechanisms behind multi-component metal chloride pyrohydrolysis. An Al-Fe-Mg-Cl-H_2O based system was selected for the study at hand. Furthermore, given that non-ferrous leaching

operations typically generate large quantities of waste liquor and that fluidized bed pyrohydrolysis facilities are generally much more cost effective for high volume processes[8-12], it was decided that the given research be geared toward fluidized bed systems.

1.2 Justification:

Industrial experience has revealed that when used to treat multi-component metal chloride waste liquors, existing fluidized bed acid regeneration facilities behave differently from those employed for the pyrohydrolysis of conventional iron chloride solutions (i.e. waste pickle liquor).[13,14] Therefore, in an effort to minimize the operating costs of such an acid regeneration plant, it was decided that an improved understanding of the mechanisms behind high temperature multi-component $MeCl_x$ hydrolysis is essential.

The significance of the project may be summarized as follows. From an environmental standpoint, the results of the given study should assist in defining the means for reducing fines emissions from the concerned acid regeneration facilities. While these fines are typically inert, they can lead to very unpleasant hygiene conditions within the plant and the immediate surroundings. Additionally, poor process efficiencies result in increased fuel consumption that obviously have negative effects on the environment. Therefore, the ability to optimize the process would result in fewer emissions (gaseous toxins and particulate matter) and therefore make a positive contribution to the preservation of the environment.

Furthermore, a better overall understanding of multi-component metal chloride regeneration fundamentals would further reassure metallurgical/chemical companies that are considering the construction and operation of HCl based leach processes. Typical hydrometallurgical installations, which include acid regeneration facilities, may cost anywhere between 250-450M$ to build; therefore, the concerned research may favour very noteworthy investments within the industry. These types of capital

projects typically benefit the financial well-being of the surrounding communities by providing job opportunities, stimulating economic activity, generating additional income/property taxes for the concerned government bodies, etc...

It should be mentioned that during the course of the given research study, the author was responsible for initiating an acid regeneration technology program for a fairly large and reputable company in the metallurgical industry, which shall remain unnamed for confidentiality reasons. This four-year program included building, commissioning, and operating a sizable pilot acid regeneration plant (i.e. multi-million dollar project), as well as conducting numerous trials to understand the effects of various parameters on process performance and to support the commercial operation. Several bench scale tests were performed in parallel to further the research team's comprehension of related fundamentals. As a result, the author was fortunate enough to have the support of many highly skilled research professionals during his studies and has therefore gained a considerable amount of experience in the area of acid regeneration technology. Clearly, the scope of the research performed for the purposes of the concerned doctoral study was partly derived from the author's experience as well as from input provided by his colleagues.

1.3 Objective:

The ultimate objective of the author's research was to define the conditions required for the efficient and environmentally friendly regeneration of a spent Al-Fe-Mg-Cl liquor generated by the non-ferrous metals industry. While fluidized bed pyrohydrolyzer performance is no doubt dependant upon numerous parameters such as fluidizing gas velocity, bed granulometry, $MeCl_x$ solution distribution within the reactor etc..., chloride conversion mechanisms must be well understood from the start. Until now, the thermal decomposition of the said aqueous metal salts has been simply described by the following chemical reactions.

$$MeCl_{2\,(s,l,g)} + H_2O_{(g)} \rightarrow MeO_{(s)} + 2HCl_{(g)} \qquad (1)$$

$$2MeCl_{2\,(s,l,g)} + 2H_2O_{(g)} + 1/2O_{2\,(g)} \rightarrow Me_2O_{3\,(s)} + 4HCl_{(g)} \qquad (2)$$

Therefore, a study was initiated in an attempt to characterize the reactions that take place and the sequence in which they occur, from the moment at which the nearly saturated solution is injected into the reactor. This investigation will also serve to challenge industry claims that aqueous metal chloride pyrohydrolysis in fluidized bed reactors is simply a ***vapour deposition process***.[1,15] Fundamental considerations suggest that such a declaration may be misleading.

In an effort to characterize the transformation of an aqueous yet saturated Al-Fe-Mg-Cl solution (at ~ 105°) upon injection into a reactor at 850°C, initial plans consisted of building a laboratory scale fluidized bed pyrohydrolyzer, complete with an offgas cyclone, and gas scrubbing facilities. The proposed set-up would have allowed for an accurate simulation of the gaseous atmosphere and dynamics within such a reactor, as well as complete mass balance calculations. While this would have been ideal, the author's experience with a similar set-up and much larger pilot acid regeneration facility revealed that the given lab installation would have been literally impossible to operate reliably. A more detailed description of this test rig is provided in Section 3.1.1.

As a result, it was decided to proceed with a series of experimental studies (three phases) instead. The trials were designed to help define the sequence of reactions that take place as the liquor converts into oxide.

Phase I:

Preliminary testwork was conducted with a simplified experimental set-up to study the physical behaviour of the chloride liquor as it is exposed to the high temperature reactor environment, and to identify the various phases of the overall transformation process. Visual observations, temperature

measurements, and sample analyses were used to study the mechanisms by which the multi-component metal chloride solution pyrohydrolyzes as its temperature increases within the reactor.

Phase II:

In light of the observations made during Phase I, controlled bench scale trials were performed to define the crystallization path that occurs as the H_2O in solution evaporates and to identify the compounds that form.

Phase III:

Further experiments were undertaken within a fully instrumented tube furnace, to elaborate on the sequence in which the chlorides of interest (i.e. $FeCl_2$, $FeCl_3$, $AlCl_3$, and $MgCl_2$) actually pyrohydrolyze. Typical pyrohydrolysis conditions were more closely simulated during the concerned series of tests.

To conclude, thermochemical modelling studies were undertaken to assist with the interpretation of the experimental results obtained during the studies mentioned above.

It should be mentioned that Fourrier Transform Infra-Red spectroscopy (FTIR) combined with ThermoGravimetric Analysis (TGA) was considered as a means to defining the saturated $MeCl_x$ solution transformation process. Unfortunately, FTIR-TGA could not be used due primarily to the corrosive nature of the $HCl_{(g)}$ generated by the pyrohydrolysis reactions and due to the presence of water vapour in the system. Further details are provided in Section 3.1.2.

2.0 LITERATURE REVIEW:

2.1 Introduction:

The use of a spray roaster to pyrohydrolyze a metal chloride waste liquor, for hydrochloric acid (HCl) regeneration purposes, was first proposed and patented by a world renowned process engineering company, Lurgi GmbH, in 1935 (DP No. 721358).[1] At that time, Lurgi engineers had also almost simultaneously developed a process involving fluidized bed reactor technology for the roasting of pyrite and/or sphalerite concentrates. Lurgi eventually decided to adopt the use of a fluidized bed reactor for the pyrohydrolysis of metal chloride waste liquors as well, and abandoned the spray roasting alternative which was ultimately taken over by Ruthner-Andritz (Vienna, Austria).[1,16]

With the introduction of commercially available HCl regeneration facilities, the steel industry turned to the use of this muriatic acid, to replace sulphuric acid (H_2SO_4), for the pickling of steel. The waste pickle liquor generated by the use of H_2SO_4, to remove the oxide layer from the surface of raw steel products, was neutralized or its ferrous sulphate content was crystallized to recover the free acid. The resulting environmentally unfriendly waste sludges were then disposed of. Given that the previously mentioned hydrochloric acid regeneration technologies resulted in close to 99% HCl recovery and the production of very stable iron oxide (a sometimes sellable by-product), many steelmaking companies (such as DOFASCO, and STELCO) decided to replace their existing pickling and waste liquor treatment facilities with HCl based processes.[3,9-11,16-25]

Over the years, Lurgi and Ruthner succeeded in further improving their respective acid regeneration processes.[1,12,15-17,22,23] In 1995, Peek[1] reported that over 200 spray roaster type acid regeneration facilities had been erected worldwide within the chemical and metallurgical industries. It is worth mentioning that a number of these installations were designed and built by a competing process engineering

company, Babcock-Woodall-Duckham (Crawley, England)[3,26]. Since 1968, Keramchemie GmbH or KCH (another multi-disciplinary engineering company) has marketed the Lurgi fluidized bed acid regeneration technology and has constructed 71 related plants for the iron and steel industry.[1,11,14,24] The growing popularity of the aforementioned acid regeneration processes inspired others to develop and patent derivations of the Lurgi and Ruthner technologies[2,5,6,26-35]. Additional concepts, such as the Wean-Pori Process[36-38], a diffusion dialysis technique[39], the Vicarb Process[40], the use of anion exchange[41], the APU Process[42], and a few others[43-48] were also developed for the treatment of waste pickle liquors. Despite these efforts, spray roaster and fluidized bed pyrohydrolysis still dominate as the acid regeneration technologies of choice within the steelmaking, minerals, and non-ferrous extraction industries.[1,3,4,7,9-18,20,23,24,25]

2.2 Available Hydrochloric Acid Regeneration Processes:

As discussed in the previous section, hydrochloric acid may be recovered from spent liquors by either of the following methods;

- ***pyrohydrolyzing a concentrated waste acid in either a fluidized bed reactor (800-900°C)[1,8-12,15,20,22,24,49,50] or spray roaster (600-700°C)[1,3,4,7,16-18,20,23,25,26,51,52] to generate an HCl:H_2O bearing offgas stream and stable metal oxide particles.*** The resulting offgas is typically quenched by direct contact (in a venturi scrubber, for example) with the spent liquor to;

  - cool the gas stream before feeding it to an adiabatic absorption column
  - concentrate the waste acid prior to pyrohydrolysis.

  A scrubber is typically installed at the tail end of the process to minimize $HCl_{(g)}$ emissions to the atmosphere.

- ***oxidizing ferrous chloride ($FeCl_2$) to ferric chloride ($FeCl_3$) and subsequently hydrolyzing the latter to generate HCl and hematite (Fe_2O_3). This technology is referred to as the WEAN-PORI PROCESS.***[36-38] The waste $FeCl_2$ liquor is concentrated in a gas/oil-fired evaporator and subsequently fed to a stirred pressure vessel where the ferrous chloride is oxidized at a temperature of approximately 150°C and a pressure of 690 kPa. The resulting $FeCl_3$ and black Fe_2O_3 mixture is then hydrolyzed by contacting the slurry (T = 155-160°C) with the combustion gases (of a burner) in a venturi scrubber. The $HCl_{(g)}$ generated by the hydrolysis reaction reports to an absorber for hydrochloric acid production, and the Fe_2O_3 rich slurry is subjected to settling. The unreacted $FeCl_3$ liquor returns to the hydrolyzer vessel.

- ***diffusion dialysis membrane separation technique, operating at ambient temperature and pressure.***[39] A recirculating bath of spent acid is separated from a water bath by an anion exchange membrane diaphragm; therefore, acid molecules diffuse into the water, which contains a lower acid concentration. By maintaining counter-current flows of the absorbing water and spent acid on the opposite sides of the diaphragm, a significant percentage of the acid is recovered in the water. With this process, the spent acid is basically stripped of its HCl content, but the metal chloride concentration remains essentially unchanged; therefore, the resulting effluent requires further treatment.

All three techniques have been commercialized at one time or another. On the other hand, with over 40 years of commercial scale operation, high temperature pyrohydrolysis based processes (i.e. fluidized bed reactor or spray roaster) are considered well established and are most commonly employed for the regeneration of metal chloride waste liquors generated by the steelmaking, minerals, and non-ferrous extraction industries. [1,3,4,7,9-18,20,23,24,25]

Given that the research at hand will focus on characterizing the transformation of a multi-component metal chloride solution within a fluidized bed reactor, a brief description of this HCl regeneration technology is certainly in order.

2.3 Keramchimie - HCl Regeneration Process:

Overall, this type of acid regeneration plant (ARP) is composed of the following; fluidized bed reactor, hot gas cyclone, venturi, gas/liquid separating vessel, adiabatic HCl absorption column, exhaust fan, and a tail gas scrubber. A schematic illustration is shown in Figure 1.

Generally speaking the process involves pyrohydrolyzing a saturated metal chloride solution (at ~ 105°C) in the fluidized bed (as per reactions 1 and 2), at temperatures of 800-900°C, to generate an HCl bearing offgas and stable disposable or saleable oxide granules. Once cooled, the HCl is recovered as regenerated acid to be reused in the pickling plant or for leaching purposes.

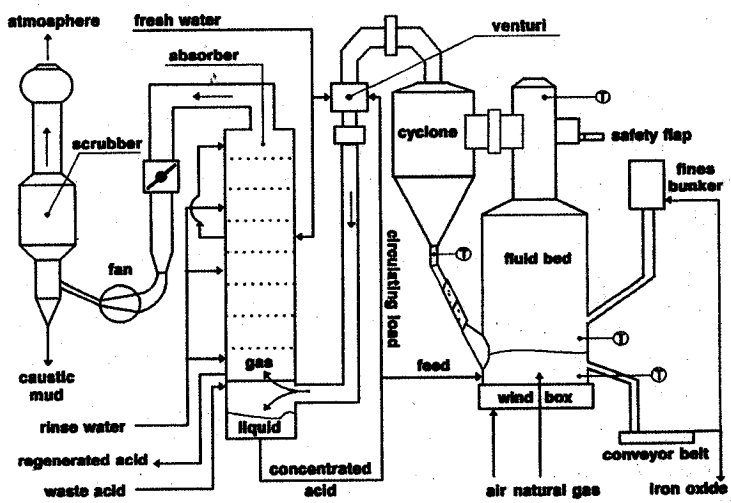

Figure 1: Schematic illustration of the Keramchemie/Lurgi Acid Regeneration Process.

As shown in Figures 1 and 2, spent acid (i.e. $MeCl_{x\,(aq)}$) units are introduced into the process through the separator vessel (in the pre-evaporator circuit), and are

ultimately used to cool the reactor off-gases in the venturi to approximately 95-105°C, for the subsequent $HCl_{(g)}$ absorption stage. The direct quenching of the hot reactor off-gas with spent liquor, results in the evolution of a predominantly $H_2O_{(vap)}$ phase (containing between 0-5% $HCl_{(g)}$) that reports along with the quenched off-gas. The resulting aqueous solution is usually concentrated to just below the saturation limit to avoid the onset of metal chloride precipitation, while simultaneously maximizing the amount of water removal from the incoming spent acid. Up to 30% of the solvent water in the feed can be evaporated in this manner. The ability to eliminate as much of the water within the waste liquor prior to feeding it into the reactor translates into lower fuel costs per unit of HCl recovered. It is also worth mentioning that the given venturi scrubber configuration also allows for the capture of particulate matter that may have made it past the off-gas cyclone, as well as its return to the reactor. Given that the waste liquor is concentrated to its saturation limit when it is used to cool the reactor off-gases, the venturi/gas-liquid separating vessel combination is commonly referred to the pre-evaporation or pre-concentration circuit. It should be noted that process water is sometimes also added to the pre-evaporation circuit, when the incoming waste acid is relatively concentrated to begin with or when the reactor off-gas contains too much enthalpy, to suppress the onset of metal chloride crystallization.

While most of the HCl (i.e. 99.5%) in the quenched reactor offgas is recovered as hydrochloric acid[1,11,15,22] (14-19 wt% strength) in the adiabatic absorption column, a fraction of the pre-concentrated liquor is bled from the recirculation loop and is introduced to the pyrohydrolyzer (i.e. reactor). A very characteristic feature of Keramchemie (KCH) technology is that the aqueous reactor feed is usually injected into the fluidized bed to ensure that the hydrolysis reaction occurs on the surface of existing oxide particles within the vessel. This results in the production of fairly large (0.2-2mm) and dense granules that are periodically or continuously discharged from the bed. In order to minimize atmospheric emissions, any remaining trace

$HCl_{(g)}$ in the absorber offgas is recovered by a scrubber at the tail end of the process. The slightly acidic scrubber water is recycled to the absorber for $HCl_{(aq)}$ generation.

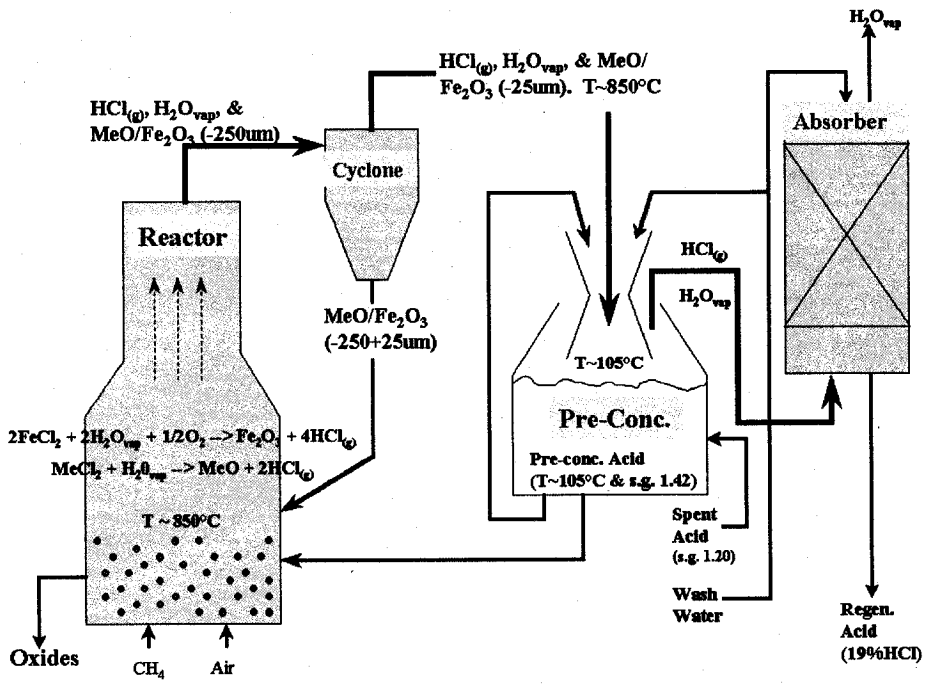

Figure 2: Simplified flowsheet for the regeneration of HCl from metal chloride solutions with the KCH process.

The performance of an acid regeneration plant is governed by a number of considerations (such as gas/liquid equilibria in the pre-concentrator and absorber, feed water distribution in the towers), but the process is most dependent on the high temperature hydrolysis of the $MeCl_x$'s in the reactor. The thermal decomposition reactions themselves are influenced by kinetics and thermodynamics, $MeCl_x$ solubility in the liquor, surface tension/viscosity of the solution, etc... Therefore, any academic studies aimed at better defining the fundamentals behind multi-component metal chloride pyrohydrolysis are certainly justified.

Of the major components that make up the KCH acid regeneration process, the fluid bed reactor influences plant performance and efficiency most. While the venturi, cyclone, absorber, and tail end scrubber are essential for economical and

environmentally sound ARP operation, the latter three are standard equipment that have no special design features that are specific to the Keramchemie process. In fact, when designing an acid regeneration plant for a specific application, KCH generally provides only duty specifications for the absorber and scrubber, and subsequently subcontract the manufacture to typical suppliers such as KOCH engineering. In light of these considerations, only the fluidized bed reactor will be described in detail.

2.3.1 Fluidized Bed Pyrohydrolyzer:

The fluidized bed reactor is a vertical, refractory lined cylindrical vessel with a combustion zone located at the base (i.e. hearth) to maintain the desired operating temperature. The front view of the bottom section of an existing commercial fluidized bed pyrohydrolyzer is shown in Figure 3.

Fluidizing/combustion air and gaseous fuel (e.g. natural gas) are evenly distributed through the hearth by a number of vertical tuyeres that enter from the base of the reactor. The available technical literature suggests that a reactor with an internal diameter of 2.5m, is typically fitted with 60-70 tuyeres. The concerned tuyere design is considered Keramchemie intellectual property; therefore, further details cannot be provided. On the other hand, it is worth mentioning that the tuyeres are designed to deliver a well-blended air/fuel mixture to the nozzle openings. This is reported to favour complete fuel combustion in the hearth, and minimize the possibility of after-burning in the upper sections (i.e. freeboard) of the reactor.[1,15,22]

Adequate fuel and air volumetric flowrates are required to generate the heat for hydrolysis, provide oxygen for the reactions, and fluidize the bed of oxide granules in the reactor. KCH claims that fluidization of the solids induces thorough mixing in the bed, which in turn favours a relatively homogeneous temperature distribution in the reaction zone (i.e. base of the

pyrohydrolyzer).[53] It should be mentioned that the superficial gas velocities typically maintained in practice (i.e.~ 2 m/s) and are apparently based on production capacity instead of ideal fluidization behaviour.[1,53]

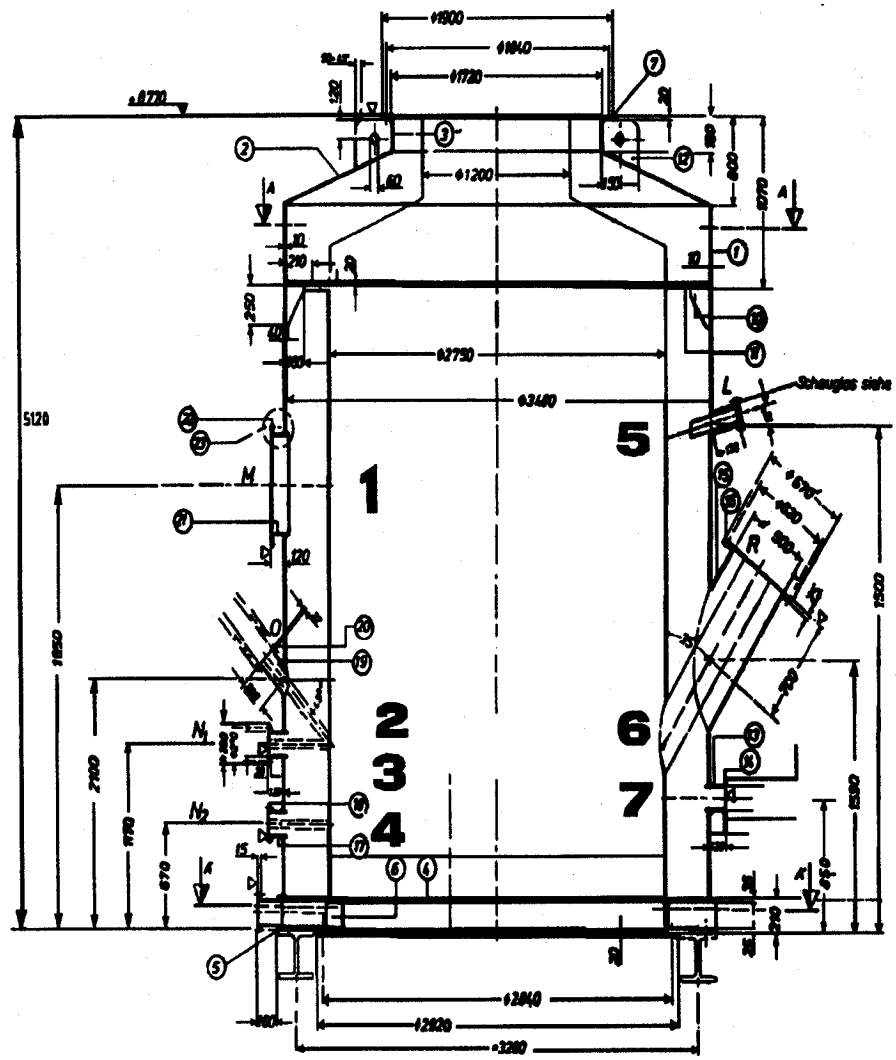

Figure 3: Blueprint of the fluid bed reactor design (bottom section) typically employed in KCH Acid Regeneration Plants[1]

Where:

1 - indicates manhole location
2 - shows inlet for oxide particles (i.e. to establish initial bed or for periodic seed addition)
3,4 - thermocouple locations
5 - points out site glass
6 - indicates point at which elutriated fines return via cyclone underflow
7 - shows pre-concentrated acid feed lance location

While smaller bed particles will be elutriated by the upward moving gas stream, a relatively homogeneous mixture is periodically discharged from the bottom of the reactor. Despite the fact that fluid bed reactors are typically designed with an expanded freeboard (i.e. vessel diameter is larger at the top than at the base), the KCH pyrohydrolyzer is designed with a much narrower freeboard (as shown in Figure 1) to minimize the capital cost.[1,22,53] As a result, the installation of a hot gas cyclone at the reactor exhaust, is essential for the recovery of any elutriated solids which are then subsequently fed back into the pyrohydrolyzer.

Although the mass and volume of the fluidized bed is dependent upon the size of the reactor, the literature suggests that the bed is typically composed of 3-8 tonnes of oxide particles (when referring to iron oxide).[1] As the oxides within the bed grow gradually during pyrohydrolysis, and the finer particles circulate between the reactor and the cyclone, it is not surprising that typical solids retention times will range from 1-8 hours. Oxide discharge from the reactor is regulated by bed weight (i.e. constant windbox pressure).

With regards to the manner in which pre-concentrated acid is introduced into the reactor, the literature has clearly revealed that the solution is not sprayed, but injected as a robust liquid stream (between ¾ - 1 ½" in diameter). This "rope-feeding" technique has been promoted by KCH to encourage the formation of large droplets that will not be carried away by the upward flowing combustion gases, and actually remain in the bed.[1,15,22] This, in turn, provides the reactor feed liquor with the opportunity to be quickly distributed throughout the thoroughly mixed fluidized bed and ultimately ensure that the pyrohydrolysis reaction occurs on the surface of the bed particles; thus favouring oxide growth.

Three methods of pre-concentrated acid injection are currently employed by existing installations.[1,53] KCH originally favoured the use of two or three titanium lances, equally spaced from one another around the circumference, to inject the pre-concentrated acid through the sides of the reactor, at approximately 0.2m above the hearth. The lances were typically installed to ensure that the pre-concentrated liquor was injected downwards toward the hearth. In an effort to reduce ultrafine oxide formation when pyrohydrolyzing waste pickle liquor, DOFASCO decided to inject the pre-concentrated acid vertically upward and parallel to the gas stream through three titanium lances, installed through the bottom of the reactor. Krupp Hoesch Stahl (Bochum, Germany) has also refrained from injecting through the sides of the reactor, and is currently feeding the pre-concentrated acid downward into the vessel through a top lance located just above the bed.

2.4 Pyrohydrolysis Fundamentals:

Generally speaking, pyrohydrolysis may be described as the thermal decomposition of metal chlorides ($MeCl_x$), in the presence of water vapour and oxygen, into metallic oxides (Me_yO_z) and gaseous hydrogen chloride. Metal chloride pyrohydrolysis may be theoretically characterized by either of the following chemical reactions.[1,15,22]

$$2MeCl_{(s,l,g)} + H_2O_{(g)} \leftrightarrow Me_2O_{(s)} + 2HCl_{(g)} \quad (3)$$

$$MeCl_{2\,(s,l,g)} + H_2O_{(g)} \leftrightarrow MeO_{(s)} + 2HCl_{(g)} \quad (4)$$

$$2MeCl_{3\,(s,l,g)} + 3H_2O_{(g)} \leftrightarrow Me_2O_{3\,(s)} + 6HCl_{(g)} \quad (5)$$

$$MeCl_{4\,(s,l,g)} + 2H_2O_{(g)} \leftrightarrow MeO_{2\,(s)} + 4HCl_{(g)} \quad (6)$$

$$2MeCl_{2\,(s,l,g)} + 2H_2O_{(g)} + \tfrac{1}{2}O_{2\,(g)} \leftrightarrow Me_2O_{3\,(s)} + 4HCl_{(g)} \quad (7)$$

$$3MeCl_{2\,(s,l,g)} + 3H_2O_{(g)} + \tfrac{1}{2}O_{2\,(g)} \leftrightarrow Me_3O_{4\,(s)} + 6HCl_{(g)} \quad (8)$$

$$2MeCl_{3\,(s,l,g)} + 3H_2O_{(g)} + O_{2\,(g)} \leftrightarrow Me_2O_{5\,(s)} + 6HCl_{(g)} \quad (9)$$

The difference between the former and latter series of reactions is that the metal species undergo a change in valency (i.e. oxidation) during pyrohydrolysis reactions 7 through 9. While the metal chloride may hypothetically be reduced to the metallic

state, it is less common during pyrohydrolysis as oxidizing (or at worst slightly reducing) conditions are typically maintained within both fluidized bed reactors or spray roasters. In light of the basic chemical reactions shown above, thermodynamic and phase equilibria considerations clearly suggest that metal chloride pyrohydrolysis is dependent upon; temperature, metal chloride stability/volatility, and oxygen partial pressure.

2.4.1 Thermodynamic Considerations:

Based on a review of the available literature[1,15,16,46,52], it appears as though single component Standard Gibbs Free Energy ($\Delta G°$) has been generally used to predict how various metal chlorides behave when exposed to high temperature hydrolyzing conditions. One reference[1] has used the following *"rule of thumb"* in a general discussion on the pyrohydrolysis of several metal chlorides:

- when $\Delta G° < -15$ kcal/mole (the equilibrium constant, $K > 10^{10}$), the reaction is expected to go to completion
- the reaction is not very likely to proceed when $\Delta G° > 15$kcal/mole (i.e. $K < 10^{-10}$).

Standard Gibbs free energy data (per mole of H_2O) of several metal chloride pyrohydrolysis reactions are provided as a function of temperature in Figures 4 through 8. The manner in which the vapour pressure of these metal chlorides varies with temperature is shown in Figure 9. The need to take vapour pressures into consideration when discussing metal chloride pyrohydrolysis will become rather clear in the following paragraphs.

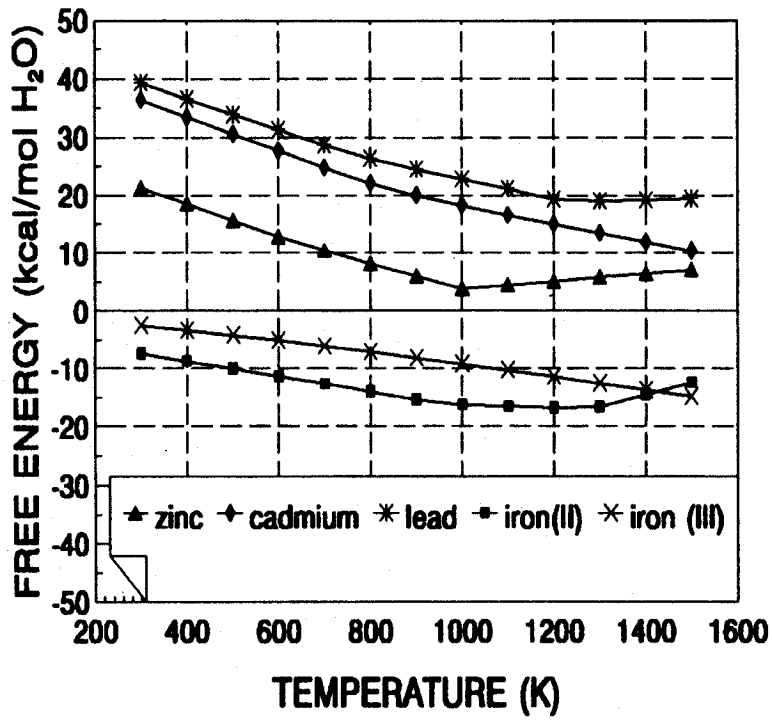

Figure 4: Standard Gibbs Free Energy as a function of temperature for the pyrohydrolysis of ferrous and gaseous ferric chloride, as well as zinc, lead, and cadmium chloride.[1]

As mentioned previously, most of the existing acid regeneration installations involve ferrous chloride pyrohydrolysis. With the assumption that the above-mentioned *"rule of thumb"* is indeed valid, Figure 4 suggests that a $FeCl_2$ solution will be fully pyrohydrolyzed at reaction temperatures of 900-1300K (i.e. 627-1027°C). It is therefore, not surprising that most iron chloride pyrohydrolyzers maintain operating temperatures of 600-900°C. As far as ferric chloride is concerned, Figure 9 reveals that this trivalent compound is much more volatile than $FeCl_2$. It is generally accepted within the industry that aqueous ferric chloride injection into conventional spray roasters or fluidized beds results in instantaneous vapourization, and ultimately to the entrainment of the metal chloride vapour into the reactor offgas phase.[1,3,10,11,22,23,50] Despite the fact that the standard Gibbs free energy data (Figure 4) implies that temperatures as high as 1400K (1127°C) are required for the gaseous ferric chloride pyrohydrolysis

reaction to go to completion, operating experience indicates otherwise. In fact, the literature suggests that $FeCl_3$ hydrolyzes in the vapour state and results in ultrafine hematite formation that fosters a number of operating difficulties and inefficiencies within the more conventional acid regeneration processes. Clearly, even ferric chloride hydrolysis does not appear to be very well understood.

With regards to lead and cadmium chloride, Figure 4 reveals that it is very difficult, thermodynamically to pyrohydrolyze these compounds, even at temperatures as high as 1400K. While the standard free energy for ZnCl pyrohydrolysis reaches a minimum at 1000K, it is unfortunately still positive; therefore, the reaction may not necessarily go forward. The literature[1] does, on the other hand, suggest that if the ZnCl and water vapour concentrations are high enough, then the chloride will partially hydrolyze.

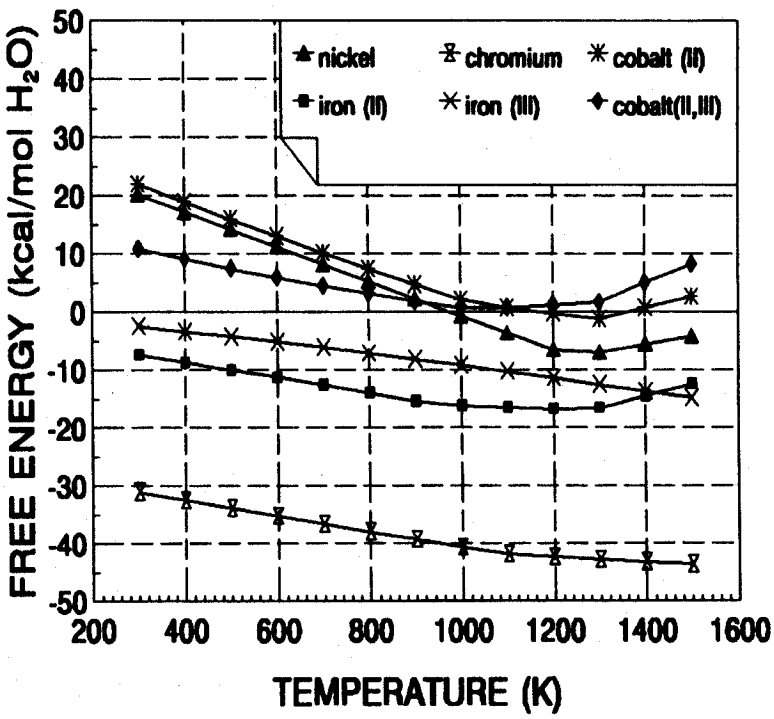

Figure 5: Standard Gibbs Free Energy Diagram for the pyrohydrolysis of ferrous, gaseous ferric, nickel, cobalt, and chromium (IV) chloride.[1]

Based on the data provided in Figure 5, chromium oxide appears to be more stable than hematite. Unfortunately, the regeneration of Cr bearing pickle liquors in industry has revealed that the formation of highly volatile complex chromium (III, IV) chloride species results in negligible Cr_2O_3 formation during pyrohydrolysis.[1] It is unknown whether the complex itself hydrolyzes in the vapour state, but operating experience with chromium bearing waste pickle liquors has confirmed that the Cr will actually accumulate in the recirculating loop between the reactor and pre-concentration circuit. While the thermodynamic data (Figure 5) does not necessarily suggest that nickel and cobalt chlorides will convert into oxides when exposed to typical spray roaster or fluidized bed reactor operating conditions, these metal chlorides have been successfully pyrohydrolyzed at the commercial scale. The literature[1,15], once again, mentions that high reactant and low product concentrations are essential for reasonable $NiCl_2$ and $CoCl_2$ hydrolysis rates.

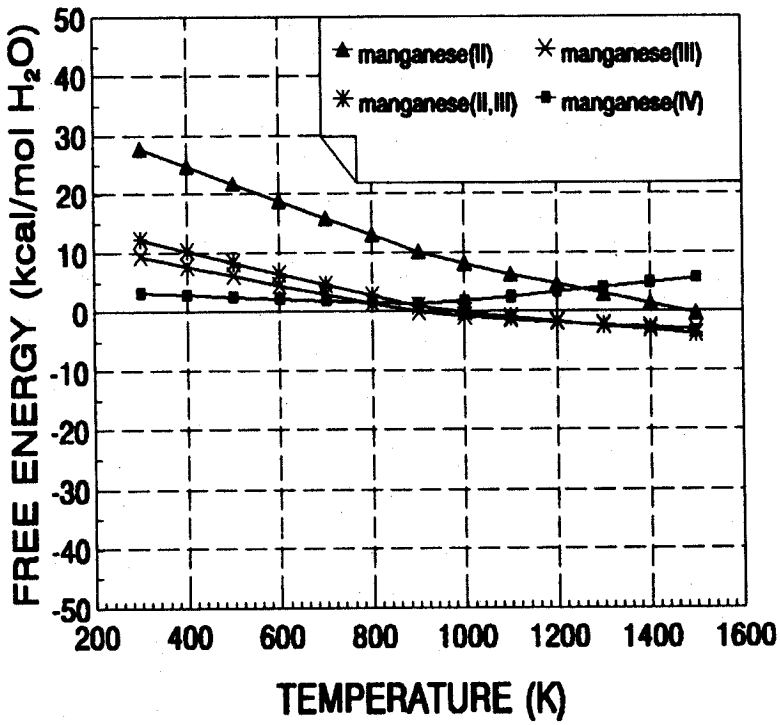

Figure 6: Standard Gibbs Free Energy Data for the hydrolysis of $MnCl_2$ over a range of temperatures into a number of manganese oxides.[1]

As shown in Figure 6, while manganese chloride pyrohydrolysis is not that favourable from a thermodynamic point of view, one of the references claims that when a relatively concentrated $MnCl_2$ solution reacts with excess water vapour, Mn_2O_3 and Mn_3O_4 are likely to form.[1] Figure 7 clearly reveals that silica, cassiterite (SnO_2) and titanium dioxide are very stable over a wide range of temperature. As a result, it is not surprising that $SiCl_4$, $SnCl_4$, and $TiCl_4$ hydrolyze readily, even at room temperature.

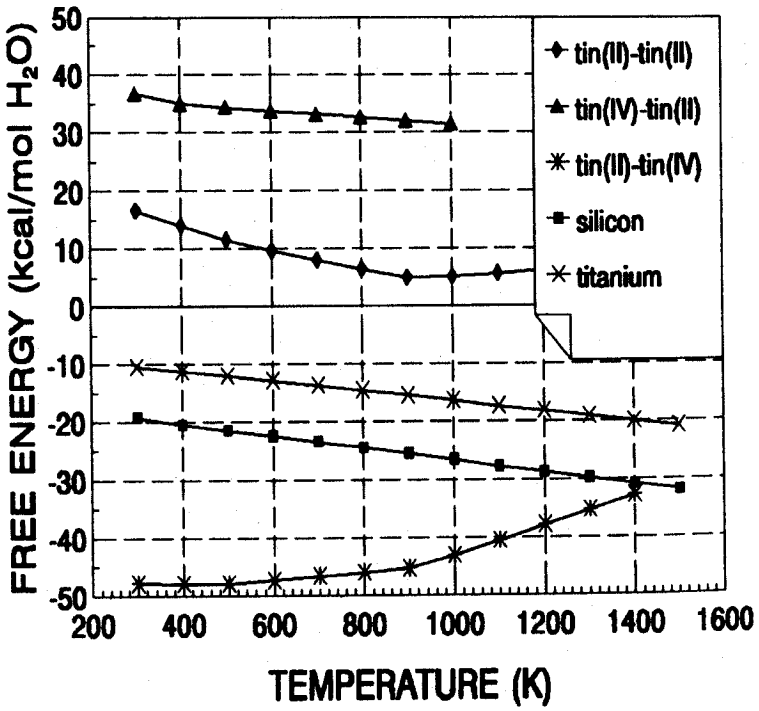

Figure 7: Standard Gibbs Free Energy data illustrates that while $TiCl_4$ & $SiCl_4$ hydrolyze readily, $SnCl_2$ will transform into SnO_2 & not SnO.[1]

Finally, the Standard Gibbs free energy diagram for the hydrolysis of sodium, potassium, calcium, and magnesium is shown in Figure 8. While the curves suggest that $MgCl_2$ is likely to hydrolyze at temperatures in excess of 1200K, the other alkali earth metal chlorides are not expected to convert into oxide.

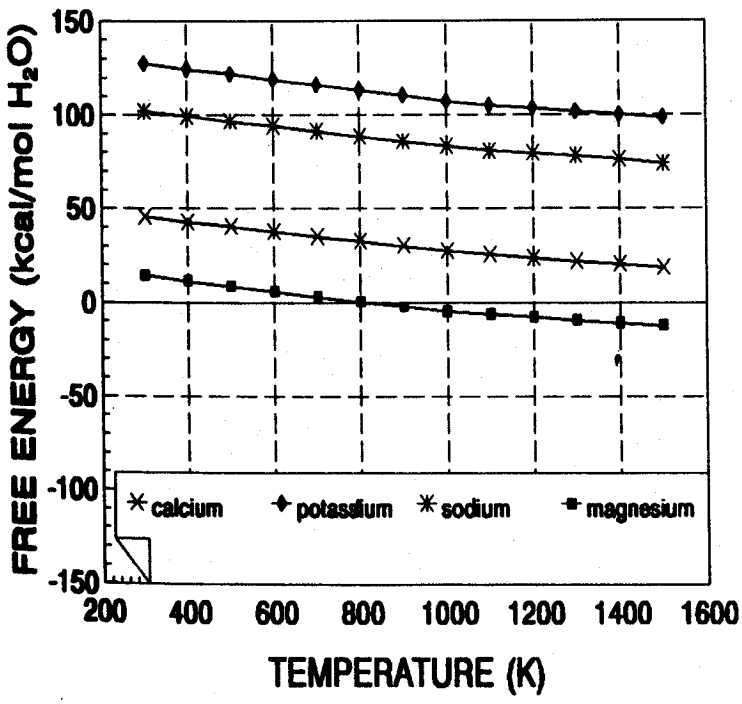

Figure 8: Standard Free Energy Diagram for the pyrohydrolysis of alkali earth chlorides.[1]

While the thermodynamic considerations provide a basic indication as to how various metal chlorides behave in the presence of high temperature hydrolysis conditions, the discussion was limited to single component systems. The presence of several metal species within a waste chloride solution (i.e. non-ferrous leach liquors) will certainly influence the hydrolyzing tendency of the mixture or the individual components involved, by affecting activities, though complexation in the aqueous phase, etc. This must therefore be taken into consideration when using the data in Figures 4 through 8 to predict whether a metal chloride in a multi-component solution will actually react with water vapour and oxygen at high temperature (as per either of reactions 1 through 9). Based on the literature[1,15,53] it appears as though the rather simplified thermodynamic data has been typically used along with pilot plant trials to select the reaction temperatures for most of the metal chloride solution pyrohydrolysis units currently in operation.

The thermodynamic data presented above also reveals that the stability of a metal chloride, in the presence of water and oxygen, is related to the valency of the metal species within the salt. The monovalent chlorides (e.g. NaCl, PCl) are extremely stable, and temperatures in excess of 2000°C are required for hydrolysis. Tetravalent compounds such as titanium, tin, and silicon chlorides are very instable and will readily convert into oxides. As for the di- and tri-valent metal chlorides, it appears as though temperature and the ability of the metal species to undergo a valency change are the dominant factors that influence the hydrolysis reaction. Aluminum chloride, for instance, hydrolyzes readily at relatively low temperatures (below 200°C)[54,55], and a minimum of 425°C is required for the hydrolysis of aqueous ferric chloride at atmospheric pressure.[15] While some divalent chlorides, such as nickel and cobalt chloride, may be pyrohydrolyzed at temperatures of 750°C and up, lead and cadmium chloride will never really convert into oxides. This may be explained by the fact metal chloride stability, which essentially governs hydrolysis tendency, is related to both metal valence state and ion size.

In light of the fact that the trivalent metal chlorides appear to hydrolyze much more readily and at lower temperature than their divalent counterparts, it is reasonable to suggest that the ability to oxidize a divalent metal to the trivalent state should result in a more favourable pyrohydrolyzing tendency. The disadvantage with trivalent chlorides is that they are typically quite volatile (see $FeCl_3$, $SbCl_3$, & $AsCl_3$ vapour pressures in Figure 9); therefore, pyrohydrolysis of these compounds may occur in the vapour state, and therefore result in the production of extremely fine oxides.

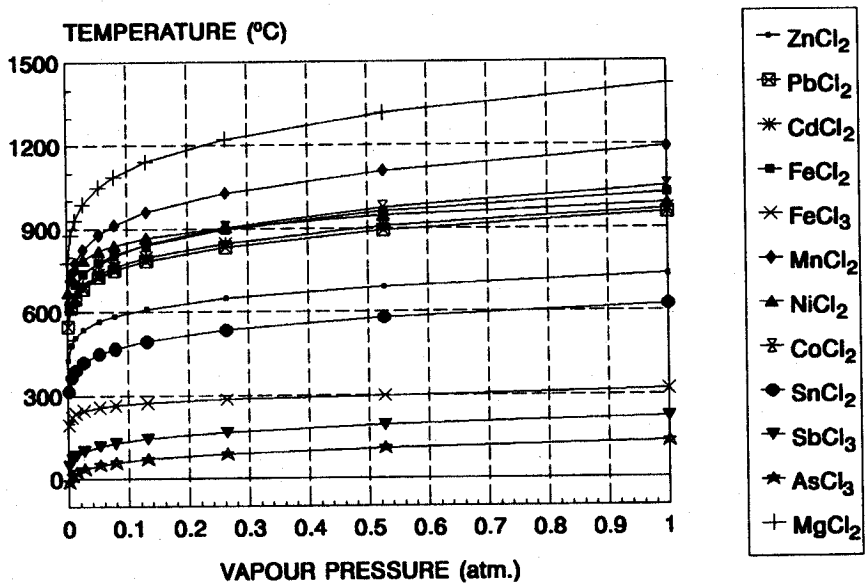

Figure 9: Various metal chloride vapour pressures as a function of temperature.[1]

As mentioned previously, spray roasting and fluidized bed acid regeneration technology has been employed extensively by the steel industry during the last 40 years for the pyrohydrolysis of waste pickle liquors. Despite this, the actual mechanisms behind $FeCl_2$.decomposition are still not yet fully understood. The concerned spent liquors are primarily composed of $FeCl_2$, with measurable quantities of $FeCl_3$ and unreacted HCl. While it is presumed that the $FeCl_2$ pyrohydrolysis reaction is oxygen assisted to produce hematite (as per reaction 7), the actual mechanisms and order in which they occur, are still somewhat unknown[1]. For instance, it is not clear whether ferrous chloride hydrolyzes to produce wustite (FeO) which is then further oxidized to hematite (as per reactions 10 and 11), or whether the $FeCl_2$ is oxidized to ferric and the latter is immediately pyrohydrolyzed to hematite. In fact, neither the scientists nor the engineers who have performed research or have practiced in the field of pyrohydrolysis have been able to provide an indisputable explanation of the phenomenon that occurs during the conversion of iron chloride to hematite.

$$2FeCl_{2\,(s,l,g)} + 2H_2O_{(g)} \leftrightarrow 2FeO_{(s)} + 4HCl_{(g)} \quad (10)$$

$$2FeO_{(s)} + \tfrac{1}{2}O_{2\,(g)} \leftrightarrow Fe_2O_{3\,(s)} \quad (11)$$

$$2FeCl_{2\,(s,l,g)} + 2H_2O_{(g)} + \tfrac{1}{2}O_{2\,(g)} \leftrightarrow Fe_2O_{3\,(s)} + 4HCl_{(g)} \quad (12)$$

$$3FeCl_{2\,(s,l,g)} + 3H_2O_{(g)} + \tfrac{1}{2}O_{2\,(g)} \leftrightarrow Fe_3O_{4\,(s)} + 6HCl_{(g)} \quad (13)$$

Assuming that ferrous chloride is pyrohydrolyzed to wustite and then subsequently oxidized to hematite, the enthalpies of reactions 10 and 11 confirm that reaction 12 is indeed exothermic at typical pyrohydrolysis temperatures (i.e. $\Delta H°_{1100K}$ = -56.5 kJ/mol Fe). If fuel rich conditions were maintained in the pyrohydrolyzer, $FeCl_2$ might react with $H_2O_{(vap)}$ to produce magnetite, as per reaction 13 ($\Delta H°_{1100K}$ = -17 kJ/mol Fe). The oxygen partial pressure (pO_2) within the system obviously influences the nature of the oxide produced by the reaction (i.e. hematite or magnetite). The Fe-O-H-Cl phase stability diagrams in Figures 10 and 11 clearly illustrate that by decreasing the pO_2 from 10^{-2} to 10^{-5} atm (at 1100K), typical pyrohydrolyzer operating conditions (indicated by the square at the top right hand corner) approach the magnetite stability region.

It is worth mentioning that despite the lack of any firm conclusions on the mechanisms behind the $FeCl_2$ decomposition reaction, it does appear to be generally accepted that ferrous chloride pyrohydrolysis is a chemical vapour deposition process.[1,15,22] It is unclear as to how the authors have come to this conclusion.

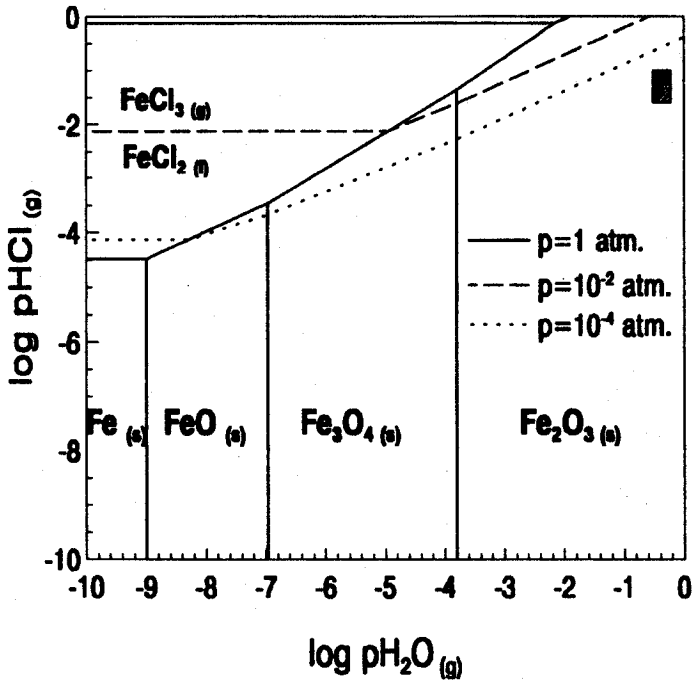

Figure 10: The Fe-O-H-Cl phase stability diagram at 1100K and an oxygen partial pressure of 10^{-2} atmosphere.[1]

With regards to $CoCl_2$ pyrohydrolysis, the literature review has revealed that a spray roaster is employed for the production of high grade cobalt oxide (CoO) by Union Minière (Métallurgie Hoboken) in Olen, Belgium, through a two step reaction mechanism which is dependent on the operating temperature.[1] While reaction 14 will proceed at temperatures as low as 460°C, much higher temperatures (T>870°C) are required for reactions 15, and ultimately 16, to go forward.

$$3CoCl_{2\,(s,l,g)} + 3H_2O_{(g)} + \tfrac{1}{2}O_{2\,(g)} \leftrightarrow Co_3O_{4\,(s)} + 6HCl_{(g)} \qquad (14)$$

$$Co_3O_{4\,(s)} \leftrightarrow 3CoO_{(s)} + \tfrac{1}{2}O_{2\,(g)} \qquad (15)$$

$$3CoCl_{2\,(s,l,g)} + 3H_2O_{(g)} \leftrightarrow 3CoO_{(s)} + 6HCl_{(g)} \qquad (16)$$

Given that CoO is known to react with $HCl_{(g)}$ to generate $Cl_{2\,(g)}$ (see reactions 17 and 18) at temperatures below 700°C, adequate controls are required when pyrohydrolyzing $CoCl_2$. In fact, if it is impossible to reliably control the offgas temperature, a chlorine removal stage must be integrated within the reactor exhaust system.

$$3CoO_{(s)} + 2HCl_{(g)} + O_{2\,(g)} \leftrightarrow Co_3O_{4\,(s)} + H_2O_{(g)} + Cl_{2\,(g)} \qquad (17)$$

$$Co_3O_{4\,(s)} + 8HCl_{(g)} \leftrightarrow 3CoCl_{2\,(s,l,g)} + Cl_{2\,(g)} + 4H_2O_{(g)} \qquad (18)$$

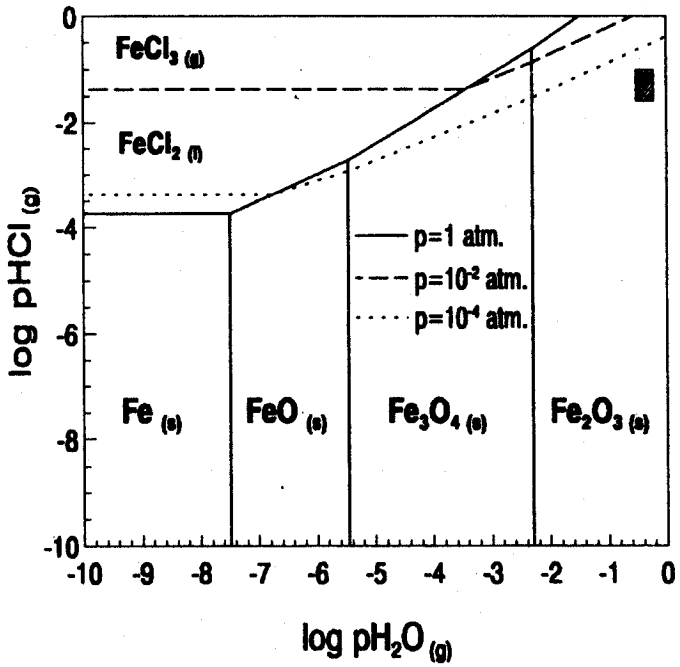

Figure 11: The Fe-O-H-Cl phase stability diagram at 1100K and an oxygen partial pressure of 10^{-5} atmosphere.[1]

2.4.2 Oxide Nucleation & Growth Phenomena:

As mentioned in section 2.3, when fluidized bed technology is used for acid regeneration purposes, the concentrated metal chloride solution is injected into a fluidized bed of oxides to ensure that the pyrohydrolysis reaction takes place on the surface of a particle. This is often referred to heterogeneous pyrohydrolysis. While previous research studies have failed to provide an accurate account of the physical

mechanisms that take place as a metal chloride transforms on the surface of the granules in the fluidized bed, metallographic examinations have confirmed that the final product is made up of several oxide layers (see Figure 12).

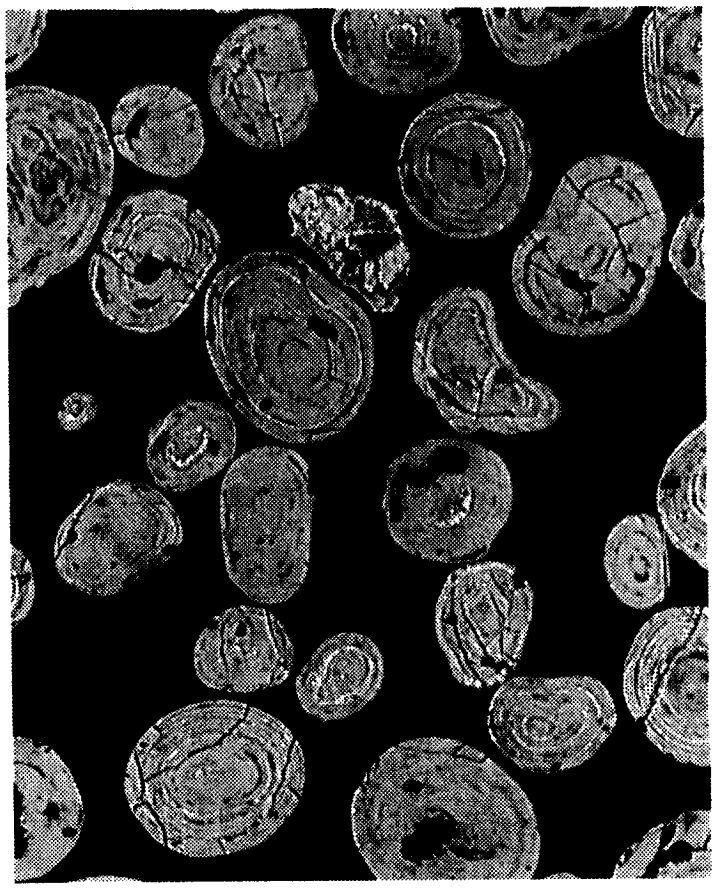

Figure 12: Cross-sectional view of the oxides produced in a fluid bed reactor that illustrates the onion-skin structure (low magnification).[1]

The resulting multi-layered calcine particle morphology is typically referred to as an onion-like structure. Common sense suggests that the onion-like configuration is the result of the following series of events.

- At the start of the oxide growth cycle, given that the original nucleus is presumably a very small particle, it will undoubtedly be entrained by the fluidizing/pyrohydrolysis gases, and ultimately captured by the cyclone.

Nuclei particles are most likely the result of liquor droplet pyrohydrolysis in free space or bed particle fragmentation.

- Upon returning to the bed via the cyclone underflow, the fine particle will very likely be coated with incoming liquor that subsequently pyrohydrolyzes and transforms into an oxide layer.

- In light of the fact that layers are quite thin and numerous, it is reasonable to assume that the said particle circulates between the fluidized bed and the cyclone a number of times, before it is finally large enough to remain in the bed and eventually exit the reactor. The particle must therefore be coated with a metal chloride layer (which ultimately converts into oxide) during several of these cycles and therefore explains the rather long calcine residence times mentioned in Section 2.3.1.

While the suggested onion-skin formation phenomenon is conceivable, it does not appear to have been confirmed by fundamental studies or experimental work. It is, for example, quite possible that the multiple oxide layers are simply the result of periodic contact between the seed particles and the pre-concentrated acid feed, as the gradually growing calcine moves around in the bed.

Given that a fluidized bed is made up of a number of oxide granules, particle size distribution plays an important role in governing whether pyrohydrolysis occurs on existing calcine surface or in the free space between the solids. This results from the fact that for a relatively constant bed mass, the total surface available for the reaction is actually dictated by the size of the particles within the bed. Obviously, since finer particles have a higher surface area to volume ratio than larger granules, a finer bed dp_{50} will naturally result in more favourable conditions for heterogeneous pyrohydrolysis (i.e. chloride conversion on the surface of calcine in the bed).

The importance of the relation between particle size and pyrohydrolysis efficiency within fluidized beds appears to be well understood by the industry as it has been addressed by several of the references.[1,10,11,22,49,50,53] In addition to surface area considerations, uniform metal chloride distribution throughout the bed is also an essential requirement for heterogeneous hydrolysis. Assuming that adequate surface area is available for the reaction, the solution must coat nearly ***ALL*** of the solid particles within the bed to ensure that the majority of the metal chloride pyrohydrolyzes on existing calcine in the reactor.

For the sake of completeness, it is worth mentioning that while a narrow particle size distribution is not necessarily required for heterogeneous pyrohydrolysis, the literature suggests that with relatively heavy oxides (i.e. hematite; s.g. = 5.7g/cm^3) a wide distribution is undesired as it is likely to result in slugging behaviour in the bed. In fact, the literature review has revealed that a narrow particle size distribution of relatively fine calcine (typically 0.2-0.4 mm) is more favourable when dealing with iron oxide systems.

2.5 Aqueous Metal Chloride Transformation – State of Current Knowledge:

The majority of the spent hydrochloric acid regeneration related technical publications that were reviewed during an initial benchmarking exercise dealt with overall process and/or specific equipment descriptions.[1,3,4,7,8-12,15-18,20,22-26,49,50] The results of general plant scale testwork performed to demonstrate the importance of bed particle size and the need for adequate surface area for *"heterogeneous"* pyrohydrolysis were also provided.[1,10,11,22,49,50,53]

Most of the available metal chloride pyrohydrolysis literature has been geared toward the thermal decomposition of iron (primarily ferrous) chloride solutions. Despite the number of studies undertaken in this area, there still appears to be some confusion as to the actual mechanisms behind the conversion of this relatively simple system (see equations 10 through 13). While thermodynamics suggest

otherwise, ferric chloride (which is also present in waste pickle liquors) is believed to decompose in the gaseous state and lead to the production of very fine hematite that results in plant operating difficulties.

The fact that very general chemical reactions (see equations 1 through 9) are typically used to describe aqueous metal chloride pyrohydrolysis, further suggests that the conversion mechanisms are still not very well understood. The literature search has also revealed that the thermal decomposition of multi-component metal chloride solutions does not appear to have been studied very much either.

Moreover, a few references[1,15,22,53] have claimed that aqueous metal chloride pyrohydrolysis in fluidzed bed reactors is generally presumed to be a ***vapour deposition process***. Fundamentals, on the other hand, would suggest that once injected into the reactor, the nearly saturated metal chloride solution at T~ 105°C would begin by boiling vigorously, followed by the precipitation of the metal salts contained within, dehydration, and eventually hydrolysis.

In light of all this, as well as the fact that acid regeneration plant performance is highly dependant on the spent liquor pyrohydrolysis step, it was decided that a better overall understanding of the manner in which a metal chloride solution transforms is certainly in order. Based on recent industrial experience[13-14], this is particularly true for multi-component waste liquors. Therefore, a secondary literature review was performed to benchmark any studies that may support the proposed transformation process or provide a more undisputable description of the mechanisms behind fluidized bed pyrohydrolysis, especially for multi-component systems. More specifically, the author has elected to focus on the transformation of an Al-Fe-Mg-Cl solution.

Given that thermodynamic modelling, using the FactSage System[1] and data generated by the FACT Consortium, was also considered as a means to defining the aqueous Al-Fe-Mg-Cl transformation process, efforts were also geared toward gathering as much solubility and thermodynamic data as is currently available for the system at hand. The most relevant findings are summarized in the following.

2.5.1 Chemical & Kinetic Considerations:

Gardner and Messing[56] studied the evaporative decomposition of various magnesium solutions, including $MgCl_2$, into MgO. The characteristics of the salts were determined using differential thermal analysis and thermogravimetric analysis. Tests were performed at heating rates of 10 and 100°C/min, and used either N_2 or air as a purging gas at a flow rate of 250 ml/min. The samples used were in the order of 32.5 mg, and a temperature correction was applied to determine the sample weight to initial salt weight ratio. Solutions of 1 M were prepared and atomized in the EDS (evaporation decomposition of solutions) furnace (Figure 13).

For all experiments, a solution flow rate of 4 ml/min and an atomizer gas pressure of 0.13 MPa were targeted. The set-up yielded a median droplet size of 10 μm in diameter. The nominal EDS furnace temperature ranged between 500 and 1000 °C, and the furnace atmosphere was maintained by the atomizing gas.

Upon heating $MgCl_2 \cdot 6H_2O$ at 10°C/min, three distinct phases were observed. At temperatures less than 300°C, the sample underwent dehydration. In the range of 400 to 800°C, the sample decomposed to MgO. In the early stages of hydrolysis (~450 °C), Mg(OH)Cl was also identified in the sample. The corresponding reaction equations are:

[1] Thermochemical Software and Databases. Registered Trademark of Thermfasct Ltd. (except for ChemSage).

$$MgCl_2 \cdot H_2O \rightarrow Mg(OH)Cl + HCl \quad (19)$$

$$MgCl_2 \cdot H_2O \rightarrow MgO + 2HCl \quad (20)$$

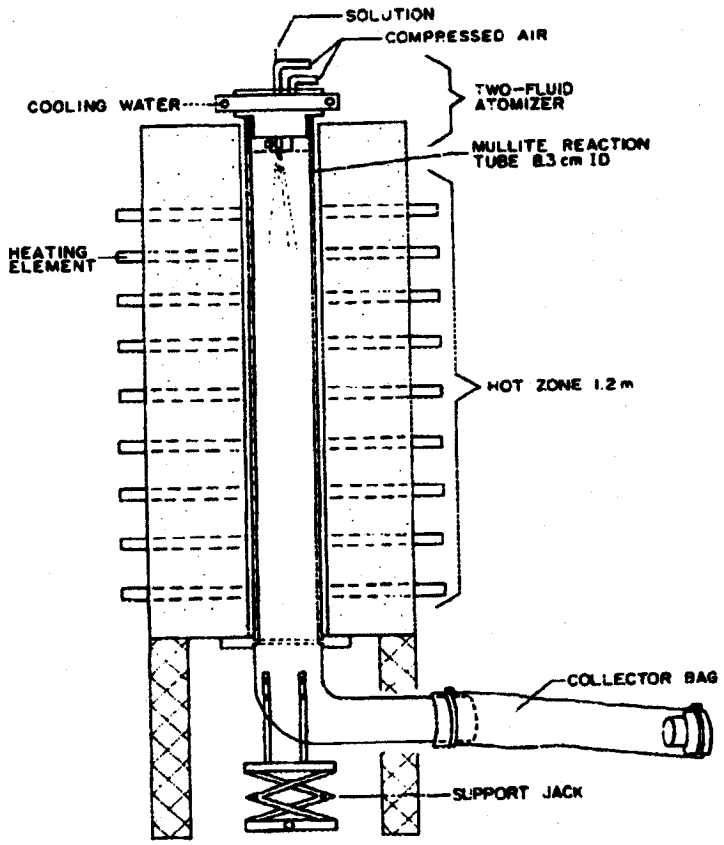

Figure 13: Schematic of the EDS furnace.[56]

The third phase involves the melting of anhydrous $MgCl_2$. At the melting point of 714°C, any anhydrous salt still present in the sample transforms to liquid. The liquid $MgCl_2$ preferentially decomposes to MgO, therefore the formation of Mg(OH)Cl stops at this point. It is the authors' opinion that the general reaction of the EDS furnace is a combination of the two mechanisms. This is supported by their identification of both species in the samples at various stages of decomposition. The decomposition of $MgCl_2$ is highly dependent on the partial pressure of water vapour during transformation. Peak temperature of decomposition was found to be 425 or 460°C, depending on the instrument, the peak temperature of the final stage of decomposition was 805°C, and the

temperature of full decomposition 830°C. When the heating rate was increased to 100°C/min, the peak temperature of decomposition shifted to 530 °C, the peak temperature associated with the final stage of decomposition was 1117°C and the full decomposition temperature increased to 1080°C. Droplets sprayed in the EDS furnace at 1000°C produced particles of a fractured hollow sphere morphology. Crystal fur was observed where the still liquid interior of the droplet spilled when the hollow sphere fractured. The smooth surface of the particle suggests that the $MgCl_2$ crust melted before hydrolyzing. Only partial decomposition of the chloride was observed at that temperature.

Dutt et al.[57] have investigated the thermal decomposition of magnesium chloride hexahydrate in a muffle furnace. It was observed that initially, five of the water of hydration molecules evolve. Recalling equations 19 and 20, the resulting $MgCl_2 \cdot H_2O$ undergoes one of the two decomposition reactions.

The first reaction (i.e. equation 19) begins at a temperature of 200°C, but it is extremely slow. This reaction is optimized at temperatures in the range of 450 to 500°C, where it is very rapid and may go to completion in a short period of time. The second reaction (i.e. equation 20) begins at 500°C and is very rapid at temperatures over 650°C. It has been reported that at temperatures above 527°C, MgO is produced rather than Mg(OH)Cl. It has been suggested that the equilibrium HCl pressure reaches 1 atm at 555°C, the temperature above which Mg(OH)Cl is unstable in the presence of HCl at 1 atm. The experiments were carried out in a muffle furnace at temperatures of 250-650°C. Tests in the range of 700 to 1000°C were performed in a kerosine-fired crucible furnace. 20g samples of $MgCl_2 \cdot 6H_2O$ were used, and the samples were removed after a specified residence time, cooled, and weighed. The weight loss was used to estimate the nature of the decomposition products. It was observed that between 350 and 450°C, the only product of decomposition was Mg(OH)Cl, as the weight loss remained constant with time. At temperatures above 650°C, the sample

converted completely to MgO and HCl. Higher temperatures did not have a significant effect on the composition and percent recovery of magnesium, and the optimal temperature range was determined to lie between 700 and 750°C and the optimal decomposition time 90 to 120 minutes.

Vilcu et al.[58] studied the kinetics of anhydrous $FeCl_2$ hydrolysis, in the 580-620°C temperature range. The purpose of this study was to develop a mathematical model of the conversion kinetics of the system. The tests were conducted in a H_2 reducing atmosphere and the reaction observed was:

$$3\ FeCl_{2\ (s)} + 4\ H_2O \leftrightarrow Fe_3O_{4\ (s)} + 6HCl_{\ (g)} + H_{2\ (g)} \quad (21)$$

When the H_2/H_2O flowrate ratio was above 1.1, at T= 823K, the reaction occurred in 2 steps:

$$3\ FeCl_{2\ (s)} + 3\ H_2O \leftrightarrow 3\ FeO_{\ (s)} + 6HCl_{\ (g)} \quad (22)$$

$$3\ FeO_{\ (s)} + 3\ H_2O \leftrightarrow Fe_3O_{4\ (s)} + H_{2\ (g)} \quad (23)$$

The reaction rates were computed as:

$$V_R = C_w^0 \alpha_w / 4\tau m_{FeCl2} \quad (24)$$

Where C_w^0 is the initial water stream concentration, α_w the concentration of water, τ the space time and m_{FeCl2} the non-reacted $FeCl_2$ mass.

Significant amounts of α-Fe_2O_3 was found in the products, which was explained by the following reaction:

$$Fe_3O_{4\ (s)} + 2HCl_{\ (g)} \leftrightarrow FeCl_{2\ (s)} + \chi\text{-}Fe_2O_3 + H_2O_{\ (g)} \quad (25)$$

The kinetics data was analyzed using different models of solid-gas interaction. The control of the reaction rate by the diffusion of gaseous water through an adsorbed layer of gas at the solid particle surface was rejected. The non-reacted

core model was also rejected. Based on the data, the homogeneous model was retained. The homogeneous model, as described by Froment and Bischoff[59], can be applied to very porous material, when the transport through both reacted and non-reacted structures is relatively fast compared to the true reaction rate. Therefore, the kinetics are actually governed by the reaction rate. It is assumed that there are no significant concentration gradients inside the particle. In other words, the particle reacts evenly throughout its whole volume, as opposed to from the outside in.

The kinetic study resulted in the following equation:

$$(C_w^0/m_0)(d\alpha/dt) = 380\exp(-121000/RT)(C_w)^{-3.2} \qquad \alpha<0.8 \qquad (26)$$

where C_w^0 is the initial water stream concentration, m_0 the initial mass of $FeCl_2$, α is the fraction of $FeCl_2$ converted, R the universal ideal gas constant, T temperature, and C_w is the water stream concentration. It should be mentioned that the experiment was conducted away from equilibrium conditions.

Dutrizac and Riveros[60, 61] studied the precipitation of hematite from a ferric chloride solution. Other impurities were also present in the liquor. The two main equations describing the system under investigation were:

$$FeCl_3 + 2H_2O \rightarrow FeO{\cdot}OH \text{ (akaganeite)} + 3HCl \qquad (27)$$

$$2FeCl_3 + 3H_2O \rightarrow Fe_2O_3 \text{ (hematite)} + 6HCl \qquad (28)$$

At temperatures over 150 °C, the rate of hematite production is so fast, that the precipitate is composed uniquely of hematite. At 100 °C, reaction time had a significant effect on the composition of the product. During the first 20 hours of the experiment, the precipitates formed were composed exclusively of akaganeite. The precipitates formed after 96 hours of reaction were composed exclusively of

hematite. The precipitates formed in between those periods were a mixture of the two. The results confirm that akaganeite is metastable relative to hematite, but that the akaganeite to hematite rate of transformation is slow. The authors propose the following mechanism that involves a combination of two pathways. The first involves akaganeite precipitating "fast" and reaching equilibrium with the solution. Once hematite starts precipitating from the ferric chloride solution, the equilibrium is upset, therefore dissolving the akaganeite back into the solution. The newly formed hematite seed promote the direct precipitation of hematite over that of akaganeite. The precipitation of hematite produces a more acidic solution, therefore inhibiting the further precipitation of akaganeite. The second mechanism is the direct transformation of akaganeite to hematite via a dissolution-precipitation mechanism. The net result is the rapid conversion of akaganeite to hematite as well as direct precipitation of hematite from the solution.

Tests were conducted to determine the effect of temperature on hematite precipitation. The range studied was 50 to 170 °C. A constant reaction time of two hours, and five hours were investigated. Results indicated that as temperature is increased, more product precipitates, but as mentioned earlier akaganeite is present at lower temperatures.

The study also demonstrated that the addition of hematite seed promoted the precipitation of hematite at the expense of akaganeite, and increased the rate of hematite precipitation. As expected from the governing equation, a higher initial concentration of $FeCl_3$ led to higher product yield, whereas higher HCl concentration led to decreased yields.

The effect of other species in the starting solution was investigated. It was shown that adding sodium and calcium chloride to the solution decreased the hematite yield, but their presence had no significant effect on the purity of the precipitates.

Zinc chloride, on the other hand, did not modify the amount or the composition of the precipitates produced.

As part of a study performed to define an alternative process for alumina production, Hamer, of Canmet[54] performed a few experiments to study $AlCl_3$ pyrohydrolysis. The proposed process consists of leaching the raw material, followed by a series of crystallization steps aimed at removing the impurities, and finally pyrohydrolyzing (calcining) the crystals to produce alumina. The flowsheet in Figure 14 illustrates the process in more detail.

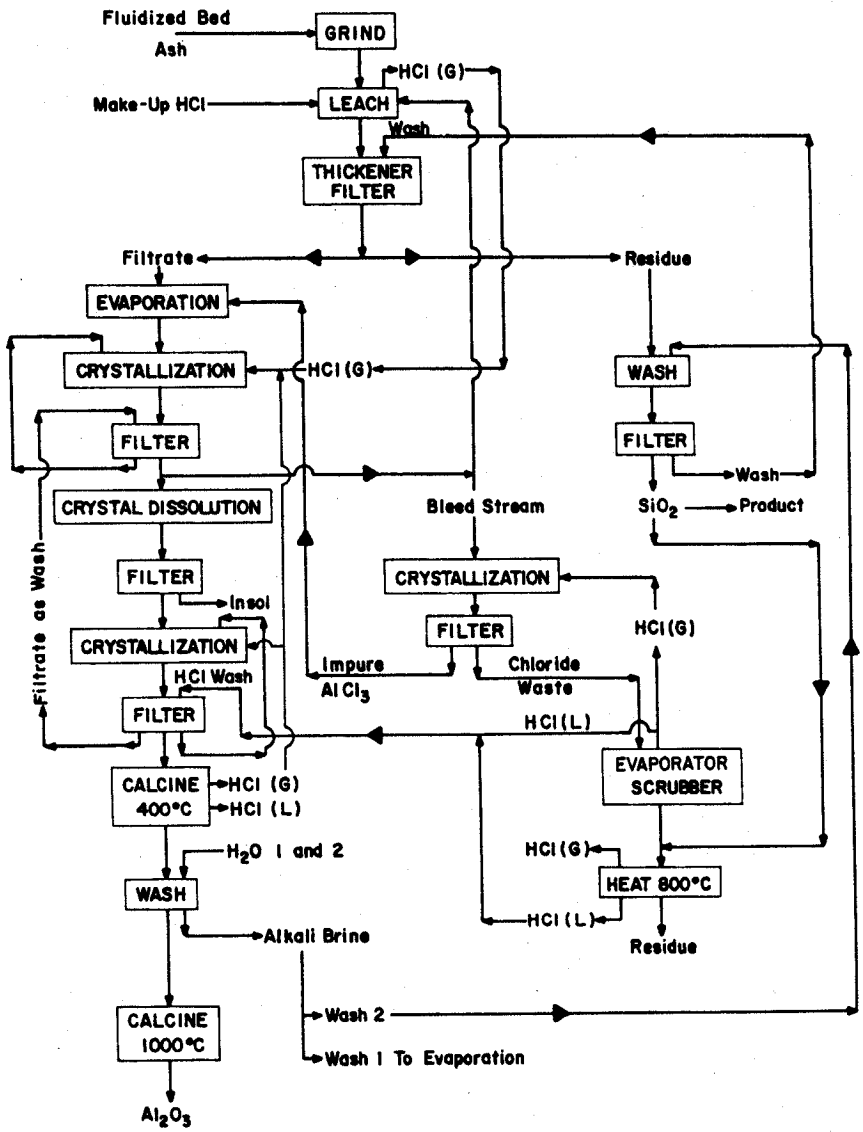

Figure 14: Flowsheet of HCl process for fluidized bed ash.[54]

The main soluble impurities found in the solution were: Fe, Ca, Mg, K, and Na, the minor impurities were: V, Ti, Zn, Ni, P, Cu, etc. Quantities varied from one solution to the next, but all were present to a certain extent.

Crystallization was achieved at low temperature (40-60 °C) by sparging HCl gas in the solution. It was observed that the solubility of $AlCl_3 \cdot 6H_2O$ dropped as HCl concentration of the solution increased, therefore sparging increased the precipitation rate. The crystallization of $AlCl_3 \cdot 6H_2O$ was not found to be too dependent on temperature, but the inclusion of impurities (NaCl, $MgCl_2 \cdot H_2O$, etc...) was.

$AlCl_3 \cdot 6H_2O$ decomposition in a fluidized bed reactor was observed to start at 118°C, but complete conversion required calcining to about 1000°C. The method used in the study to remove the impurities was calcining to 400°C, then water leaching to remove non-reacted Ca, Na, Mg and K chlorides, followed by further calcining to 1100 °C. The composition of the final calcine is shown in Table 1.

Table 1: Alumina by the hydrochloric acid-gas sparge process average of 10 leach cycles, µg/g[54]

Element	Target	1st crystallization	2nd crystallization	Water leached calcine
Fe	200	>1000	42	24
Si	115	84	52	60
Mg	12	>1000	102	14
Ca	600	430	37	Na
Cr	12	121	35	22
V	11	107	6	Na
Na	3000	>1000	>1000	Na
Mn	12	18	>8	Na
Zn	160	27	>25	Na
Ti	30	37	5	Na
P	4	Na	na	35*
K	40	52**	na	>6**

na - Not analyzed
* - average 5 samples
** - one sample

Another experiment was conducted involving an aluminum chloride bearing liquor. The solution was subjected to evaporative crystallization to produce a dry (but not necessarily anhydrous) salt that was subsequently calcined for 3 hours at 350 °C in a fluidized bed to produce a satisfactory calcine. A calcine of a tan brown colour, indicating conversion of ferric chloride to oxide, was considered of good quality. Under these conditions, magnesium chloride partially decomposed to oxides and oxychloride. Calcium, sodium, and potassium were not significantly decomposed. To purify the product, a water leach was performed. The final compositions are shown in Table 2.

Table 2: Analyses of calcine product.[54]

	Calcine 3 ½ h 400 °C m %	**Washed Calcine dried 105 °C m %**
Al_2O_3	83.6	70.2
Fe_2O_3	14.1	11.9
CaO	2.67	0.05
MgO	1.43	1.16
P_2O_5	na	0.184
Na_2O	na	<0.01
K_2O	na	<0.01
Cl	7.55	0.14
LOI	na	20.26

High temperature (i.e. 150-700°C) hydrolysis kinetics of various single component metal chlorides (i.e. Fe, Ni, Mg, Cu, Zn, Mn, and Cd) were investigated by Chunpeng et al.[62] According to the experiments, the rate constants of hydrolysis follows this order:

$$k_{FeCl2} >> k_{MgCl2} > k_{CoCl2} > k_{NiCl2} > k_{MnCl2} > k_{ZnCl2} > k_{CuCl2} > k_{CdCl2}$$

Given that the rate constant for $FeCl_2$ hydrolysis is significantly greater than the others, the authors claim that it is possible to selectively pyrohydrolyze this salt, in

the presence of air at 350°C, from a solution containing Fe, Ni, Mg, Co, Cu, Zn and Cd chlorides. It appears as though the non-ferrous impurities in the calcine were primarily in chloride form and were easily removed via a hot water leach.

The kinetics of hydrolysis for $FeCl_2$ and $MgCl_2$ at a temperature of 400°C can be described as a chemically controlled process, which changes to a phase boundary process, whose rate is controlled by diffusion. In the initial period, the kinetics are first order, and may be represented by the following equation:

$$\log\left(\frac{100}{100-x\%}\right) = K_s \cdot t + B \qquad (29)$$

Subsequently, the thermal decomposition of these salts is governed by a second order relationship:

$$\frac{dx}{dt} = k_m(1-\delta)^2 + const. \qquad (30)$$

where $x\%$ is the extent of reaction and δ is the rate equation.

2.5.2 Physical Mechanisms:

The mechanisms behind the evaporative crystallization of a salt from a liquor droplet exposed to a hot gas stream were studied by Charlesworth and Marshall[63] in the 1960's. A 275 μm droplet was suspended on a filament and an air stream was blown directly underneath the droplet at different flow rates to control the rate of evaporation. Visual observations were made and the weight of the droplet was monitored. In all cases, a reduction in droplet size was initially observed with no signs of any solid phase. Solid precipitation first appeared at the base of the droplet, and the crust grew symmetrically from the bottom up until the whole droplet was encased inside the crust. From then on, further drying depended on the physical properties of the precipitated salt. A summary of all the observations

made is provided in Figure 15. The chlorides tested were found to follow path II. Drying rates for a droplet without crust formation were similar to a pure water droplet.

Once the crust completely covers the droplet, the drying rate always decreases, but to a different extent depending on the behaviour of the crust structure. According to Charlesworth and Marshall, the water mass transfer mechanism trough a porous crust is by capillary force.

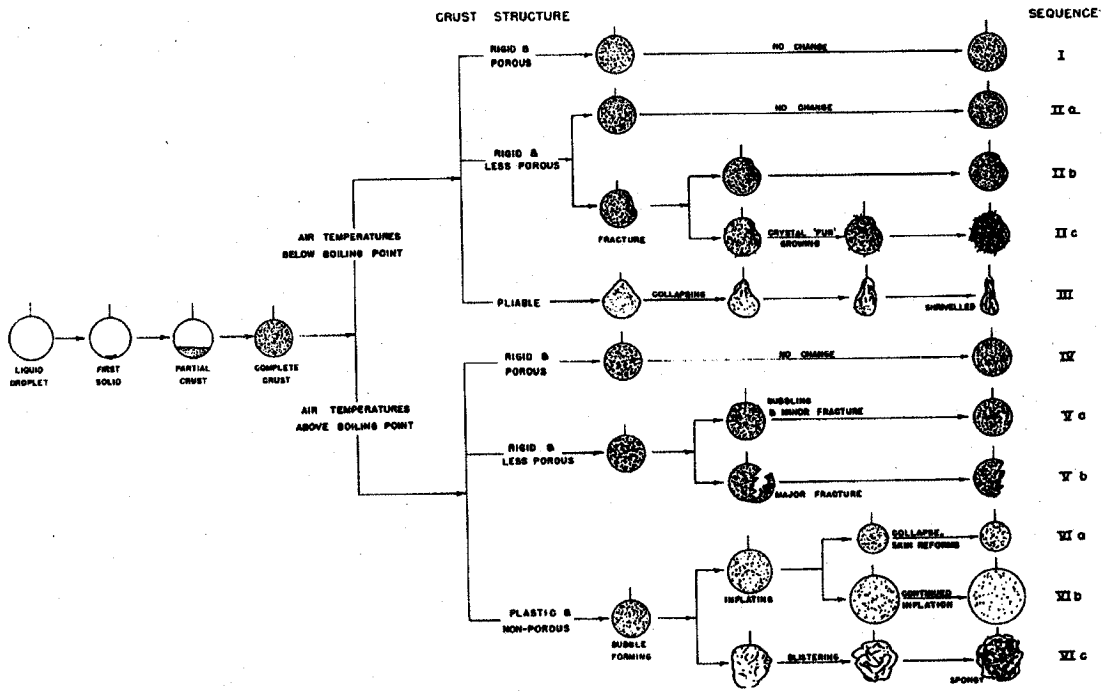

Figure 15: Appearance changes in drying droplets.[63]

Taniguchi et al.[64] devised an experimental procedure that allows for the measurement of both droplet weight and temperature versus time as an aqueous sodium chloride solution droplet evaporates. When the droplet first started evaporating, a reduction in its size was observed with no appearance of crystals. The presence of crystals was first observed at the front stagnation point of the droplet. Crystallization occurred before the average concentration inside the

droplet reached its saturation point. The crystal then proceeded to grow in the form of a shell around the droplet. A local Sherwood number analysis reveals that it reaches a maximum at the front stagnation point. This may indicate that salt concentrations inside the droplet reach a maximum at the stagnation point, which would explain the location of the initial crystallization. The time of crystal appearance was found to be related to the free-stream velocities. A model was developed to describe the system. The system is illustrated in Figure 16, and the governing model equations are presented in Table 3 and Figure 17.

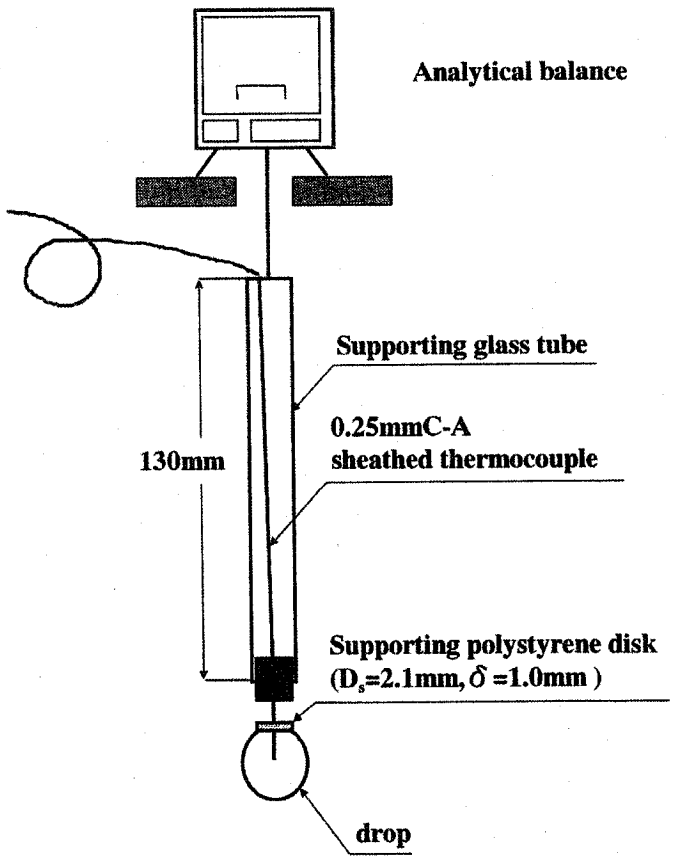

Figure 16: Detail of supporting tube.[64]

Table 3: Basic equations for simulation. [64]

Mass balance	$-\frac{dW}{dt} = N_A \cdot A_e$
Heat balance	$\frac{dT_P}{dt} = \frac{q_G \cdot A - \lambda \cdot N_A \cdot A_e + Q_c}{c_L \cdot W}$ $Q_C = \frac{A_t \cdot \kappa_t (T_\infty - T_P)}{l_t}$
Mass flux	$Sh(1-\omega_s) = 2 + 0.6 \cdot \mathrm{Re}_\rho^{1/2} \cdot Sc^{1/3}$
Heat flux	$Nu = 2 + 0.6 \cdot \mathrm{Re}_\rho^{1/2} \cdot \mathrm{Pr}^{1/3}$
Effective surface area	$A_e = \frac{\pi D_A}{2}(\sqrt{D_A^2 - D_S^2} + h)$ $\frac{\pi}{12}(4h^3 - 3D_A^2 h + D_A^3) = \frac{(\overline{C} - C^*) \cdot W}{100\,\rho_{sc}}$

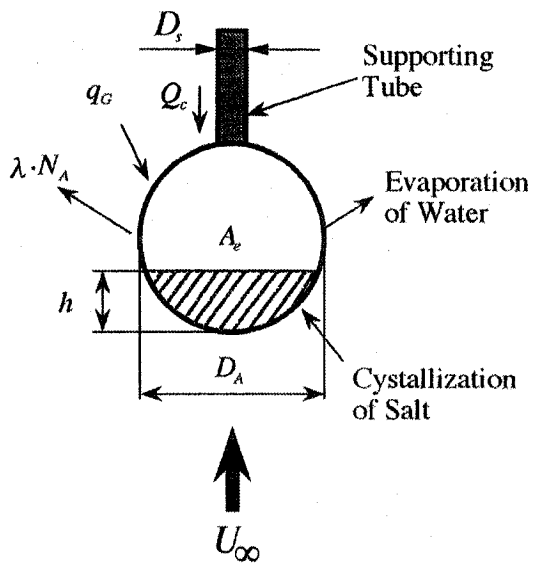

Figure 17: Schematic diagram of proposed model.[64]

Link and Schlünder[65] have investigated the coating process of fluidized bed spray granulation by performing experiments on a single particle. The authors claim that the particles can grow in one of two ways: agglomeration and layering as shown in Figure 18.

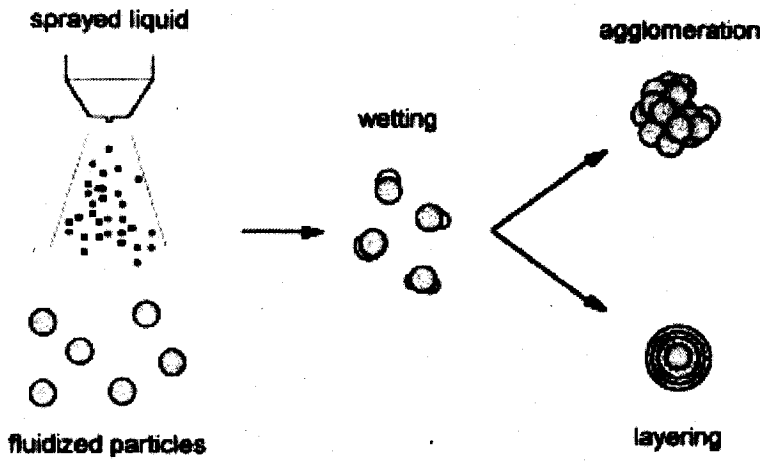

Figure 18: Agglomeration and surface layering during fluidized bed spray granulation.[65]

Depending on the operating parameters, one of the mechanisms will dominate. The main parameters affecting growth of a particle are liquid feed concentration, viscosity, and surface tension. Agglomeration occurs when liquid is present in between particles. The fast drying of the solvent leaves a solid bridge binding particles together. Although agglomeration mechanisms favour an increase in the growth rate of particles, the resulting product in not mechanically "strong" and is likely to break apart. Figure 19 illustrates six different interactions between droplet and particle, the frequency of which determines particle growth rate and size distribution. In the experiment, a single particle of aluminum (inert to the coating solids) was sprayed intermittently to simulate the movement between wet and dry zones in the fluid bed reactor.

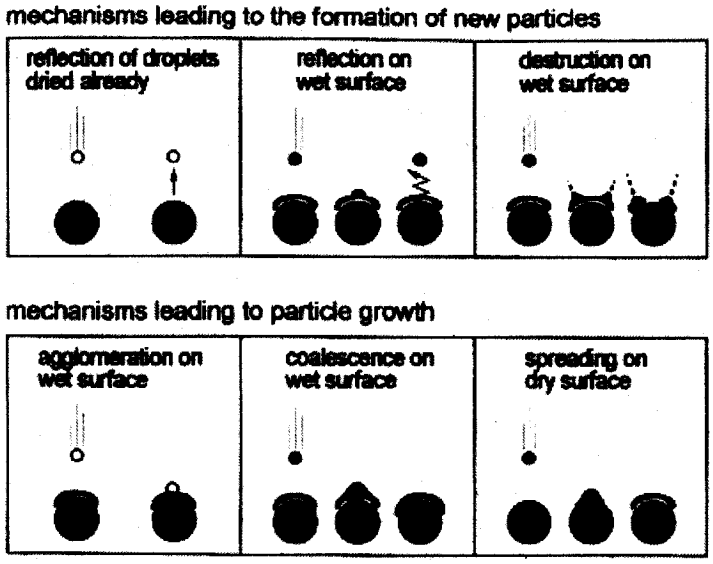

Figure 19: Mechanisms determining the adhesion-probability and therefore the particle growth rate.[65]

J. G. M. deLau[66] was concerned with densities of oxides produced by the spray drying and roasting of sulfate solutions. Although most tests performed focused on the final densities of the resulting oxides, some observations are worthy of mention. At temperatures between 800 and 1000°C, only the metallic species found in dissolved form in the feed liquor were present in the final oxide particle. It was also found that the rapid evaporation of the solvent reduces the likelihood of segregation in the final product. When the solvent evolves very quickly, ions do not have the time to diffuse and therefore stay where they are. The end result is that the final product is very homogeneous in composition. This was the case in this system due to the high temperatures and the fine droplet size (high surface area for evaporation) in the range of 10 to 20 μm. The resulting morphology of the particles was that of agglomerated, sintered, thin-walled hollow spheres.

The high-temperature solid-state reaction of a mixture of oxides to form a multi-component calcine was also discussed. The mechanism involves the mutual diffusion of cations through the oxygen lattices by way of the contact areas

between the particles of the different oxides. Oxygen diffusion is not necessary. At those high temperatures, sintering also occurs, in which both cations and oxygen ions diffuse therefore reducing the active surface of the particle. Reaction temperature and residence time must be carefully chosen to obtain a good compromise between homogeneity and sintering activity.

Chess et al.[67] are in agreement with deLau on the claim that rapid evaporation decreases segregation and produces a homogeneous product. Their work consisted of studying the production of sulfide ceramics from nitrates by atomizing aqueous solution in a 500 to 550°C oxidizing atmosphere and subsequent exposure to H_2S at 1000 °C

Panda et al.[68] have undertaken a study on spray granulation in a fluidized bed reactor. The paper mentions that the particles move randomly between humidifying and drying zones of the bed. This effect, combined with fines recycling via a cyclone gives rise to the layered, onion-skin morphology of the final product. Experiments were conducted on a single aluminum particle. The experimental set-up, as shown in Figure 20 consisted of a glass cylinder 150mm in diameter. A nozzle carries the drying air from the bottom with a velocity, *V*, towards the top. The fluidizing air temperature was regulated with the use of a heating element with a heat load, *H*. A thermo element (carrying the inlet air) was installed to touch the nozzle and was protected from liquid droplets by Teflon tape. The sample nucleus, made of aluminum of about 1.3mm in diameter, was suspended in the fluidizing air stream coming out of the nozzle (D). The solution is transported from a storage tank (cell) through a micro-dosing pump (P) to an ultrasonic atomizer (Z) suspended from the top of the granulation chamber and was atomized. A carrier air stream was used to accelerate the coagulated/agglomerated droplets (of about 40 μm). The droplets, which did not collide with the nucleus, were removed and carried away by a hot stream of air

coming out at a velocity, $V_{\text{carrier air}}$. The temperatures of all inlet and exit air streams were measured and the signals were monitored with a data logger.

The solutions that coated the particle consisted of aqueous sodium chloride (20%), calcium chloride (20%), lactose (16%), and maltodextrin (20%). Small amounts of polymer (PVP, CMC) were mixed with the lactose solution to modify its viscosity. Tests were conducted with various solution compositions, different droplet velocities, and a range of fluidizing air temperatures to determine growth kinetics. A summary of the experimental conditions employed is provided in Table 4. The morphology of the surface was examined, and densities and viscosities were measured.

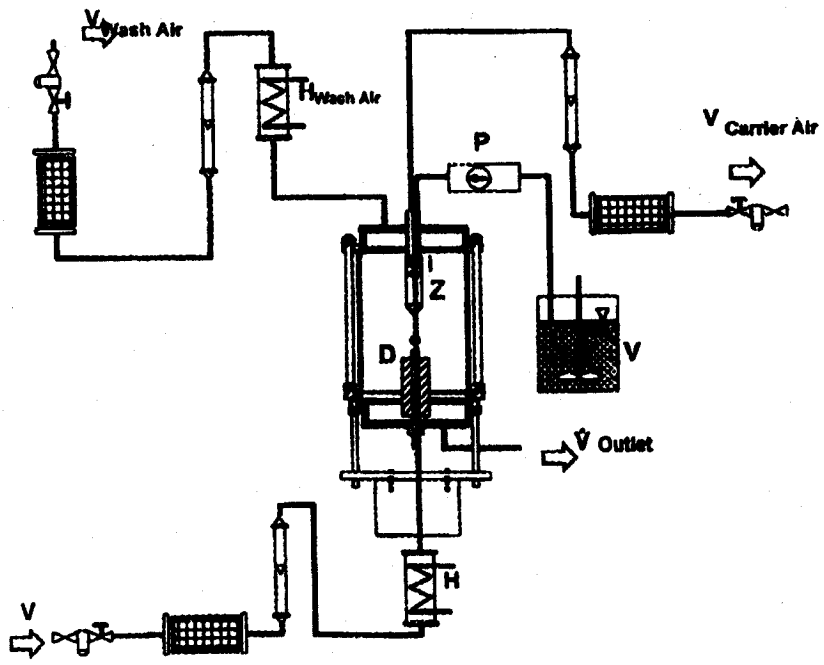

Figure 20: Experimental set-up to study spray granulation process.[68]

Table 4: Experimental Conditions[68]

$V_{wash\ air}$	200 l/hr
Distance between particle & nozzle	5 mm
Time between consecutive strokes	5 seconds
Volume of liquid sprayed per stroke	4 μL
Number of strokes	600
Duration of pause per 200 strokes for sample drying	3-5 min.

It was discovered that the growth rate was dependent on fluidizing temperature. The range of temperatures investigated lies between 30 and 100°C and tests were conducted using droplet velocities of 31, 47, 74, and 93 cm/s. For the fluids tested, some maxima and minima were observed in the particle growth rate. These seemed to correspond to changes in physical characteristics such as optimal surface tension, temperatures, changes in wettability, and the formation of an amorphous phase. It was also observed that as the fluidization temperature increases, the dust production due to overspray also increases.

It was concluded from the test with binder addition, designed to modify viscosity, that the growth rate increases with viscosity. This effect was predicted by Link[66], based on an energy balance.

The morphology of the final particle was dependent on the coating used. Lactose displayed a crystalline phase at lower temperature, but revealed an amorphous coating at higher temperatures. In the case of sodium chloride, porosity increased as fluidizing temperature increased.

To summarize, particle growth rate reaches an optimal point as drying temperature is varied. Furthermore, the growth rate decreases with increasing droplet velocity, and the physical properties (such as surface tension and viscosity) were found to have a significant effect on particle growth rate.

Kleinbach and Riede[69] have studied the coating of solids on an inert fluidized particle bed. The coating material was composed of solids in a water-based slurry. It was found that the more dilute the slurry is, the more even the coating will be. On the other hand, it was reported that slurry dilution can lead to the partial dissolution of the solid to be coated which may be undesirable. If moisture enters underneath the coating, it may lead to cracking during subsequent drying steps. Spreading the slurry in small droplets leads to a good distribution but may also foster premature drying, causing fines and deteriorating coating quality. Bed temperature has a significant effect on drying rates, and may cause particles to stick together.

2.5.3 Existing Al-Fe-Mg-Cl-H_2O Thermochemical Data:

2.5.3.1 Solid Hydrates:

H_2O-$AlCl_3$

Aluminium chloride apparently forms only one hydrate, the hexahydrate $AlCl_3.6H_2O$, according to the aqueous phase diagram at atmospheric pressure.[70] The hexahydrate is the only aluminium-containing solid phase observed in the $AlCl_3$ - H_2O, $AlCl_3$ – HCl - H_2O and $AlCl_3$ – $FeCl_3$ - H_2O systems.[70] Thermodynamic data are available for anhydrous aluminium chloride and for the aluminium chloride hexahydrate in the FACT System.

H_2O-$MgCl_2$

Six hydrates containing 12, 8, 6, 4, 2 and 1 molecules of water per molecule of magnesium chloride have been identified and their phase equilibria with aqueous solutions has been reported.[71,72] When in contact with a liquid solution under pressures greater that atmospheric, the tetrahydrate persists to a temperature of 117°C and the dihydrate persists to 184°C. Magnesium also forms a solid hydroxy-chloride, or basic chloride, MgClOH. The relative stability of the various

magnesium chloride hydrates and hydroxy-chloride solids at temperatures above the aqueous solution normal boiling point at atmospheric pressure will depend on the concentration of water and of hydrogen chloride in the gas phase.[73]

Thermodynamic data are available for the 1, 2, 4 and 6 hydrates at low temperature and ambient conditions (25°C, 1 atm).[73,74] Thermodynamic data to higher temperatures are available only for the magnesium chloride 0, 1 and 2 hydrates and for the basic chloride in the FACT System.

Vapour pressure and other data, but not solubility data, for magnesium chloride aqueous solutions are summarised by Wang and Pitzer.[75] They indicate that the available thermodynamic data for the solid hydrates and the anhydrous phases is not of sufficient quality for accurate, aqueous solubility calculations. That is, the solids and aqueous solution thermodynamic data, cannot be used to accurately reproduce published solubility data, such as that of Linke.[70] While it would have been possible to refine or optimize the thermodynamic data to accurately reproduce aqueous solubility measurements, it was decided not to for the reasons provided in Section 3.1.3. On the other hand, the available thermodynamic data are considered to be of sufficient accuracy to reasonably predict solid – gas phase equilibria.

$\underline{H_2O\text{-}FeCl_2}$

The 6, 4 and 2 hydrates of ferrous chloride have been identified in the aqueous phase diagram.[70,72] When in contact with its aqueous solution, the dihydrate persists to temperatures higher than 120°C at pressures greater than atmospheric. No low or high temperature heat capacity or heat content data have apparently been measured for any of the iron II chloride hydrates. Only enthalpy of formation data at 25°C is available for the di- and tetra-hydrates. Detailed phase equilibrium modelling of the aqueous liquid - solid system would be required to accurately estimate the missing data.

H_2O-$FeCl_3$

The 10, 6, 3.5, 2.5 and 2 hydrates of ferric chloride have been identified in the aqueous phase diagram.[70,72] When in contact with its aqueous solution, the dihydrate persists over the temperature range 50 to 73.5°C, with only the anhydrous salt being in equilibrium with the solution at higher temperatures.

2.5.3.2 Multicomponent Systems with Water

H_2O-$MgCl_2$-$FeCl_2$

Afonichkin and Gaidukova[76] investigated solubilities in this system at temperatures of 0, 15 and 25°C. They found substitution between magnesium and iron II in the hexahydrate and in the tetrahydrate. Similar substitution is found in the anhydrous salts $(Mg,Fe)Cl_2$ where a continuous series of solid solutions has been reported in the binary system.[77] Substitution of iron II for magnesium II has been found to be very common in the solid oxide systems studied by the FACT Group.[78] This is because magnesium II and iron II have a similar ionic size. Consequently, some substitution of magnesium by iron II in the magnesium dihydrate, the monohydrate and hydroxy-chloride there would be expected to occur. Unfortunately, no experimental information is available on these latter systems; therefore, pure magnesium chloride salts (in either hydrated and hydroxy-chloride form) would have to be used for any thermodynamic modelling exercise.

H_2O-$AlCl_3$-$FeCl_3$

An extensive series of solid solutions has been reported in the anhydrous binary system[79] but neither of the concerned compounds are expected to form at the conditions maintained in typical $MeCl_x$ pyrohydrolyzers. No evidence of atomic substitution has been reported in the solid hydrates.[70] This is probably because of the strong tendency of aluminium atoms in salts to direct bonding with water,

thus producing the hexahydrate grouping in the solid. Iron III does not have the same inclination in the salt; therefore, anhydrous ferric chloride can exist in equilibrium with its aqueous solution. Also, there is sufficient difference in the ionic size of aluminium III and iron III to give only limited substitution and wide miscibility gaps in the aluminium – iron III oxide systems studied by the FACT Group.[78]

2.5.3.3. Chloride Formation Reactions of Me_xO_y with $HCl_{(g)}$:

The chloride formation reactions of metal oxides with HCl gas and the reverse reactions were studied by Kasaoka et al.[80] to obtain basic information about the corrosion of materials, recovery of waste catalysts, minerals with volatilization of chlorides, and the catalytic mechanism of the Deacon reaction or oxychlorination. The experiments were carried out by using a thermobalance, X-ray diffraction, and gas analysis under atmospheric pressure and at temperatures in the range 25-500°C. Inlet gases were composed of 0-1.5% HCl, 0-21% O_2, 0 or 4% H_2O, N_2, etc., and the total gas flow rate was 500cm^3/min for 80mg of metal oxides. The metal oxides were mainly prepared by the precipitation reaction of metal salts with NaOH at 70 or 100°C. The following results were obtained.

(1) The chloride-formation reactions are brought about by

$$MO + 2\,HCl = MCl_2 + H_2O$$

for MO (MgO, CaO, NiO, CuO, ZnO, PbO, HgO, etc.) and by

$$M_xO_y + 2y\,HCl = x\,MCl_2 + y\,H_2O + (y\text{-}x)\,Cl_2 \qquad (31)$$

for M_xO_y (V_2O_5, Mn_2O_3, Mn_3O_4, Co_3O_4, Pb_3O_4, PbO_2, etc.).

Also, for CuO above approximately 300°C the reaction of

$$CuO + 2HCl = CuCl + H_2O + (1/2)Cl_2 \text{ occurs.} \qquad (32)$$

Al_2O_3, SiO_2, Cr_2O_3, Fe_2O_3, Fe_3O_4, ZrO_2, CeO_2, WO_3, etc. do not react under the present conditions.

(2) The chloride-formation reactions (Eq. 31) are the combination of

$$M_xO_y + 2x\ HCl = x\ MCl_2 + x\ H_2O + [y\text{-}x)/2]\ O_2, \text{ and}$$
$$MCl_2 + (y/2x)\ O_2 = (1/x)\ M_xO_y + Cl_2 \qquad (33)$$

which is the decomposition-oxidation reaction of metal chloride (MCl_2) with oxygen (O_2).

(3) The decomposition-oxidation reactions of chlorides in water vapour are given by

$$MCl_2 + (y/x)\ H_2O = (1/x)\ M_xO_y + 2HCl + [(y/x) - 1]\ H_2 \qquad (34)$$

at lower temperatures, and by

$$MCl_2 + H_2O = MO + 2\ HCl \qquad (35)$$

at higher temperatures. Also, in the mixtures of oxygen (O_2) and water vapour (H_2O), it is shown by

$$MCl_2 + [(y\text{-}x)/2x]\ O_2 + H_2O = (1/x)\ M_xO_y + 2\ HCl. \qquad (36)$$

(4) The catalytic mechanism of the Deacon reaction

$$4\ HCl + O_2 = 2\ Cl_2 + 2\ H_2O \qquad (37)$$

was elucidated in terms of the combination of Eqs. 31 and 33.

2.6 Summary of Findings:

The aforementioned studies can be used to help explain the mechanisms behind high temperature metal chloride hydrolysis. However, neither is specific enough to provide an accurate or undisputed account of the reactions that take place as a nearly saturated aqueous solution is introduced into a typical fluidized bed reactor. Furthermore, other than the studies performed by Dutrizac et al.[60,61], Hamer[54], and Chunpeng et al.[62], most of the aforementioned research was performed with single component systems.

Given that nearly saturated solutions at ~105°C are typically injected into fluidized bed pyrohydrolyzers, $MeCl_x$ precipitation will no doubt occur, but will the crystals be hydrated or anhydrous? If anhydrous, will the salt melt prior to hydrolysis? Will complexation, which often takes place in concentrated chloride solutions, lead to the formation of multi-component crystals (i.e. $FeMgCl_2$)? How will these salts subsequently hydrolyse? The ability to optimize multi-component chloride pyrohydrolyzer performance lies (at least partially) in the answers to these questions.

Some of the findings that may prove useful in helping to define aqueous Al-Fe-Mg-Cl hydrolysis (i.e. conversions process) are summarized below.

Firstly, Gardner and Messing[56] reported that when heating $MgCl_2 \cdot 6H_2O$ rather slowly at 10°C/min., the salt undergoes dehydration until the temperatures reaches 300°C, followed by partial decomposition to Mg(OH)Cl at ~450°C, and ultimately full hydrolysis. Given that the experiments were performed in the presence of a N_2 or air atmosphere, the presence of molten $MgCl_2$ at higher temperatures (i.e. 714°C) may be explained by the lack of H_2O for hydrolysis. Moreover, it was shown that at heating rate of 10°C/min, the temperature of full decomposition was 805°C. This temperature increased to 1080 °C with a heating rate of 100°C/min.

Based on the information provided by Dutt et al.[57], it is possible to dehydrate $MgCl_2 \cdot 6H_2O$ at temperatures as low as 200°C, and the resulting monohydrate may begin to decompose, albeit very slowly, at that point. Furthermore, the authors claimed that $MgCl_2 \cdot H_2O$ decomposes preferentially to MgO at temperatures in excess of 527°C. While optimum hydrolysis conditions were reported to lie between 700 and 750 °C and a residence time of 90 to 120 minutes, a minumum of 650°C is required for the complete transformation of the salt.

Vilcu et al.[58] developed a mathematical model for the kinetics of anhydrous $FeCl_2$ hydrolysis, in the 580-620°C temperature range and H_2 reducing atmosphere.

When the H_2/H_2O flowrate ratio was above 1.1, at T= 823 K, the reaction occurred in 2 steps:

$$3\ FeCl_{2\ (s)} + 3\ H_2O \leftrightarrow 3\ FeO_{\ (s)} + 6HCl_{\ (g)} \qquad (22)$$

$$3\ FeO_{\ (s)} + 3\ H_2O \leftrightarrow Fe_3O_{4\ (s)} + H_{2\ (g)} \qquad (23)$$

The reaction rates were computed as:

$$V_R = C_w^0 \alpha_w / 4\tau m_{FeCl2} \qquad (24)$$

Where C_w^0 is the initial water stream concentration, α_w the concentration of water, τ the space time, and m_{FeCl2} the non-reacted $FeCl_2$ mass.

Significant amounts of α-Fe_2O_3 was found in the products, which was explained by this reaction:

$$Fe_3O_{4\ (s)} + 2HCl_{\ (g)} \leftrightarrow FeCl_{2\ (s)} + \alpha\text{-}Fe_2O_3 + H_2O_{\ (g)} \qquad (25)$$

Based on the data, Froment and Bischoff's[59] homogeneous model was retained and it was concluded that the kinetics were actually governed by the reaction rate.

The kinetic study resulted in the following equation:

$$(C_w^0/m_0)(d\alpha/dt) = 380\exp(-121000/RT)(C_w)^{-3.2} \qquad \alpha<0.8 \quad (26)$$

where C_w^0 is the initial water stream concentration, m_0 the initial mass $FeCl_2$, α is the fraction of $FeCl_2$ converted, R the universal ideal gas constant, T temperature, C_w water stream concentration. Related experiments were conducted away from equilibrium conditions.

Dutrizac and Riveros[60,61] studied the precipitation of hematite from a ferric chloride solution. Other impurities were also present in the feed liquor. The two main chemical reactions describing the system under investigation were:

$$FeCl_3 + 2H_2O \rightarrow FeO{\cdot}OH \text{ (akaganeite)} + 3HCl \quad (27)$$

$$2FeCl_3 + 3H_2O \rightarrow Fe_2O_3 \text{ (hematite)} + 6HCl \quad (28)$$

At temperatures over 150 °C, the rate of hematite production is so fast, that the precipitate is composed uniquely of Fe_2O_3. At 100°C, reaction time had a significant effect on the composition of the product. The results confirm that akaganeite is metastable relative to hematite, but that the akaganeite to Fe_2O_3 rate of transformation is slow.

The study also demonstrated that the addition of hematite seed promoted the precipitation of Fe_2O_3 at the expense of akaganeite, and increased the rate of hematite precipitation.

Hamer[54] reported that $AlCl_3{\cdot}6H_2O$ decomposition in a fluidized bed reactor was observed to start at 118°C, but complete conversion required calcining to about 1000°C. The aluminum chloride was precipitated from a solution containing Fe,

Ca, Mg, K, and Na. The process actually consisted of calcining to 400°C (to oxidize the Al & Fe), then water leaching to remove unreacted Ca, Na, Mg and K chlorides, followed by further calcining to 1100 °C. The aforementioned solution was also subjected to evaporative crystallization to precipitate a dry (but not necessarily anhydrous) $AlCl_3$ salt that was subsequently calcined for 3 hours at 350 °C in a fluidized bed. A calcine of a tan brown colour, indicating conversion of ferric chloride to oxide, was produced. In this case magnesium chloride partially decomposed to oxides and oxychloride

Based on high temperature (i.e. 150-700°C) hydrolysis kinetic studies performed by Chunpeng et al.[62], the rate constant for $FeCl_2$ hydrolysis is significantly greater than that of $MgCl_2$. As a result, the authors claimed that it is possible to selectively pyrohydrolyze iron chloride, in the presence of air at 350°C, from a solution containing Fe, Ni, Mg, Co, Cu, Zn and Cd chlorides. It appears as though the non-ferrous impurities in the calcine were primarily in chloride form and were easily removed via a hot water leach.

With regards to the physical mechanisms behind aqueous metal chloride conversion, Charlesworth and Marshall[63] as well as Taniguchi et al.[64] claimed that when exposed to "evaporative" conditions, the first appearance of the solid phase was observed at the bottom of a salt bearing liquor droplet. Furthermore both studies revealed that the crust grew symmetrically from the bottom up until the entire droplet was encased within the solid phase. Taniguchi et al. claimed that crystallization occurred before the average concentration inside the droplet reached the saturation point.

Research related to the coating process observed during fluidized bed spray granulation was conducted by Link and Schlünder[65], Panda et al.[68], as well as Kleinbach and Riede[69]. The most noteworthy findings of the given studies may be summarized as follows:

1. bed particles can grow in one of two ways: agglomeration and layering (i.e. onion-skin morphology).
2. the main parameters affecting particle growth are liquid feed concentration, viscosity, and surface tension.
3. while uniform liquor distribution throughout the bed is favourable, liquor droplet size must be controlled to avoid fines formation and deteriorating coating quality.
4. bed temperature has a significant effect on drying rates, and may cause particles to stick together.

As far as the available thermochemical data is concerned, other than the $MgCl_2$-$FeCl_2$-H_2O sub-system, there does not appear to be any evidence that other mixed metal salts (anhydrous or hydrated) form in the combined $AlCl_3$-$FeCl_2$-$FeCl_3$-$MgCl_2$-H_2O system. All available information indicates that in the other cases, the concerned metal salts will precipitate as pure chloride hydrates or anhydrous chloride from the concentrated solution of interest. On the other hand, the solid solubility of iron II in magnesium chloride dihydrate, monohydrate, and hydroxy-chloride has not been measured and would require an experimental investigation. The literature review also revealed the lack of thermochemical data for both the aqueous solution phase, as well as solid compounds likely to be in equilibrium with the chloride solution.

With all of the aforementioned considerations in mind, three phases worth of experimentation was performed to characterize the transformation process that takes place as a saturated Al-Fe-Mg-Cl solution at ~105°C is exposed to typical pyrohydrolyzer operating temperatures (i.e. 850°C). Efforts were geared toward defining the sequence of reactions that take place as the liquor gradually transforms into oxide. The results are expected to help explain the differences in fluidized bed

reactor behaviour, when employed to treat single versus multi-component metal chloride solutions.

3.0 EXPERIMENTAL FACILITIES & METHODOLOGY :

3.1 General Approach & Facilities:

3.1.1 Lab Scale Fluidized Bed Pyrohydrolyzer:

In an effort to define nearly saturated $MeCl_x$ liquor conversion mechanisms, initial plans consisted of building a laboratory scale fluidized bed pyrohydrolyzer, complete with an offgas cyclone and gas scrubbing facilities (see Figure 21). The proposed apparatus would have allowed for a more accurate simulation of the gaseous atmosphere and dynamics within the reactor, as well as thorough mass balance calculations. While this would have been ideal, the author's experience with a similar but much larger pilot acid regeneration facility revealed that the given lab installation would have been virtually impossible to operate reliably.

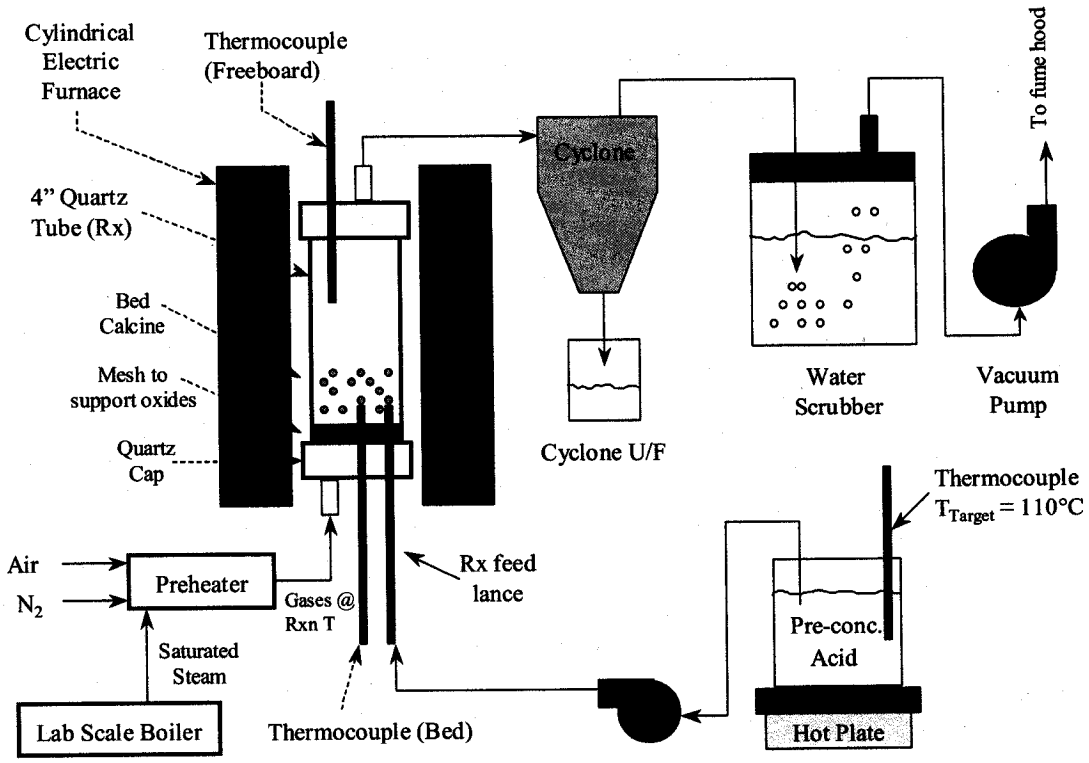

Figure 21: Schematic of proposed lab scale pyrohydrolysis set-up.

Based on personal experience with a similar bench scale set-up for an unrelated project, the ability to pre-heat the incoming gases to the targeted operating temperature would have been extremely difficult and would have required a ridiculously large heat exchanger. Furthermore, experience with a similar pilot facility revealed that it would have been literally impossible to reliably feed the saturated liquor (i.e. pre-concentrated acid) into the reactor due to $MeCl_x$ salt precipitation in the lance and the feed line. Even the use of heat tracing coupled with a very sophisticated control system would have been insufficient to avoid crystallization in the piping to the reactor. Feed line and lance blockage would have been further amplified by the very small diameter needed to maintain typical solution injection velocities.

In addition to the aforementioned considerations, a careful review of the concerned lab scale installation revealed that it was not very likely to shed any more light on the transformation mechanisms than the fully instrumented pilot plant at the author's disposition. As a result, it was decided to proceed with the series of experimental studies (three phases) briefly described in Section 1.3.

3.1.2 FTIR-TGA:

Theoretically, the use of Fourrier Transform Infra-Red spectroscopy (FTIR) combined with ThermoGravimetric Analysis (TGA) would have been preferred to define the sequence of reactions that take place as the saturated $MeCl_x$ liquor transforms into oxide. The two analytical techniques complement one another as the reaction products are identified through spectrographic analysis while the TGA unit (Figure 22) monitors sample mass. Combined the results can be used to define the reaction taking place at a specific temperature. When coupling a TGA unit to a FTIR system, any gas ions that evolve from the feed sample as its temperature increases are directed towards the FTIR device that uses discrepancies in light wavelengths to identify the molecular bonds in a compound. Therefore by combining TGA with FTIR, it is possible to better define the nature of the reaction

that takes place during a specific change in mass, as any gaseous reaction products will have been identified.

Unfortunately, FTIR-TGA could not be used to characterize the transformation process for the system at hand for the following reasons. Firstly, the FTIR is sensitive to corrosive gases and is therefore incapable of accommodating the $HCl_{(g)}$ generated by the pyrohydrolysis reactions. Furthermore, the presence of water vapour (produced during evaporation and purposely injected to simulate typical pyrohydrolyzer atmosphere) hinders FTIR analysis. Given that the starting solution contains several components and that the actual reaction mechanisms are unknown, the interpretation of the thermograms without the FTIR analysis results would have been virtually impossible.

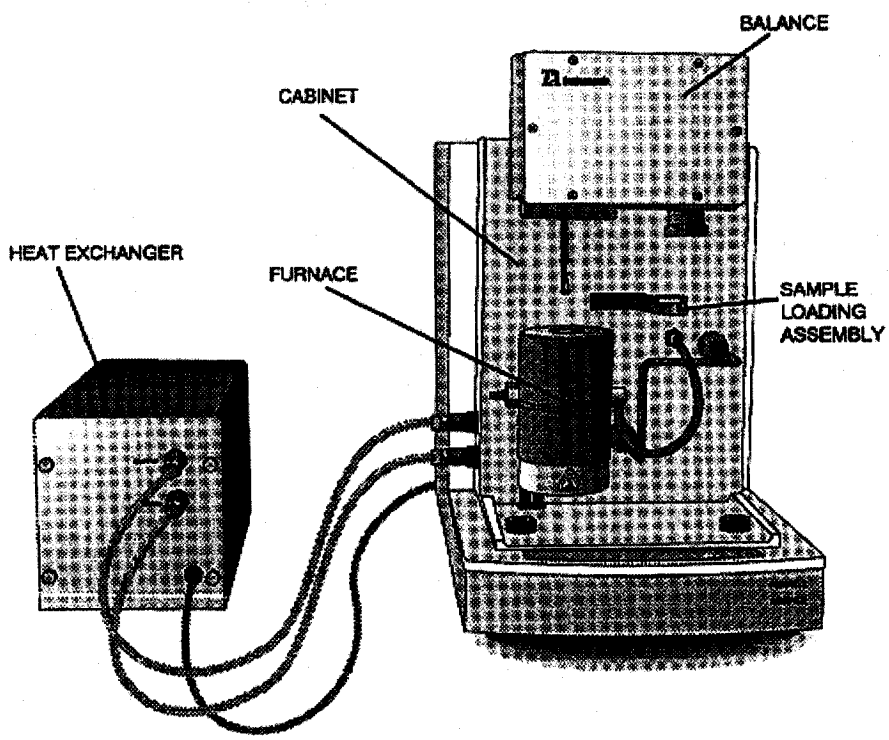

Figure 22: Typical TGA Unit.

3.1.3 Thermochemical Modelling of the Transformation Process:

As mentioned in Section 2.5, the use of the FactSage System and data generated by the FACT Consortium was also considered as a means to defining the aqueous Al-Fe-Mg-Cl conversion process. Unfortunately, the literature review revealed:

- a deficiency in thermochemical data for both the aqueous solution phase, as well as for the solid compounds likely to be in equilibrium with the chloride liquor.

- that the precipitation of simple metal chloride salts, from the starting solution, would have to be assumed due to the lack of any data that would suggest otherwise.

- that the solid solubility of iron II in magnesium chloride dihydrate, monohydrate, and hydroxy-chloride has not been measured and would require an experimental investigation.

Furthermore, fundamental considerations would suggest that heat transfer and kinetics, rather than equilibrium thermochemistry, would play a major role in determining the most likely phase assemblages at lower temperature. Therefore, detailed thermodynamic modelling would have to be restricted to temperatures of 200°C and above, and to non-aqueous oxide and chloride salt phase plus gas equilibria. These assumptions were believed to grossly oversimplify the system and cause the concerned results to be open to considerable interpretation.

Moreover, a few preliminary calculations also revealed that both the iron and aluminum chloride pyrohydrolysis reactions are irreversible and would most likely be under kinetic control. Magnesium chloride hydrolysis is reversible at lower temperature, where its chlorides are stable, and irreversible at higher temperature.

Therefore, the thermodynamic modelling results would only serve as a first approximation of the transformation process.

As a result, it was decided to proceed with the experimentation described in the sections that follow, and that thermochemical modelling be used to help interpret the results of the studies undertaken to define the saturated Al-Fe-Mg-Cl solution pyrohydrolysis process.

3.1.4 Phase I: Liquor Response to High Temperature

Initially, testwork was performed with a simplified experimental set-up to study the physical behaviour of the concerned chloride solution as it is exposed to a bed of oxides at 850°C (i.e. typical reactor operating temperature), and ultimately identify the various phases of the transformation process. Visual observations, temperature measurements, chemical analyses and mass balance calculations were used to develop a preliminary understanding of the mechanisms by which the saturated Al-Fe-Mg-Cl liquor pyrohydrolyzes. The experimental set-up employed for the given study is shown in Figure 23.

The trials were performed by injecting a fixed quantity of the saturated solution onto a known mass of iron oxide particles (from an industrial fluidized bed reactor). A Brinkmann Eppendorf Research Series 2100 adjustable volume pipette (available from Fisher-Scientific) was employed to ensure that a constant volume of solution was used for each test. The accuracy of the instrument was reported to be approximately +/-1% for a volume of 850µL.

The oxide particles were evenly spread as a thin layer over the base of a shallow Pyrex crucible. The bed was heated to the targeted system temperature with the use of a natural gas-fired Bunsen burner, located below the horizontal centre of the crucible. A spring loaded contact thermocouple (custom made by the Cole-Parmer Instrument Co.) was placed on the surface of the oxide layer and used to measure

and control the operating temperature. The shaft and housing were made of Inconel 600, due to the rather corrosive nature of the liquor, and the response time was reported to be 30 seconds. Given that this probe was simply used to set and control the bed temperature at 850°C during the tests, quicker response times were not deemed necessary. A Digi-Sense® Dual thermometer (also from Cole-Parmer) was used to display the oxides surface temperature on a continuous basis. The accuracy of the unit was reported to be +/-0.1% or 0.85°C in this particular case.

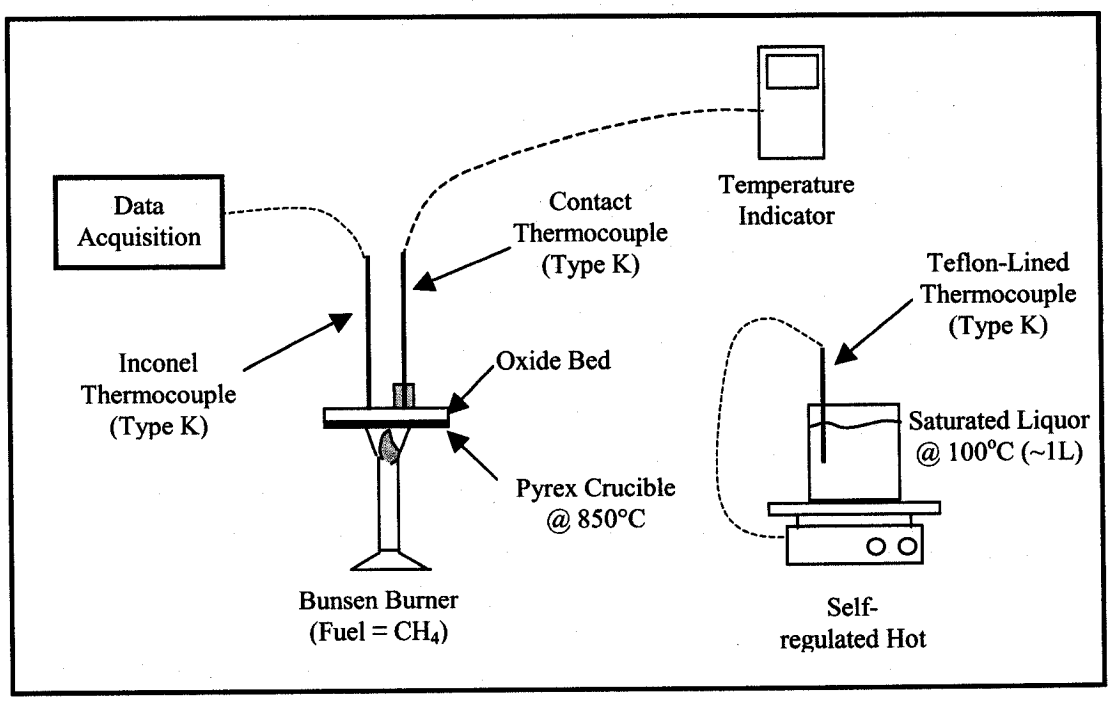

Figure 23: Experimental set-up employed to study physical behaviour of saturated feed liquor subjected to 850°C.

The second Type K thermocouple (i.e. fast-response, small diameter) was used to measure the temperature of the atmosphere 2mm above the surface of the oxides, prior to introducing the liquor into the crucible. This probe was subsequently used to measure the feed liquor temperature during transformation. As a result, an Inconel 600 shaft and quickest available response time was specified to Cole-Parmer during the purchase of these custom built thermocouples. The response time was reported to be 3 seconds (10 to 30 seconds is typical for standard probes). The temperature profile was recorded with the use of a Hewlett Packard

Data Logger (Model No. 34970A) and related BenchLink Software. Efforts were made to ensure that the thermocouple was consistently located in the centre of the pool of liquid, and that it remained in contact with the sample until the very end of each test run. The accuracy of the data acquisition system was also reported to be +/-0.1%.

A two litre batch of the concentrated liquor was prepared by adding certified reagent grade salts to hydrochloric acid (18 wt% HCl) for each series of tests. Related details are provided in Section 3.2.1.1. Subsequently, a Thermolyne MIRAK Hot-Plate with integrated temperature controller (Model No. 72725) and magnetic stirrer was employed to maintain a constant solution temperature of 105°C and to continuously agitate the bath (for homogeneity). This temperature was selected, to avoid further concentrating the liquor (i.e. boiling point approximately 125°C at atmospheric pressure), and to simultaneously minimize the risk of metal chloride precipitation. Despite this, distilled water was periodically added to the solution to make up for any evaporation that may have occurred during the course of a test run. A Fisherbrand precision specific gravity hydrometer (with integrated thermometer) with a minimum accuracy of +/-0.9% was used to continuously monitor solution density and to estimate required water additions. Liquor samples were also periodically taken throughout the course of the experiments to ensure that the composition did not drift in time.

The physical behaviour of the solution, when exposed to the hot oxide surface, was recorded with the use of a Sony Hi8 Handycam (CCD-TRV70).

3.1.5 Phase II: Crystallization Path During Evaporation

The results obtained during the aforementioned simplified pyrohydrolysis experiments revealed that during the vigorous boiling phase, the chloride liquor temperature ranged from approximately 140-170°C. At the end of the solution densification stage, the liquor temperature had risen to 260°C. Given that neither

$FeCl_2$, $FeCl_3$, $MgCl_2$, or $AlCl_3$ are expected to melt at such low temperatures, fundamentals would suggest that the violent boiling and viscous phases may be characterized primarily as the solution concentration and metal chloride ($MeCl_x$) precipitation phases. In other words, as the H_2O is driven from the solution, the liquor becomes supersaturated and $MeCl_x$ crystallization occurs.

In light of this, controlled evaporative crystallization experiments were conducted under pseudo-equilibrium conditions to define the $MeCl_x{\cdot}yH_2O$ precipitation path that takes place during the vigorous boiling phase (i.e. H_2O evaporation) and to determine whether the chlorides precipitate independently or as complex compounds.

Ideally, the ability to reproduce a gradually increasing temperature profile (as would occur upon liquor injection into the pyrohydrolyzer) during the experiments would have been preferred. Unfortunately, given the difficulties with sample manipulation at higher temperature (due to spontaneous $MeCl_x$ precipitation), the crystallization tests were performed at 105°C under progressively increasing vacuum, to maintain gentle boiling conditions and to gradually concentrate the liquor until at least 50% of the water in the saturated liquor of interest had evolved. The ability to further concentrate the solution was hampered, once again, by difficulties with sample manipulation due to uncontrollable $MeCl_x$ precipitation. The selected system temperature was based on the fact that saturated liquor is typically at 105°C as it is injected into the acid regeneration reactor.

Clearly, the proposed crystallization experiments do not simulate the dynamic intense boiling that takes place as the Al-Fe-Mg-Cl solution is injected into the pyrohydrolyzer. On the other hand, based on the author's personal experience as well as discussions with several experts in the area of $MeCl_x$ precipitation (e.g. G.P. Demopoulos, McGill University, R. Farrell & J. Sendra, Swenson Process Equipment, D. Le Flammec, GEA Kestner S.A.S), the selected approach was

considered to be the best possible compromise. Given that a rather slow evaporation rate was employed and that the system was allowed to equilibrate for 15 minutes prior to solution and crystal sample acquisition, the resulting procedure is believed to simulate pseudo-equilibrium conditions. As far as crystallization path definition is concerned, this procedure was also expected to produce reasonable sample quality and therefore, the most meaningful and reliable results.

A schematic illustration of the experimental set-up employed for the given study is shown in Figure 24. At the start of each test run, a known volume of the metal chloride solution was placed into an airtight heavy-walled, agitated Pyrex kettle (4L capacity) equipped with an electric heating mantle. CAL 3200 autotune controllers were employed to regulate the heating mantle setting and maintain a constant liquor temperature of 105°C during the experiments. Given that the boiling point of the saturated solution at atmospheric conditions is approximately 125°C, an eductor was used to gradually lower the pressure (i.e. apply vacuum) in the kettle to initiate and maintain gentle boiling for solution concentration purposes. The system temperature was controlled to within +/-1°C.

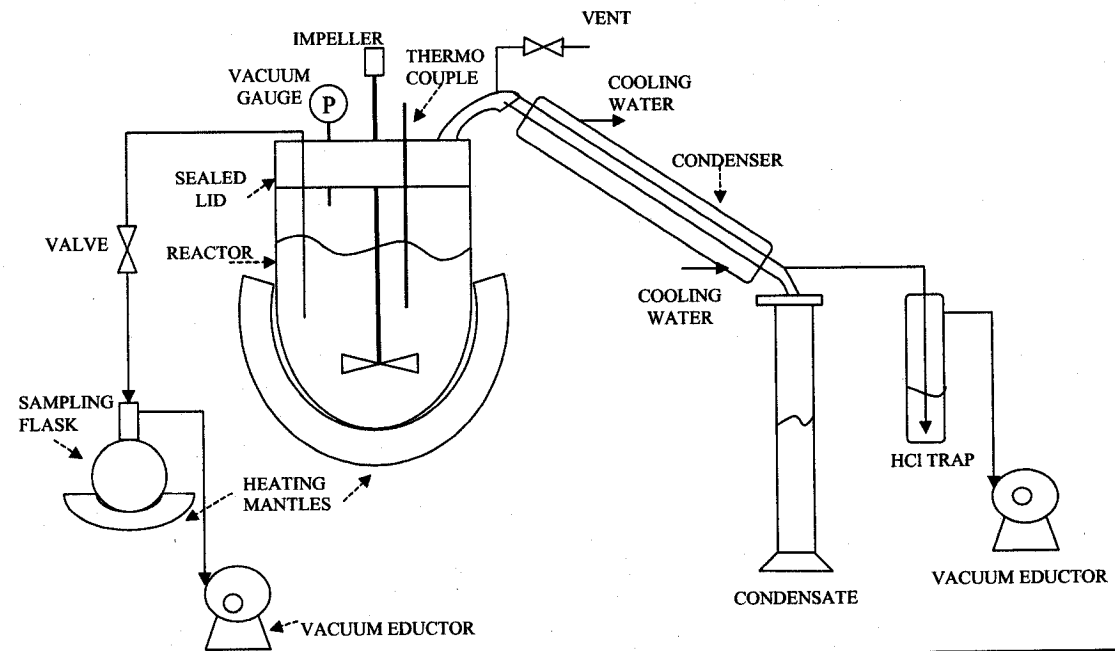

Figure 24: Experimental set-up for the evaporative crystallization tests.

At the onset of boiling (t=0), time and the total pressure in the system were periodically recorded. The degree of evaporation (or solution concentration) was determined over time by collecting and measuring the amount of water vapour and $HCl_{(g)}$ that evolved from the system. The eductor aspirated the vapour through a condenser that served to collect the gases in liquid form within a volumetric flask. A vapour trap, filled with 200ml of 1N NaOH, was used to ensure that any uncondensed HCl was recovered. It should be mentioned that a number of initial experiments were performed to define the most suitable vapour trap for maximum HCl capture.

As the solution became more concentrated, its boiling point increased; therefore, the kettle pressure was periodically lowered (in step-wise fashion) to maintain boiling at 105°C. Prior to increasing the vacuum in the system (at the end of each step), the mass of the condensate was measured, the degree of evaporation (DOE) calculated, and the [HCl] in the condensate was determined by titration (using 0.1 N NaOH). Similarly, after each vacuum (or concentration) step, the NaOH within the vapour trap was analysed to account for any HCl vapours that made it past the condenser.

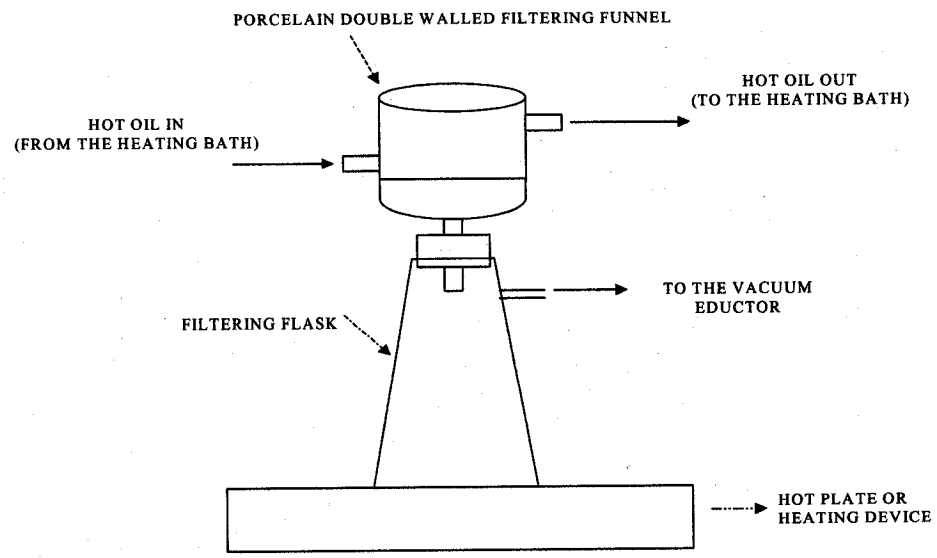

Figure 25: Schematic of the hot filtration unit.

The slurry samples, taken at specific degrees of evaporation, were vacuum filtered using a double-walled Buckner funnel through which hot oil (120°C +/- 1°C) was circulated. For DOE's of 45% or less, solution samples were aspirated through the ½" heavy gauge Teflon tubing with the use of an eductor and collected within a preheated volumetric flask. Heat tracing was used to ensure that $MeCl_x$ precipitation did not occur within the solution sampling line A schematic illustration of the hot filtration unit is shown in Figure 25.

The resulting solution and crystal samples were submitted for chemical analysis to define the crystallization path. Due to their extreme hygroscopic nature, the chloride crystals were stored in sealed bags, kept within a desiccator, and submitted for analysis as soon as possible.

3.1.6 Phase III: *Characterizing the Solution Transformation Process as a Function of Temperature*

The results of the simplified pyrohydrolysis experiments described in Section 3.1.4 revealed that as the feed sample temperature approaches 300°C, all of the solvent water has been driven from the saturated liquor. Fundamental considerations would suggest that at this point, the evaporative crystallization phase is essentially complete, and the precipitated metal salts begin to or are already dehydrating or hydrolysing as the temperature continues to rise. Based on thermodynamics (see Section 4.4.5) and reported experimental observations[54], the $AlCl_3 \cdot 6H_20$ will most likely have decomposed (at least partially) at a temperature of 300°C. A fraction of the $FeCl_{3\,(aq)}$ or $FeCl_3 \cdot xH_2O$ may have also hydrolysed.

With this in mind, a third series of experiments were performed in a fully instrumented tube furnace (Figure 26) to elaborate on the nature of the reactions (dehydration and/or pyrohydrolysis) that take place after all of the water in the starting solution has evaporated (i.e. end of metal chloride precipitation). Saturated liquor samples (32ml) at 105°C were introduced into the ThermoLyne

electric tube furnace with integrated temperature controller (Model No. F21135) and allowed to react, in the presence of a simulated pyrohydrolyzer atmosphere, to temperatures of 300, 400, 500, 600, 700, and 800°C. The system was capable of controlling the furnace temperatures to within +/-2.5 °C at 800°C, and as tight as +/-1.5 °C at 300°C.

A two litre batch of the concentrated liquor was prepared prior to starting two to three of the concerned series of tests. A Thermolyne MIRAK Hot-Plate with integrated temperature controller (Model No. 72725) and magnetic stirrer were employed to maintain a constant solution temperature of 105°C and to continuously agitate the bath (for homogeneity). As mentioned in Section 3.1.4, distilled water was periodically added to the solution to make up for any evaporation that may have taken place during the course of a test run. Furthermore, liquor samples were periodically taken throughout the course of the experiments and submitted for analysis, for an accurate measure of the starting solution composition.

After preheating the reactor to one of the aforementioned target operating temperatures and stabilizing the N_2 and $H_2O_{(g)}$ flows, the concentrated solution samples (at 105°C) were poured into a preheated Titanium Grade 7 crucible, introduced into the furnace, allowed to react for one hour, and then slowly cooled to room temperature. A 50ml pipette with 0.2ml graduations combined with a "Finnpipette Biomate" pipetting aid (available from Fisher Scientific) were employed to ensure that a constant volume of solution was used for each test. The accuracy of the apparatus was reported to be approximately +/-2% for a volume of 32mL. Gas flow into the reactor was terminated one hour after introducing the feed sample into the furnace. Titanium Grade 7 is able to withstand the corrosive nature of the concerned liquor and is typically employed for the fabrication of pyrohydrolyzer feed lances. It was selected over Pyrex, as the thermal conductivity of the metallic crucible is greater than of its silica-based counterpart and would

therefore bring the feed sample to the target operating temperature more quickly. As with all of the utensils used to handle the saturated liquor, the crucible was also preheated in the beaker of gently boiling water.

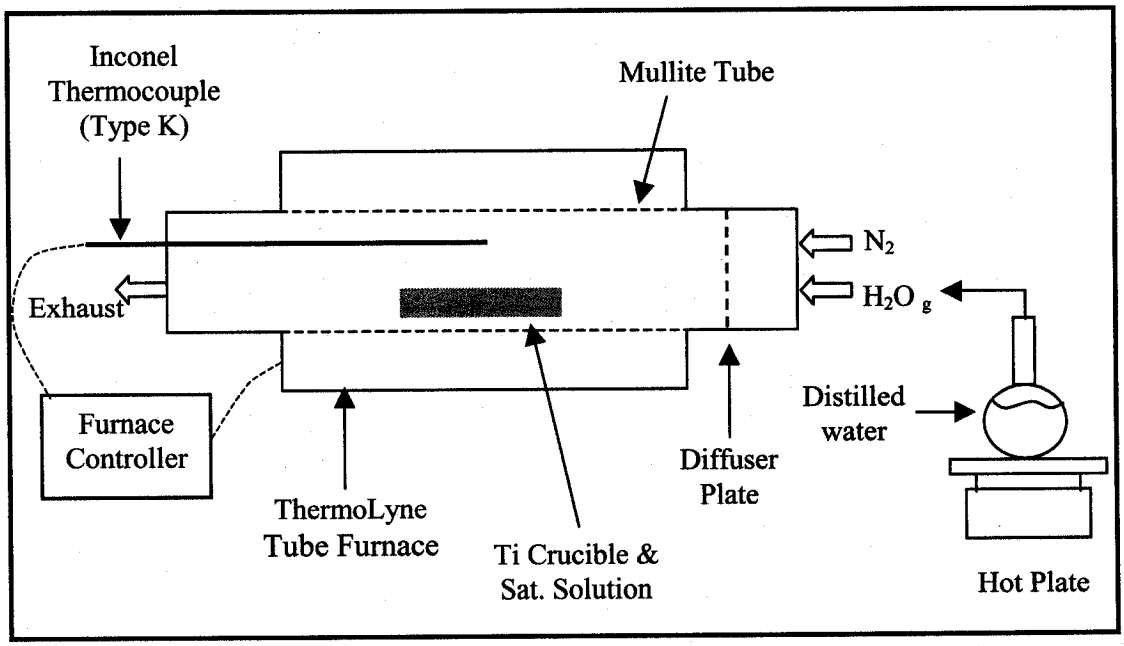

Figure 26: Bench scale facility employed to perform the Phase III pyrohydrolysis experiments.

A gas flowmeter (Model No. 4336-S from Advanced Specialty Gas Equipment) was used to regulate the N_2 injection rate into the reactor. The steam was introduced into the system by boiling distilled water in a volumetric flask and forcing the vapour through semi-rigid Teflon tubing connected to a stainless steel inlet at one end of the tube furnace. Errors related to condensation were minimized by using the shortest possible length of tubing between the volumetric flask and the furnace and by heat-tracing the line. While schematically shown as two separate entries into the reactor, the nitrogen was actually introduced into the freeboard of the boiling water flask, and used to "carry" the water vapour to the tube and through the diffuser plate that was installed at the front end of the furnace. The latter was located between the gas inlets and the centre of the reactor, to evenly distribute gas flow over the diameter of the tube. The minimum

temperature observed within this zone was measured to be approximately 200°C; therefore, $H_2O_{(g)}$ condensation ahead of the diffuser did not occur. The opposite ends of the mullite tube were sealed with customized caps, Garlock gaskets, and specialized clamps. A slightly positive pressure was maintained within the furnace to ensure that the reaction products were continuously exiting from (and not accumulating within) the system. A fume hood was used to capture the resulting exhaust gases.

An Inconel 600 sheathed Type K thermocouple (i.e. fast-response, small diameter), located in the centre of the furnace and approximately 15mm above the crucible, was used to measure and control the system temperature. The response time of the probe supplied by Cole-Parmer was reported to be 3 seconds. The thermocouple was inserted into the furnace through rigid stainless steel 9.5mm O.D. tubing to avoid it from sagging at higher temperature. The probe tip was made to protrude approximately 25mm through to the end of the supporting pipe.

Unlike the simplified pyrohydrolysis experiments (Section 3.1.4), the liquor heat-up profile was not measured during the Phase III trials due to difficulties in consistently introducing a thermocouple into the solution feed sample without causing a spill. Furthermore, actual contact between the thermocouple tip and the crucible contents could not be reliably ensured throughout the duration of each test.

At the end of each trial, the reaction products were analyzed by X-ray Fluorescence (XRF) and X-Ray Diffraction (XRD). A mass balance was conducted to quantify the degree of pyrohydrolysis as a function of temperature.

3.2 Experimental Procedures & Analytical Methods

3.2.1 Phase I: Liquor Response to High Temperature

Preliminary testwork was geared toward defining the various phases of the transformation process (i.e. physical characteristics), measuring the corresponding temperature profile, and correlating the resulting temperature data to the visual observations. The tests consisted of injecting 0.85ml of the saturated liquor (at T~105°C) onto a 30g bed of oxide particles at 850°C. The said feed solution volume was selected as it appeared to represent a reasonable liquor droplet size (from a commercial point of view), it allowed for reliable mass balance calculations, resulted in a pool of liquid that was large enough for visual inspection and that facilitated sample manipulation during the experiments. As mentioned in Section 2.3.1, the liquor is injected as a rather robust stream (i.e. 19-38 mm in diameter) into commercial fluidized bed pyrohydrolyzers to favour so-called "roping" action. This is believed to encourage the formation of large droplets that will not be carried away by the upward flowing combustion gases.[1,22,53] While final liquor droplet size in commercial units is dependant upon a number of parameters (i.e. fluidizing gas velocity, lance orientation and angle of inclination, bed fluidizing regime etc...), it is expected to be considerably larger than those generated by a spray nozzle.

The solution was introduced onto the hot bed surface, after equilibrating the oxides at 850°C for approximately 15 minutes. It should be mentioned that all the utensils used to handle the pre-concentrated acid (including the pipettes) were preheated in a 3L beaker of gently boiling water to avoid any $MeCl_x$ precipitation. This procedure was used during the Phase II and III experiments as well.

The initial composition of the liquor (including maximum allowable variations) and solids employed during the test program are provided below.

Solution Composition		***Oxide Composition***	
$[FeCl_2]$ =	10 +/- 0.2wt%	$[Fe_2O_3]$ =	98.3 wt%
$[FeCl_3]$ =	12 +/- 0.2wt%	[MgO] =	0.21 wt%
$[MgCl_2]$ =	18.5 +/- 0.3wt%	$[Al_2O_3]$ =	0.41 wt%
$[AlCl_3]$ =	8.5 +/- 0.2wt%	$[Mn_2O_3]$ =	0.32 wt%
[HCl] =	1.5 +/- 0.005wt%	$[SiO_2]$ =	0.20 wt%
		[CaO] =	0.12 wt%
		$[Cl^-]$ =	0.15 wt%

The starting solution preparation procedure is described in Section 3.2.1.1.

Visual observations during preliminary trials revealed that the solution begins by boiling vigorously, followed by densification (result of metal chloride precipitation), and ultimately chemical conversion (i.e. dehydration and pyrohydrolysis of the hydrated chlorides).

A series of tests were then subsequently performed to define the various reactions taking place during transformation (as a function of temperature). This was accomplished by taking samples of the partially reacted liquor at 225, 300, 500, 750 and 850°C. The reaction was allowed to progress until the desired temperature was reached at which point the entire sample was removed from the crucible, cooled with a gentle flow of gaseous nitrogen at ambient temperature, and weighed. To generate sufficient material for chemical analysis, five repetitions were needed for each stage. All five samples (see Figure 28) were then used to generate a composite that was submitted for analysis (X-Ray Fluorescence). Sample contamination with bed oxide particles was impossible to avoid; therefore, the mass of entrained oxide (which was known to contain 0.15% Cl) was measured after each test and accounted for during the mass balance calculations.

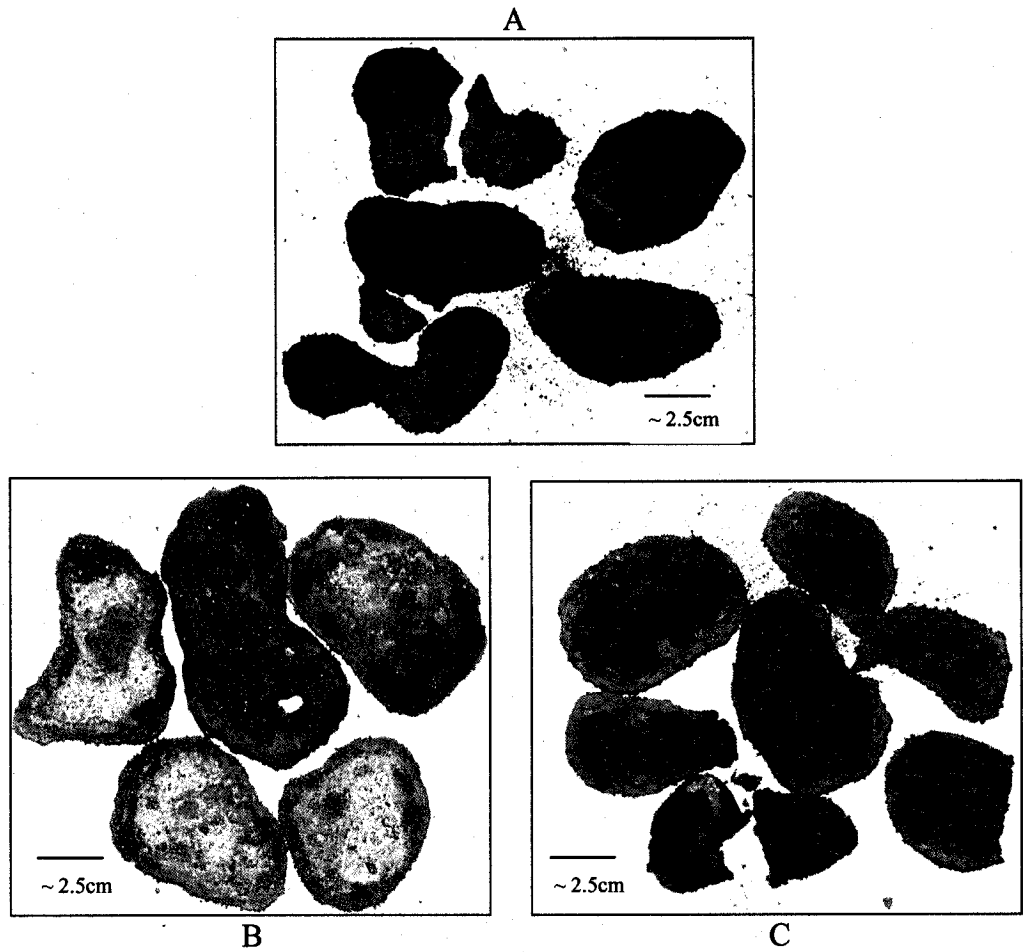

Figure 28: Photos of the samples taken at: A) 300°C (i.e. end of liquid phase, sample composed primarily of dark crystals), B) 500°C (i.e. middle of crystal pyrohydrolysis phase), C) 750°C (i.e. near end of full pyrohydrolysis).

Clearly, a number of tests needed to be performed to generate all of the samples required for the study at hand. A total of 29 experiments were conducted (4 were rejected) just to collect the samples, and based on visual observations alone, the process appeared to be very repeatable. All of the concerned tests were performed in a span of five days to minimize the effects that any variations in lab atmosphere may have had on the results.

The resulting chlorine concentration was used to calculate the relative degree of transformation, which was expressed as the percentage of chlorine remaining in the starting sample as a function of time and temperature.

While the concerned experimental set-up does not accurately simulate the conditions that exist within typical fluidized bed pyrohydrolyzers, the results were used as a first approximation of the transformation process, and also served to define the nature of any future work that need be performed (i.e. Phases II & III).

3.2.1.1 Starting Solution Preparation:

The saturated solution employed as feed for all of the experiments (Sections 3.1.4, 3.1.5, and 3.1.6) was synthetically produced by adding reagent grade $AlCl_3 \cdot 6H_2O$, $MgCl_2 \cdot 6H_20$, $FeCl_2 \cdot 4H_2O$ crystals, and anhydrous $FeCl_3$ to hydrochloric acid at 18 wt% HCl. These reactants were purchased from Fisher-Scientific. While available in hexahydrate form, anhydrous ferric chloride was used as it was of higher purity and could be obtained as powder. Certified $FeCl_3 \cdot 6H_2O$ was only sold as lumps. The other hydrated chloride salts were purchased in the form of relatively fine crystals.

In the case of the Phase I and III trials, 400ml of the acid was agitated with a magnetic stirrer and heated to approximately 50°C, before gradually adding 414g of the aluminium chloride to the solvent. The liquor temperature was monitored at all times. Given that $AlCl_3 \cdot 6H_2O$ dissolution is rather favourable, a slight increase in system temperature was usually observed. Once the crystals were fully dissolved, 422g of the ferrous chloride tetrahydrate, followed by 323g of the $FeCl_3$ were added to the solution. After each addition, the temperature was allowed to stabilize for approximately 5 minutes before introducing any other salt. 1062g of the magnesium chloride were then slowly added to the stirred bath until solid crystals were no longer observed in the solution. Given the rather opaque colour of the final liquor,

samples were periodically taken after the last of the $MgCl_2 \cdot 6H_2O$ additions and filtered through the heated Buckner funnel described in Section 3.1.5.

It took just over an hour to prepare the starting solution for each test and despite all the precautions taken, the resulting liquor was sampled and submitted for analysis by ICP to confirm the starting solution composition. The procedure proved to be quite practical and reliable, as the variation in the desired chloride concentrations was rather narrow (see Section 3.2.1) and very few batches of the synthetic liquors or test results were disposed of due to the composition being off target.

The starting solution preparation methodology was based on pure component solubility[81] and thermodynamic data, as well as a few initial experiments. The $AlCl_3 \cdot 6H_2O$ was added first as it is quite soluble at low temperature and while exothermic, was not expected to favour a significant increase in solution temperature. The ferrous chloride was added immediately afterward as its solubility is relatively low (compared to the others) and it also resulted in additional H_2O units in the solvent for the anhydrous $FeCl_3$ dissolution. The ferric chloride and $MgCl_2 \cdot 6H_2O$ were kept for last as these are extremely soluble (especially at the higher temperatures) and their dissolution quite favourable from a thermodynamic point of view; therefore, these salts were expected to readily dissociate despite the increasing salt concentration in the liquor. The heat released during the addition of these two chlorides would raise the solution temperature to approximately 90°C. The hot plate was then used to heat the liquor to 105-110°C to ensure that the crystals were fully dissolved. Clearly, the HCl content dropped from 18% in the initial solvent to approximately 1.5% in the product liquor due to the dissolution of the waters of hydration within the crystals and the evaporation of some HCl during the salt additions.

Given that the solution preparation procedure and the evaporative crystallization tests were quite long, it was decided that a large batch (approximately 20L) of the feed liquor of interest be produced for the Phase II study.

3.2.1.2 Analytical Methods:

Inductively Coupled Plasma (ICP)

A Perkin Elmer Optima 4300 DV Inductively Couple Plasma Spectrometer was employed to analyse the starting solution used for each of the experiments. This analytical method is based on the principle of atomic emissions, which are defined as the radiation emitted by atoms or ions that have been energized to their excited states by an arc, spark or flame. In this particular case, a plasma torch is used to heat the aqueous sample to temperatures of 8000 to 10000K to excite the atoms or ions contained within. This excited condition does not last very long and upon returning to their normal state of existence, excess energy is released in the form of electromagnetic radiation. When an atom of a specific element is excited, it emits light with a characteristic wavelength when it returns to its initial orbitals. The resulting light is then filtered to obtain the spectra for the elements in the sample. A photomultiplicator is used to measure the intensity of the resulting rays, which are proportional to the concentration of the corresponding element in the solution.

Prior to submitting the saturated Al-Fe-Mg-Cl liquor for ICP analysis, it is diluted 100:1 (volume basis) in slightly acidified distilled water (pH = 4-5). Furthermore, synthetic reference samples are used to regularly confirm that the unit is functioning properly and providing reliable results. The accuracy of this analytical device is reported to be within +/-0.1%.[83] When taking sample preparation into consideration, the ISO 9002 lab used to analyse the samples certifies that the error lies within +/-1%.

X-Ray Fluorescence (XRF)

A Rigaku 3270 XRF was employed to analyse the solid composite samples collected at the various stages of the transformation process. This analytical technique consists of bombarding a solid sample with X-rays that, in turn emit electrons at different wavelengths that are reflected by a crystal to a detector for analysis. The crystal and detector rotate, through the use of a goniometer, at angles that satisfy the Bragg relationship $n\lambda=2d\sin\theta$ and allows for all the elements in the sample to be identified. Collimators are located in front of the crystal and detector to select the x-rays of interest. A generator is used to supply the 50kV and 50mA of current required by the X-ray tube during analysis. The unit is regularly calibrated with reference standards, dependant on the type of samples being analyzed (i.e. chlorides, oxides, metals, etc...).

XRF can be used to analyse for any element whose molecular weight is greater than that of fluorine, and the accuracy of the reported analytical data is estimated at +/1% (or as much as +/-3% absolute).[84]

Before submitting a solid sample for analysis by XRF, a fused button must be prepared. The sample of interest must be ground (to –325 mesh), and a few grams must be well mixed with a lithium meta- and tetra-borate (50-50 blend) on a 1:14 basis (by weight), respectively. The mixture is then heated to approximately 950°C (in a Claisse Fluxy 10), at which point the submitted sample dissolves completely into the flux. The crucibles employed to make the fused buttons are rotating (so as to stir the sample/lithium borate blend) to ensure the homogeneity of the sample that will be analyzed.

Given that the chlorine in the partially reacted liquor samples will evolve if heated to 950°C, a pressed pill is used for chlorine analyses with the XRF.

The corresponding sample preparation technique is described in Section 3.2.2.2.

3.2.1.3 Sources of Error:

In addition to the inaccuracies associated with the analytical methods, instruments, and procedures employed during the experiments described in sections 3.1.4 and 3.2.1, a summary of the other miscellaneous sources of error that may have affected the results is summarized in the following.

Firstly, the chemical composition of the oxides used during the trials is a based on a composite sample taken from two 10L pails. While efforts were made to collect a representative sample for analysis through the use of splitters, some variation in the oxide assay may have been incurred from one test run to the next. Furthermore, the oxides were manually spread as a uniform layer over the base of the crucible. Variations in bed thickness and compaction over the 3" crucible diameter may have lead to deviations in heat flux from one experiment to another.

The partially reacted liquor samples taken as a function of temperature were also manually acquired; therefore, the exact temperature at which the various samples were recovered to generate the composite may have varied by a few degrees. Moreover, given that the samples were not "quenched" to ensure that no further reactions are taking place after it has been removed from the bed of oxides, it may not necessarily be an exact representation of the degree of conversion that has taken place to that point in time.

While it is difficult to accurately quantify the degree of error that may have resulted by the aforementioned conditions, a review of sections 3.1.4, 3.2.1 and 3.2.1.2 suggests that the solid sampling method, XRF analyses of the oxides and acquired samples (+/-1%), the precision of the pipette (+/-1%), and material losses have the

greatest impact on the accuracy of the results. It is estimated that the reported results are accurate to within +/- 6-7%.

3.2.2 Phase II: Crystallization Path During Evaporation

3.2.2.1 Procedure:

Two to three litres ($V_{Initial}$) of the starting solution were poured into an airtight heavy-walled Pyrex "kettle" and heated to 105°C, while maintaining gentle agitation (375 – 400rpm) to ensure uniform temperature throughout the bath. At atmospheric conditions, the liquor does not boil at the prescribed temperature. Upon equilibrating the system at 105°C, a sample of the starting solution was taken.

Given that the synthetic solution preparation procedure (see Section 3.2.1.1) and the evaporative crystallization tests were quite long, it was decided that a large batch (approximately 20L) of the feed liquor of interest be produced for the study at hand. Since the Al-Fe-Mg-Cl solution is saturated at 105°C, cooling to room temperature would result in $MeCl_x$ precipitation, as ferric, ferrous, and magnesium solubility are temperature dependant.[82] The resulting synthetic feed liquor was therefore diluted with distilled water (1 part water per 3 parts liquor), stored in sealed 10 litre pails, and used for the concerned series of experiments. This approach was also favoured as it was expected to minimize any errors that may have been incurred by the use of different starting solutions for each test.

Vacuum was gradually applied to the kettle (using the eductor) until the solution began to boil gently (P_{Abs} ~73kPa). This marked the beginning of a trial run (t=0). The time and total pressure in the system were periodically recorded from this point onward. The remainder of the experimental procedure may be summarized as follows.

1. As boiling stopped, the degree of evaporation (or solution concentration) was determined by weighing the condensate collected in the graduated cylinder and measuring the corresponding [HCl]. Similarly, the NaOH within the vapour trap was analysed to account for any HCl vapours that may have made it past the condenser. Subsequently, the NaOH in the vapour trap was replaced with 200ml of fresh solution. Furthermore, the liquor/slurry was let to stand for 15 minutes (for equilibration purposes) prior to moving on to the next step.

2. Solution/slurry samples were taken from the kettle, filtered and diluted with slightly acidified distilled-water, and eventually submitted for chemical analysis. At the lower degrees of evaporation (DOE<45%), approximately 25ml of solution was drawn from the bath through the ½" Teflon piping with the use of a vacuum source (i.e. eductor). The more concentrated liquor (i.e. DOE>45%) was sampled by temporarily cutting the vacuum, removing the lid from the reactor, and pouring a small quantity of the slurry (100-200ml) directly into the hot filtration set-up. In doing so, further metal chloride precipitation, due to the rapid cooling of the solution, is avoided thanks to the rather high thermal inertia of the reactor contents. Filtrate dilution serves to avoid any error or difficulties with crystallization as the solution cools. Regular filter paper was unable to resist the rather high temperature (i.e. 120°C) HCl-based application and was carbonized; therefore, Whatman glass microfibre filters (type GF/D) were used instead. The crystals were washed with diethyl ether directly in the funnel and then dried overnight in the oven at ~ 50°C. Subsequently, the chloride crystals were stored in sealed bags and kept within a dessicator.

3. The system pressure was lowered once again until the onset of gentle boiling was re-established within the kettle. Once boiling ceased, Steps 1 and 2 were repeated.

This overall procedure was repeated until 74% of the water in the initial liquor had evaporated. The absolute pressure required to maintain boiling to this point was measured to be approximately 6 kPa. Given that the starting solution employed for these experiments is actually a diluted version of the Al-Fe-Mg-Cl liquor of interest, the actual degree of evaporation is in the order of 62%. Beyond this point the solution was extremely supersaturated and was simply too difficult to work with. The ability to take reliable and representative liquor or crystal samples was often hampered by uncontrollable (catastrophic) crystallization.

For the sake of completeness it is worth mentioning that four preliminary experiments were performed with the experimental set-up to fully define and fine-tune the aforementioned test procedure.

With regards to the washing of the crystal samples, diethyl ether was selected because it did not appear to dissolve the salts, as did some of the other alcohol-based agents that were tried. Moreover, as the viscosity of the slurry increased, larger quantities of the diethyl ether and more intense washing was required for the samples recovered at higher DOE, to avoid the crystals from cementing together with entrained solution.

As mentioned in Section 3.1.5, the solution and crystal samples were submitted for chemical analysis (i.e. ICP, XRD, and SEM-EDS) to define the crystallization path as a function of DOE. In an attempt to avoid analytical errors related to crystal hydration, efforts were made to submit related samples for analysis as quickly as possible. With the mass of water collected in the condenser, its HCl concentration, along with the quantity of HCl recovered in the vapour trap after

each vacuum step, it was possible to calculate P_{H2O} and P_{HCl} in the offgas phase as a function of the DOE. While the results are not presented in this thesis for confidentiality reasons, the P_{HCl} data will be used to further support conclusions regarding the onset of crystallization.

3.2.2.2 Sample Preparation & Analytical Methods:

Acid-Base Titration

The HCl concentration in the condensate, at different degrees of evaporation (vacuum levels), were monitored by titration with NaOH 0.1N. An automatic titrator (Radiometer Copenhagen Titralab™90), equipped with a high precision ABU 900 Autoburette System and glass pH electrode (i.e. Fisher Accu-pHast), was employed. Similarly, HCl 0.1 N was used to titrate the liquid collected by the vapour trap to quantify the mass of $HCl_{(g)}$ that made it past the condenser.

Solution & Crystal Sample Analysis by ICP

The Perkin Elmer Optima 4300 DV Inductively Coupled Plasma Spectrometer described in Section 3.2.1.2 was employed to analyse the concentrated solution and filtrate samples collected as a function of the DOE.

The 25ml liquor samples taken at DOE's of less than 45%, were initially diluted up to 100ml with acidified distilled water (pH 1) in a volumetric flask, to avoid any $MeCl_x$ precipitation as the mixture cooled to room temperature. . The saturated filtrate samples (100-200ml) recovered at DOE's of 45% and higher were immediately diluted to 500ml with the acidified distilled water (pH 1). Prior to submitting the resulting solutions for analysis, they were subsequently diluted 50:1 (volume basis) in slightly acidified demineralized water (pH = 4-5). The accuracy of the volumetric flasks employed is reported to be +/-1%.

The crystals were analyzed by dissolving 1g of the washed sample into 100ml of the acidified distilled water (pH = 4-5). The salts were still in crystalline form prior to dissolution.

X-Ray Diffraction (XRD)

A Phillips PW1710 XRD was used to analyze the crystal samples collected, to identify the nature of the resulting metal chlorides and to quantify the number of crystallization water molecules associated with each of the precipitated salts. This analytical technique consists of bombarding the submitted sample with X-rays (emitted from a Cu tube) at different angles. Upon reflection, the X-rays emit wavelength which form a pattern that is characteristic of each crystalline phase within the sample. A graphite monochrometer is used to record the patterns.

The phases present within the salts were then identified by comparing the major spectral lines obtained for each of the samples to the characteristic peaks of reference standard spectra contained within the computer's database ($MeCl_x \cdot yH_2O$, where Me = Fe, Mg and Al, respectively). Clearly, the reliability of this technique is somewhat dependant on the availability of standard spectra for every possible compound that may be present in the sample. The identification of the phases within the sample is further complicated by the fact that the presence of more than one compound in the matrix may cause the spectral lines to shift from where they should actually be, and therefore go unidentified. Furthermore, if a compound is present in amorphous (instead of its crystalline) form, it will go undetected. When the crystal structure of the compounds within a sample are not well formed, the resulting X-ray diffraction pattern will show a considerable degree of background noise which may also complicate the interpretation of the data.

The crystals samples were manually ground with a pestle and mortar, poured into an aluminium capsule and then compressed with a 70ksi load for 3 seconds, to produce the pressed pill required for analysis by XRD.

Scanning Electron Microscopy (SEM)

Due to its ability to provide images of high spatial resolution for solid specimens with minimal sample preparation, a JEOL 840A SEM operating with an accelerating voltage of 15 keV was used to examine the crystals generated during the experiments. Given the fairly large size of the concerned particles (i.e. 300-400μm), the magnification employed ranged between x16 to x200. Prior to analysis, the samples were gold-coated in a Hummer VI plasma sputter coater. The images obtained were used to visually characterize sample morphology, texture, and quality.

The SEM was equipped with a Noran *Energy-Dispersive Spectroscope (EDS)* that was used to perform spot analyses on individual crystal particles within the samples to determine whether the chlorides were precipitating as basic or complex salts. EDS analyses can vary by as much as +/-20% and are therefore rather subjective. It is generally accepted that for reliable EDS analyses, a polished, flat, homogeneous sample is required. This is physically impossible to guarantee for a single crystal; therefore, EDS analyses were performed on the flattest possible surfaces available within a crystal sample.

3.2.2.3 Calculation Formulae:

- *Degree of Water Evaporation:* **DOE (%) = ($m_{Cond}/m_{H2Oinitial}$)*100**, where:

m_{Cond} = mass (weight) of condensate collected for a certain vacuum step (g)

$m_{H2Oinitial}$ = quantity of water present within a given mass of the starting solution (g). This was determined by subtracting the weight of the known elements (metal cations, Cl^-, HCl) from the overall initial

liquor mass and therefore includes the dilution water added to the saturated solution of interest.

- *Acid Titration for the Condensate:* $\mathbf{m_A = N_A * E_{g,A} * Wt_{cond.} * 10^{-3}}$, where:

  m_A = the mass of HCl within the condensate (g)
  $N_A = N_B * V_B / V_A$: HCl normal concentration
  V_A = volume of analyte used in titration (ml)
  V_B = volume of NaOH used in titration (ml)
  N_B = NaOH normal concentration (0.1 N)
  $E_{g,A}$ = 36.45: HCl gram-equivalent (g/mol)
  $Wt_{cond.}$ = the quantity of condensate collected (g)

- *Base Titration for the Trap*: $\mathbf{m_B = N_B * E_{g,B} * Vol_{trap} * 10^{-3}}$, where:

  m_B = the mass of NaOH reacted with the HCl in the trap (g)
  $N_B = N_A * V_A / V_B$: NaOH normal concentration
  V_B = volume of analyte used in titration (ml)
  V_A = volume of HCl used in titration (ml)
  N_A = HCl normal concentration (0.1 N)
  $E_{g,A}$ = 40: NaOH gram-equivalent (g/mol)
  Vol_{trap} = the quantity of NaOH in the trap (ml)

- *Partial Pressures:*

  Partial pressure of species "i" in the gas mixture: $\mathbf{P_i = y_i * P_{tot}}$
  Mole fraction of species "i" in the vapour phase: $\mathbf{y_i = n_i / n_{tot}}$, where:

  P_{tot} = absolute pressure (kPa)
  n_i = moles of species "i" in the vapour phase
  n_{tot} = total quantity of moles in the vapour phase

- *Percent HCl in the Vapour Phase:* $\mathbf{\% \ HCl = (n_{HCl} / n_{total}) * 100}$

- *Solids Density of Crystal Sample:*

$$\mathbf{SD(\%) = \frac{\text{mass of crystals}}{\text{mass of slurry}} \times 100}$$

3.2.2.4 Sources of Error:

A summary of the errors that may have been incurred during the experiments and that may have affected the results are summarized in the following.

While ICP results are reported to be accurate to within +/-1%, differences of 0.6 to 13.5% were observed between the actual and theoretically calculated $AlCl_3$ and $FeCl_2$ concentrations of the solution samples taken before the dilution water had evaporated (i.e. DOE < 32%). These values should have been nearly identical. The degree of error was less pronounced for $MgCl_2$, and the agreement between actual and theoretical values for $FeCl_3$ was actually quite good (i.e. within ~8%). Careful review of the experimental and sample preparation procedures suggest that dilution is the most probable culprit for the observed differences. This may be explained by the fact that the solution samples were diluted in steps (upon acquisition and again just prior to analysis) and that a volumetric flask was used to measure and dilute during the experiments. Volumetric flasks are much more subjective than pipettes and are therefore more prone to producing error. The explanation for the much larger deviations observed for $AlCl_3$ and $FeCl_2$ (as compared to $MgCl_2$ and $FeCl_3$) is much less obvious.

Despite the significant differences between the actual and calculated solution concentrations, the reader is reminded that the objective of these experiments was to define the crystallization path and the nature of the salts that form. Efforts were not geared toward defining the degree of supersaturation required for $AlCl_3$ to precipitate homogeneously from solution, for example. Therefore, the accuracy of the DOE's and solution concentrations at which the chlorides precipitate are not that critical for the study at hand. On a more positive note, it is worth mentioning that the experiment was repeated and the overall results were very similar from one run to the next.

With regards to the crystals, despite efforts made to avoid further hydration of the samples after they were taken (i.e. drying, placing the crystals in sealed bags and storing them in a dessicator, etc...), it is very difficult to confirm with certainty that no additional water pickup occurred.

Other noteworthy sources of error, such as the effects of crystal sample washing with diethyl ether, were provided along with the results in Sections 4.2.2.1 and 4.2.2.2.

3.2.3 Phase III: Characterizing Solution Transformation as a Function of Temperature

3.2.3.1 Procedure:

During the third series of experiments, six 32ml saturated liquor samples (at 105°C) were individually introduced into the ThermoLyne electric tube furnace and allowed to react, in the presence of a simulated reactor atmosphere, to temperatures of 300, 400, 500, 600, 700 and 800°C, respectively. Prior to starting the tests, a sample of the feed solution was submitted for chemical analysis by ICP. The composition of the liquor employed during the concerned experiments was similar to that provided in Section 3.2.1. The starting solution preparation procedure was described in Section 3.2.1.1.

After preheating the reactor to one of the aforementioned target operating temperatures and stabilizing the N_2 and $H_2O_{(g)}$ flows, a concentrated liquor sample (at 105°C) was poured into a Titanium Grade 7 crucible, introduced into the furnace, allowed to react for one hour, and then slowly cooled to room temperature. A 50ml graduated pipette along with a pipetting aid were used to accurately measure the required feed solution sample volume (i.e. 32 ml) and subsequently pour it into the crucible that was preheated in the beaker of gently boiling water (mentioned in Section 3.2.1) to avoid $MeCl_x$ precipitation and to help minimize the drop in furnace temperature as it is introduced into the mullite tube. A reaction time of one hour was selected in an effort to favour pseudo-equilibrium conditions at each of the given temperatures and therefore generate samples that would produce meaningful and reliable XRD results. While a flowmeter was used to regulate the N_2 injection rate, a few trials were performed

(with the use of nitrogen as a carrier) in advance of the pyrohydrolysis experiments to define the hot-plate set point required for the desired steam flowrate.

The crucible was inserted into the reactor as quickly as possible through the exhaust end of the furnace to avoid disturbing the desired gaseous atmosphere during charging. In an effort to minimize the duration of the temperature drop incurred during this operation, the furnace controller was programmed to heat at maximum power until the system was within 10°C of the setting. At this point, a heating rate of 1°C/min. was specified to avoid significantly overshooting the target operating temperature. The time required to re-establish system temperature during the concerned series of tests varied between 12 and 18 minutes and a maximum overshoot of 8°C was observed.

It should be mentioned that the vigorous boiling observed during the simplified pyrohydrolysis experiments was detected once again, when the saturated liquor was placed within the reactor. In fact, the starting solution volume of 32ml was selected to avoid liquid overflow and material losses during the experiments. The concerned feed sample volume was also chosen to generate sufficient reaction product for chemical analyses. Interestingly enough, the degree of bubbling and frothing observed upon introducing the sample into the furnace was relatively constant, regardless of system temperature. Furthermore, no splashing was observed, and no material was found on the sides or ceiling of the mullite tube.

At the end of each test, the resulting product samples were recovered from the crucible, weighed, and submitted for chemical analysis (X-Ray Fluorescence and X-Ray Diffraction). The accuracy of the scale was reported to be +/-0.2%. Special care was taken to minimize material losses upon retrieving the concerned reaction products. The crucible was weighed at the end of each trial to estimate the quantity of reaction product (if any) that remained glued to the walls. The

degree of conversion was quantified by calculating the percentage of chlorine loss realized at each stage of the transformation process (i.e. as a function of temperature). XRD was used to identify the phases/compounds present in the product generated during each of the tests. The accuracy of each of these analytical methods was provided in Sections 3.2.1.2 and 3.2.2.2.

3.2.3.2 Test Condition Definition:

Given that natural gas is typically burned with air (using an air/fuel ratio of approximately 9.8) to generate the heat required for the pyrohydrolysis reactions and to maintain the target operating temperature, the combustion gas (prior to liquor injection) is essentially composed of CO_2, H_2O, and N_2. In light of this, as well as the fact that the CO_2 is considered inert (stoichiometrically speaking) when it comes to the pyrohydrolysis reactions, it was simply replaced by N_2 during the experiments. Therefore, the combustion gas (i.e. 9%CO_2, 73%N_2, & 18%H_2O) was simulated by injecting 82%N_2 and 18% steam into the furnace. The flowrates employed were based on maintaining the same combustion gas volume/liquor injection rate as that of a commercial unit, where the 32 ml of feed solution were assumed to be injected over a period of two minutes (i.e. time required for liquor to reach 850°C during Phase I experiments). This is considered a conservative estimate, as the time required for the feed solution to reach the target operating temperature in the tube furnace is likely to be much faster than that realized with the crucible/Bunsen burner set-up used during the simplified pyrohydrolysis trials. In other words, an excess of reagent (i.e. water vapour and oxygen) was most likely made available for the reactions of interest. It is certainly worth mentioning that the surplus $H_2O_{(g)}$ available in commercial pyrohydrolyzers has been estimated to lie between 1100-1400%. 60-70% of this excess comes from the evaporation of the water contained with the feed liquor alone. Therefore, the experimental procedure was designed to ensure that once the target system temperature was reached, the same excess (if not a little more) was provided to the feed solution. As a result, once the furnace set-point was

attained, designated $H_2O_{(g)}$ and N_2 flows in the reaction chamber were maintained for a duration of two minutes, after which the water vapour flow was cut and a simple nitrogen purge was maintained until the end of the trial. For the sake of completeness, it should be mentioned that the oxygen required for the pyrohydrolysis of the $FeCl_2$ in the feed solution came from the specially produced grade of N_2 that contained 0.24% O_2.

The actual combustion gas volume/liquor injection rate employed and the data used to calculate the excess amount of water vapour available in commercial reactors are not provided for reasons of confidentiality.

As far as the steam flowrate is concerned, the mass of the distilled water in the volumetric flask was measured at the start and end of each test, and the difference was used to calculate the injection rate incurred over the concerned time interval. The trials performed to define the hot-plate set point required for the desired steam flowrate revealed that once stabilized, the $H_2O_{(g)}$ generation rate is relatively constant over time.

All of the concerned tests were performed in a span of two weeks to minimize the effects that any variations in atmosphere in the lab may have had on the results.

3.2.3.3 Sample Preparation:

As mentioned in Section 3.2.1.2, the starting solution samples periodically taken throughout the course of the Phase III experiments were diluted 100:1 (volume basis) in slightly acidified distilled water (pH = 4-5) prior to analysis by ICP.

The test procedure described in Section 3.2.3.1 resulted in the production of approximately 12g of reaction product that was divided in two with the use of an appropriate splitter. Half was submitted for analysis by XRD and the other by XRF.

Due to presence of chlorine, all of the samples were manually ground with a pestle and mortar.

Given that the reaction product generated during the lower temperature tests (i.e. <500°C) were likely to contain hygroscopic chlorides, they were stored in a dessicator to avoid moisture pick-up prior to analysis. Furthermore, efforts were made to analyze the samples as quickly as possible after they were produced.

In light of the fact that the chlorine in the reaction product evolves if heated to 950°C, a pressed pill was used for chlorine analyses via XRF. The corresponding sample preparation technique is described in Section 3.2.2.2.

Moreover, the manually ground reaction product was poured into an aluminium capsule and then compressed with a 70ksi load for 3 seconds, to produce the pressed pill required for analysis by XRD. Fused buttons were avoided to conserve any chlorides that may be present in the samples generated at lower reaction temperature (i.e. <500°C).

3.2.3.4 Sources of Error:

In addition to the inaccuracies associated with the analytical methods, instruments, and procedures employed during the experiments described in sections 3.1.5 and 3.2.3, some of the other miscellaneous sources of error that may have affected the results are summarized in the following.

Firstly, while test work was performed to ensure that the $H_2O_{(g)}$ flow to the furnace was relatively constant over the course of the test, the actual flowrate was not regulated or monitored as for the nitrogen. On the other hand, the experiments were run with an excess of water vapour; therefore, if the flow did vary, this condition is not likely to have significantly affected the results.

Furthermore, while efforts were made to recover all of the reaction product from the crucible prior to proceeding to the next trial, residual amounts of solid remained glued to the walls, especially after the tests performed at 300 and 400°C. The impact of any error that this may have caused was minimized by weighing the crucible before and after each experiment.

A careful review of the experimental procedure and methods of analysis suggests that the sources of error that are most likely to have affected the results arise from the accuracies related to:

- the pipette employed to measure the starting solution volume (+/- 2%)
- the balance used to weigh the product sample and the crucible (+/- 0.2%)
- feed liquor and reaction product assays (+/-1%).

In light of this, it is estimated that the reported results are accurate to within +/- 4-5%.

4.0 RESULTS & DISCUSSION:

4.1 Phase I: Liquor Response to High Temperature

4.1.1 Initial Findings:

The visual observations made during the simplified pyrohydrolysis experiments revealed that the saturated Al-Fe-Mg-Cl solution transformation process consists of four distinct phases:

- rapid H_2O evaporation (i.e. vigorous boiling) and onset of metal chloride precipitation.
- slurry densification due to a gradual increase in crystal content (i.e. $AlCl \cdot 6H_2O$, $FeCl_2 \cdot xH_2O$, and $MgCl_2 \cdot xH_2O$).
- crystal drying and onset of pyrohydrolysis.
- thermal decomposition of the remaining metallic salts ($MeCl_x \cdot yH_2O$).

Clearly, the presence of several metal chlorides in the liquor favours a certain degree of overlap between each of these stages due to differences in solubility and the stability of the individual compounds over the temperature range of interest. The physical characteristics of each of the aforementioned phases are shown in Figures 29 through 32. A clearer image of the intense boiling stage is shown in Figure 33. The temperature profile observed upon injecting the saturated liquor onto the static bed of hot oxides is provided in Figure 34. When superimposing the profiles measured during each trial, the degree of variation was calculated to be approximately +/-5%.

Figure 29

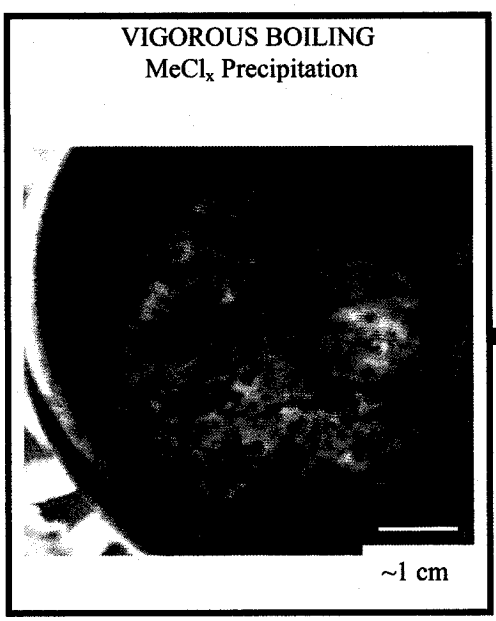

Figure 30

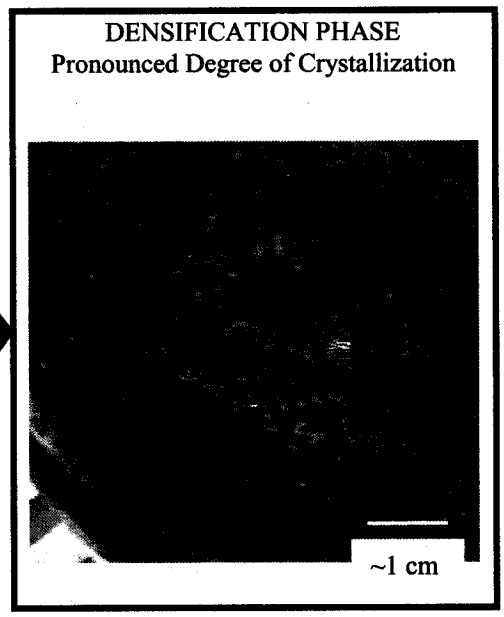

Figure 31

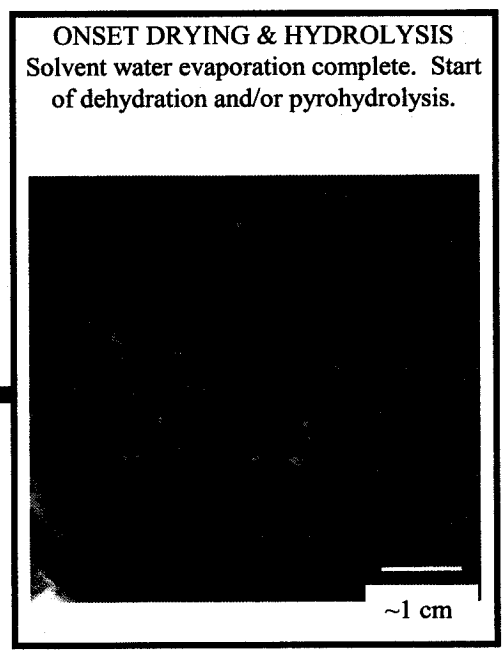

Figure 32

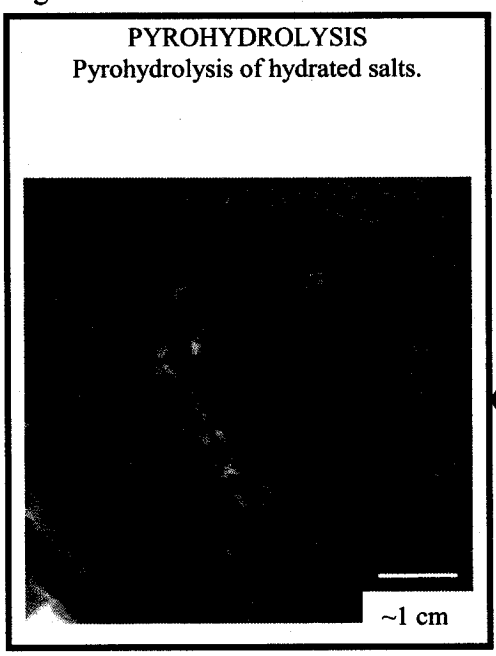

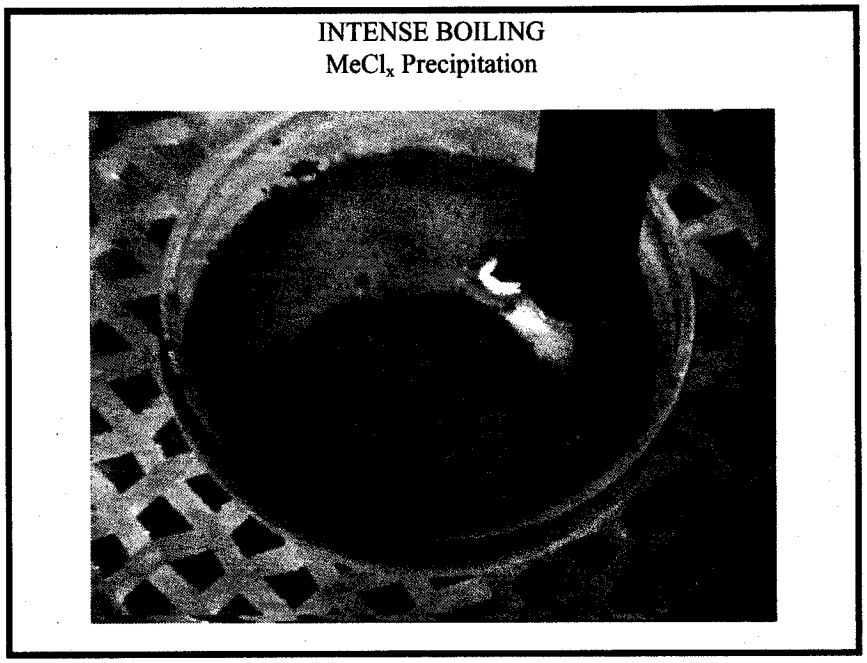

Figure 33

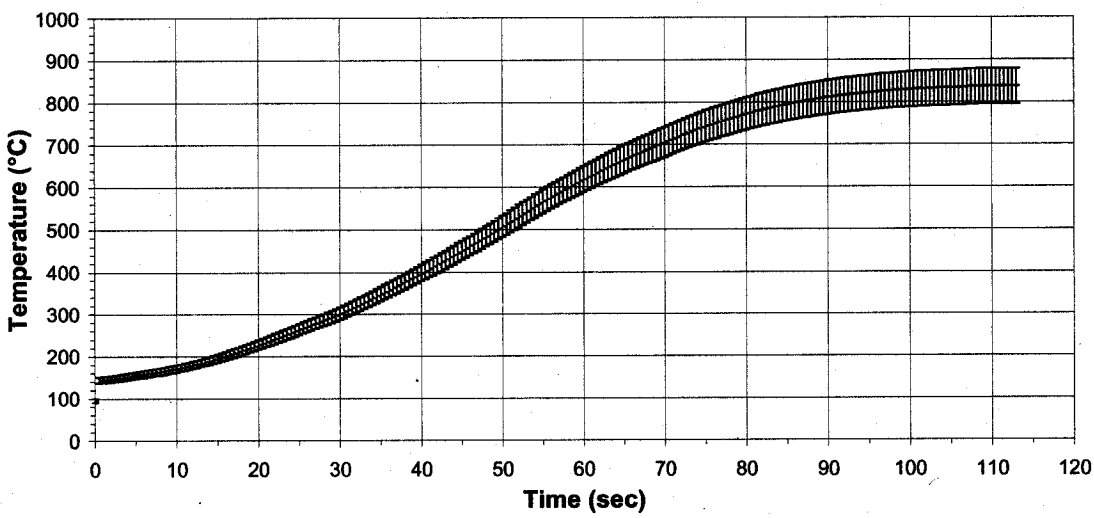

Figure 34: Average temperature profile measured upon injecting saturated chloride liquor onto hot oxides.

The various stages of transformation were initially classified by qualitative process, namely colour and state changes. The feed liquor temperature profile and fundamental considerations were used as a preliminary means of defining the phases present or the reactions taking place during each stage. Once all of the concerned phases had been observed, subsequent tests were conducted to quantify

the transformations occurring during each stage (Section 4.1.2). An initial attempt to describe the conversion process as a function of temperature (based on the profile, visual observations, and theoretical considerations) is provided in the following paragraphs.

During the intense boiling phase, the chloride solution temperature ranged from approximately 140 to 170°C. Obviously, as the saturated liquor came into contact with the hot oxide bed, the vapour pressure of the water contained within the solution increased to a level greater than atmospheric and thus favoured boiling. As H_2O is driven from the solution, the liquor becomes supersaturated and theoretically $MeCl_x \cdot yH_2O$ crystallization will occur (see Section 4.2.1). The chlorides will precipitate as hydrated salts since the crystals will be in intimate contact with a water-saturated atmosphere. The rapid rise in the solution boiling point (i.e. 30°C in 10 seconds) may be explained by the steadily increasing salt concentration. Given the differences in the solubilities of $AlCl_3$, $FeCl_2$, $FeCl_3$, and $MgCl_2$, the dissolved metal concentration will continue to rise until the saturation limit of the most soluble species (or the degree of supersaturation required for that salt to precipitate) has been reached. Increased solute concentration raises the entropy of the system by augmenting the random arrangement of molecules. For the solvent water to vaporise, the dissolved salts must precipitate, which lowers entropy because it increases the order of the system. Therefore, to vaporise the water, additional heat is required to increase the probability that all the solute atoms in any given area of the solution should leave that area by random movement. In other words, as the solute concentration increases, so must the energy required for the water to vaporise because there are greater concentrations of solute atoms that must be displaced before vaporisation can occur.

Beyond 170°C, the froth observed upon initial contact between the liquor and hot oxide particles collapsed into a thicker, slow bubbling, tar-like substance. Fundamentally, the increase in viscosity is directly related to the rise in

precipitated metal chloride crystal concentration as the solvent water continuously evolves from the solution. The viscous phase exists for approximately 15 seconds and attains a temperature of nearly 250°C. The last remaining pools of viscous liquor disappear at approximately 300°C.

In light of the aforementioned considerations and given that neither $FeCl_2$, $FeCl_3$, or $MgCl_2$, are expected to melt at such low temperatures, fundamentals would suggest that the violent boiling and solution densification stages may be characterized primarily as the liquor concentration and metal chloride ($MeCl_x$) precipitation phases. While anhydrous $AlCl_3$ can theoretically melt at 193°C, it is not very likely to occur as this salt has a very high affinity for water and the hydrated crystal has been reported to start hydrolysing at temperatures as low as 118°C.[54] It should be mentioned that the absence of any molten chloride phase during transformation was further confirmed by thermochemical modelling (see Section 4.4).

It is worth mentioning that the so-called "viscous" phase (during which the salts are precipitating) may be prolonged by hydrated metal chloride drying. In other words, the last few units of liquid phase observed during the liquor densification stage may actually be water molecules released during the dehydration of previously precipitated salts (such as $FeCl_2 \cdot 4H_2O$).

As the feed sample temperature approached 300°C, all of the solvent water appeared to have been driven from the saturated liquor, leaving behind a dark green (nearly black) hydrated crystal-like phase. Theoretical considerations would suggest that at this point, the evaporative crystallization phase is essentially complete, and any remaining hydrated metal salts begin to "dry" as the temperature continues to rise. This is further supported by visual observations which revealed that from this point onward, the colour of the sample in the crucible began to transform from black to yellow-green, which is characteristic of metal chloride crystals.

It should be mentioned that $AlCl_3 \cdot 6H_20$ decomposition is extremely favourable (thermodynamically) at a temperature of 200°C. Under oxidizing conditions, both ferrous and ferric chloride hydrolysis is also quite favourable at such low temperatures. On the other hand, these chlorides are likely to undergo a certain degree of dehydration prior to decomposition. In light of this, it is reasonable to suggest that only iron and magnesium chloride will undergo drying as per the following chemical reactions, provided that the said metal ions precipitate as pure and not complex multi-component salts.

$$FeCl_2 \cdot 4H_2O_{(s)} \rightarrow FeCl_2 \cdot 2H_2O + 2H_2O_{(g)} \quad (38)$$
$$MgCl_2 \cdot 6H_2O_{(s)} \rightarrow MgCl_2 \cdot 4H_2O_{(s)} + 2H_2O_{(g)} \quad (39)$$
$$MgCl_2 \cdot 4H_2O_{(s)} \rightarrow MgCl_2 \cdot 2H_2O_{(s)} + 4H_2O_{(g)} \quad (40)$$
$$MgCl_2 \cdot 2H_2O_{(s)} \rightarrow (MgOHCl) + HCl_{(g)} + H_2O_{(g)} \quad (41)$$

The onset of iron chloride decomposition was highlighted by yet another significant change in sample colour; from yellow-green to the characteristic terra-cotta colour of Fe_2O_3. Samples taken when the system temperature reached 750°C, after a considerable fraction of the crucible contents had turned reddish-brown, contained close to 15% Cl which suggested that the magnesium chloride had not yet fully pyrohydrolyzed.

4.1.2 Preliminary Quantification of the Transformation Process

In an effort to quantify the above-mentioned observations, a series of tests were initiated to collect data at specific points along the transformation process. In other words samples of the liquor, which had reacted to a certain degree, were taken at predefined temperatures over the profile shown in Figure 34. 0.85mL of the saturated solution was introduced onto the surface of a static 30g bed of iron oxides at 850°C. The aforementioned oxides were produced in a commercial fluidized bed waste pickle liquor regeneration facility, and were used due to the absence of any magnesium or aluminium; thereby reducing the probability of error during the mass balance calculations. The reaction was allowed to progress until the desired temperature was reached at which point the entire sample was

removed from the crucible. To generate sufficient material for chemical analysis, five repetitions were needed for each stage of transformation to produce a composite that was submitted for chemical analysis. The resulting chlorine concentration was then used to calculate the relative degree of transformation, expressed as the percentage of chlorine remaining in the feed sample as a function of time and temperature. The results are shown in Figures 35 and 36.

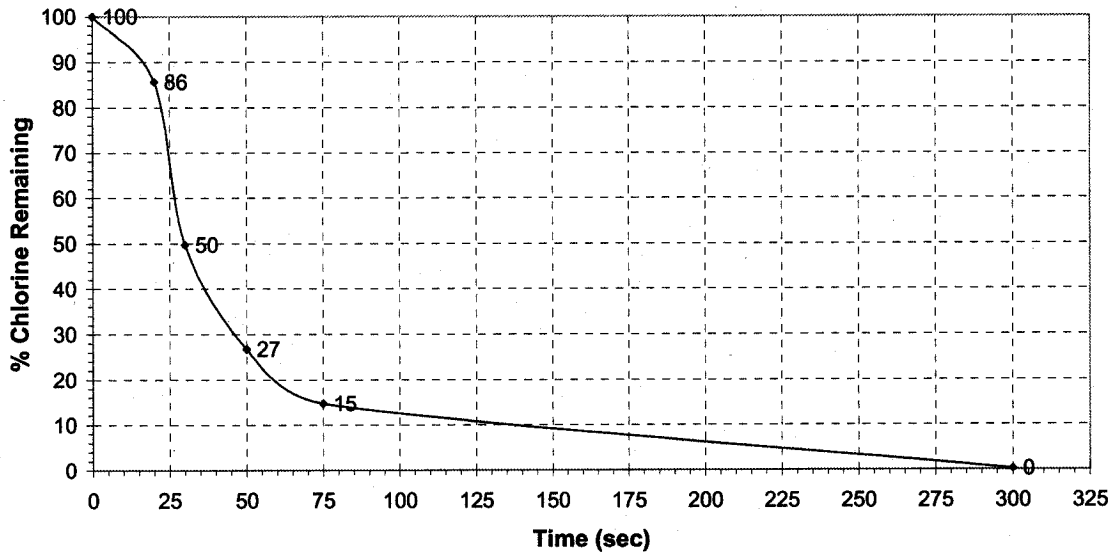

Figure 35: Degree of pyrohydrolysis expressed as a function of chlorine remaining in the starting sample over time.

As shown in Figure 36, approximately 14.5% of the chlorine in the starting solution evolved by the time that the system temperature has reached 225°C (i.e. middle of liquor densification stage). Based on fundamentals, this suggests that most of the HCl has evaporated and close to 55% of the $AlCl_3$ in the feed sample has hydrolysed. Combined, the HCl and $AlCl_3$ make up 23.2% of the chlorine units in the saturated liquor of interest.

Once the system reached 300°C, just over 50% of the originally available chlorine has been consumed. Given that the HCl, $AlCl_3$, and $FeCl_3$ make up approximately 45% of the chlorine units in the starting solution, thermodynamic considerations

would suggest that all of the aluminum and ferric chloride as well as a small fraction of the $FeCl_2$ have hydrolyzed at this time.

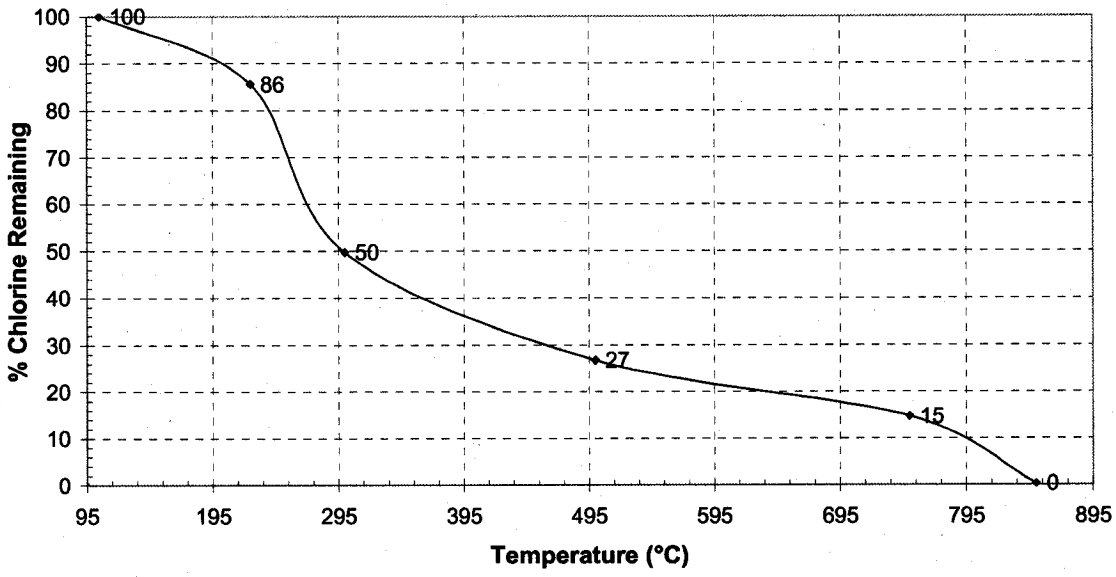

Figure 36: Degree of pyrohydrolysis expressed as chlorine remaining in the starting sample as a function of temperature.

Just under 27% of the initial chlorine units were left in the sample taken at 500°C. This result, combined with the fact that $MgCl_2$ accounts for close to 39% of the chlorine in the feed sample, indicates that all but 69% of the magnesium salts have pyrohydrolyzed at this point. Given that as much as 38% of the original $MgCl_2$ related chlorine units are still present at 750°C, it is reasonable to suggest that the hydrolysis of this salt may be kinetically and not thermodynamically controlled. The lack of H_2O vapour in the atmosphere surrounding the sample, with the given experimental set-up, may also be partially to blame for incomplete $MgCl_2$ conversion at 750°C. On the other hand, Figures 35 and 36 do show that given enough time, the magnesium salt will fully decompose at 850°C.

4.1.3 Implications on Commercial Reactor Performance:

In an effort to help further explain the aforementioned observations and their impact on fluidized bed reactor performance, the temperature profile measured during the transformation of the saturated Al-Fe-Mg-Cl solution was compared to that generated during the pyrohydrolysis of a typical waste pickle liquor (i.e. saturated, primarily $FeCl_2$ solution). These spent solutions are reported to contain 85-95% ferrous and 5-15% ferric.[1] Clearly, the phases observed upon injecting the saturated ferrous chloride liquor onto the hot oxide bed is similar to that of the Al-Fe-Mg-Cl system; intense boiling, followed by solution densification, dehydration, and hydrolysis. The main difference is that the duration of each of these phases is much shorter, and the reacting sample reaches the system operating temperature in 30% less time.

As shown in Figure 37, once the $FeCl_2$ solution comes into contact with the hot surface, it boils at a constant temperature of 119°C for approximately 7.5 seconds, before the vigorously bubbling froth collapses into the viscous phase. This observation may be explained by the fact that once saturated in $FeCl_2$, the boiling point remains constant until the majority of the solvent has evaporated and the salt precipitated. Under the same conditions, it takes closer to 10.5 seconds to densify the Al-Fe-Mg-Cl liquor into the dense tar-like sludge. This is due to the presence of $MgCl_2$ and much more significant quantities of $FeCl_3$ (which have higher solubilities) in the system; therefore, higher degrees of solution concentration must be reached before these salts precipitate. The duration of the crystal drying and decomposition phases were also observed to be much shorter with the iron chloride solution. This is, once again, explained by the fact that there is only one and not a multitude of salts (with differing solubilities and stabilities) that needs to undergo dehydration and hydrolysis.

Given that fluidized bed pyrohydrolyzer performance is dependant on the need for the majority of the injected liquor to coat and react on existing particle surfaces,

the impact of the aforementioned observations on the process are rather straightforward. The longer it takes for the chlorides to precipitate from solution, to provide the relatively hot crystals with the opportunity to adhere to bed particles and to fully transform, the higher the probability that the incoming liquor will be carried off by the fluidizing gas. This, in turn, favours an inefficient recirculating loop and negatively impacts on process performance. Solid chlorides are known to be quite sticky at elevated temperature.

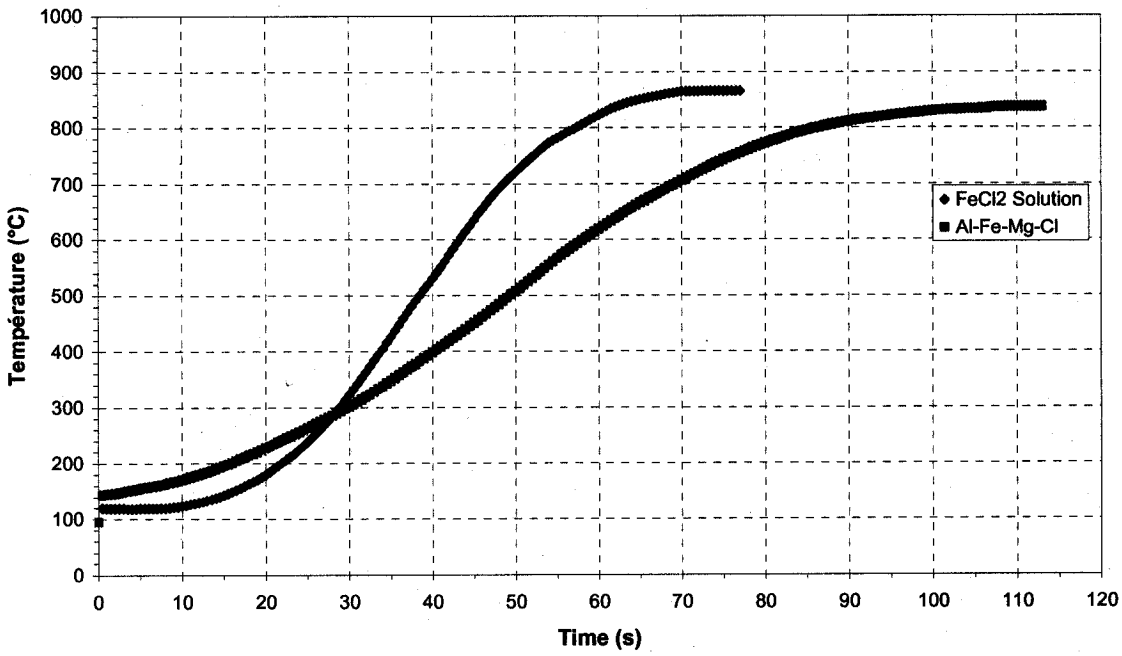

Figure 37: Average temperature profile observed upon injecting saturated $FeCl_2$ and Al-Fe-Mg-Cl solutions onto hot oxide surface.

Clearly, given that typical fluidized bed reactor operating conditions (i.e. atmosphere, dynamics, heat flux/unit volume of solution, etc...) were not simulated during the simplified pyrohydrolysis experiments, all of the above-mentioned findings may only be considered as indicative of what truly takes place. On the other hand, the trials were quite instrumental in generating a preliminary understanding of the mechanisms by which the Al-Fe-Mg-Cl solution of interest transforms into oxide. Furthermore, the corresponding test results served to

define the nature of the experimental studies that needed to be performed to further elaborate on the sequence of reactions that take place as the saturated liquor temperature increases within the pyrohydrolyzer (i.e. Phase II and III testwork).

4.2 Phase II: Crystallization Path During Evaporation

4.2.1 Fundamentals:

In the hydrometallurgical industry, crystallization is a process that involves precipitating a solid phase from an aqueous solution that is usually laden with dissolved metals. Crystallization takes place via nucleation and growth. Nucleation may occur spontaneously (i.e. homogeneous), or may require the presence of some type of solid-liquid interface upon which the crystal will form (i.e. primary heterogeneous or secondary). Primary heterogeneous refers to the precipitation of a salt onto the surface of a solid compound of similar composition, while crystallization that takes place on a foreign object (i.e. dissimilar to aqueous species of interest) is referred to as secondary (or surface) nucleation.

The driving force behind nucleation and growth is supersaturation. An aqueous solution has the capacity to dissolve a fixed quantity of a metallic species at a given temperature and pressure. This is referred to as the solubility or saturation limit. The solubility of a metal species can actually increase or decrease with temperature and is dependant upon the presence of other ions in solution. Based on crystallization fundamentals, the dissolved salt concentration must exceed the solubility limit before the metal compound of interest can precipitate from the liquor. A supersaturated solution is characterized by significant solute concentrations that lead to extensive ion-association (due to a reduction in a_{H2O}) and ultimately fosters electrically neutral ion-pair formation. Supersaturated liquors favour the aggregation-polymerization of the solute species that promotes ion-pair/molecule cluster formation (10-1000 monomers per cluster).

As shown in Figure 38 for a classic cooling crystallization system, when the temperature (T_F) of a dissolved metal bearing solution drops to T*, it is essentially saturated in that species. Upon further cooling, the liquor enters a metastable zone where crystal growth occurs, provided that a solid surface is available. No spontaneous nucleation takes place at this point. Once the system temperature drops below T_M, it enters the labile zone where both crystal growth and nucleation can occur simultaneously and compete for solute.[82] Clearly, a higher degree of supersaturation is needed for primary homogeneous nucleation to occur.

While many of the solid phases that precipitate from aqueous solutions are originally amorphous in nature, they will eventually age to form a crystalline compound. Generally, high solution temperatures and lower degrees of supersaturation favour the formation of crystalline salts upon precipitation.[85]

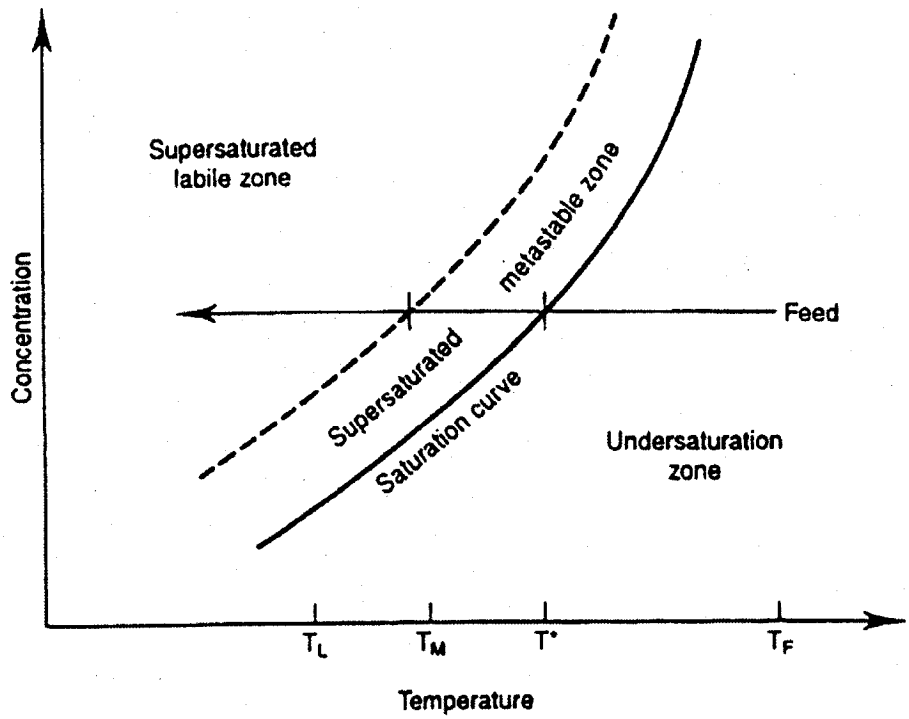

Figure 38: Classic solubility and supersaturation curves for a salt bearing aqueous solution.[82]

These same principles hold true for evaporative crystallization. In this case, the solution is being concentrated in metallic salts by driving off water molecules from the liquor. Therefore, each of the dissolved species will eventually reach and exceed their respective saturation limits and ultimately result in the precipitation of the corresponding salts from solution. Given that no solid particles were present in the Al-Fe-Mg-Cl starting solution, a relatively high degree of supersaturation was required to initiate the crystallization process.

4.2.2 Crystallization Sequence & Resulting Compounds:

Crystallization studies are typically performed to obtain solubility data for a system of interest at specific conditions (i.e. temperature and pressure). Therefore, the related apparatus and test procedures are usually designed to ensure that equilibrium conditions exist between the liquid and solid phases. In this particular case the experiments were performed under pseudo-equilibrium conditions (Section 3.1.5 & 3.2.2), as the main objectives were to define the order in which the aluminium, ferrous, ferric, and magnesium salts precipitate as the solvent water is driven from the liquor, as well as to identify the resulting solid phases. Efforts were not geared toward defining solubility limits of the individual metal chlorides or the degree of supersaturation required for precipitation to occur.

The sequence in which the dissolved $MeCl_x$'s precipitate was determined by plotting actual salt concentrations alongside theoretical values (based on the amount of water removed alone), both as a function of the degree of evaporation (DOE). The results for the individual metal chlorides are shown in Figures 39 through 42. The onset of crystallization for each of the salts is defined as the point at which the actual and theoretical metal chloride concentrations begin to deviate considerably. The composition of the crystal samples recovered from the liquor at various degrees of evaporation, were also used to support any conclusions drawn through the analysis of the previously mentioned data.

As a reminder, the saturated Al-Fe-Mg-Cl liquor of interest was diluted (1 part water per 3 parts liquor, on a volume basis), and the resulting mixture was used as the starting solution for the evaporative crystallization experiments. The dilution water is eliminated from the mixture (i.e. typical pyrohydrolyzer feed) as the DOE approaches 32%.

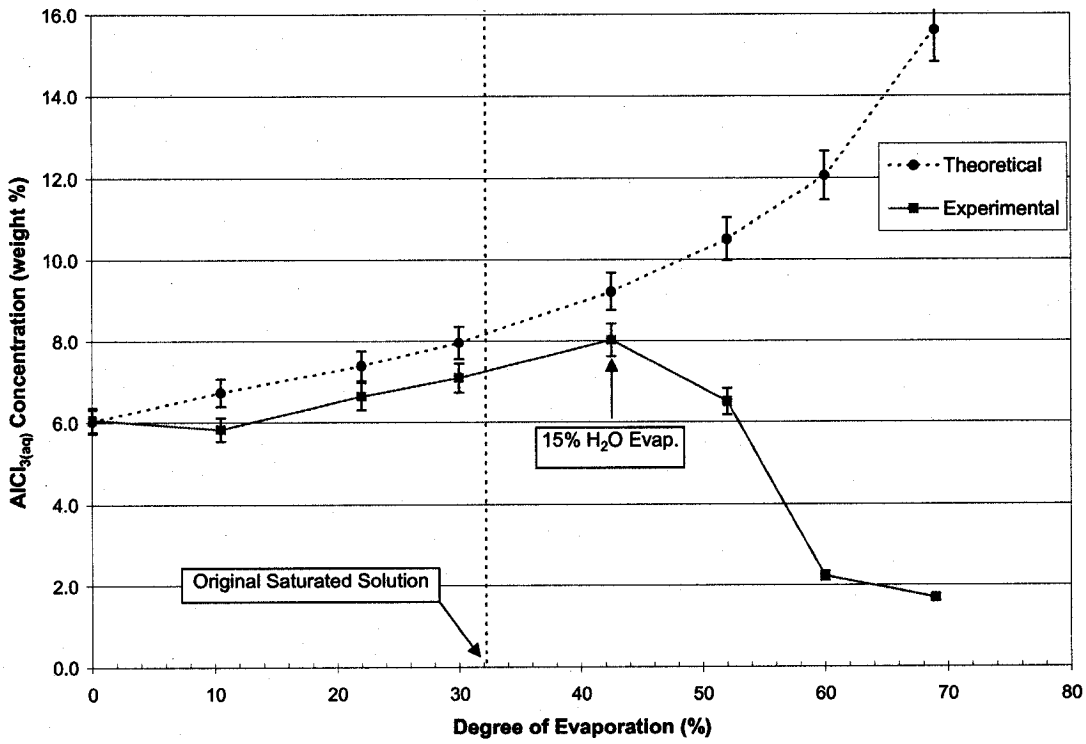

Figure 39: $AlCl_{3(aq)}$ concentration as a function of the degree of evaporation.

In light of this, Figure 39 reveals that the aluminium chloride precipitates once at least 15% of the solvent water has evaporated from the original saturated (undiluted) liquor (i.e. DOE > 42.5%). This observation coincides with the corresponding profile for P_{HCl} as a function of solution concentration, which is not presented for confidentiality reasons. It reveals that the partial pressure drops significantly after increasing exponentially to the peak observed at a DOE of approximately 45%. This decrease in P_{HCl} indicates that the equilibrium of the system has been disturbed and suggests that $MeCl_x$ precipitation has begun. Clearly, as long as all the metal

chlorides remain in solution, HCl will be driven from the aqueous phase in increasing quantities (due to rising degrees of supersaturation) during evaporation, as it is the most volatile of all in the system of interest. Once a salt begins to precipitate from the solution, the degree of supersaturation rises less dramatically with the DOE, and the HCl is not as compelled to evolve with the solvent water. This argument is supported by a levelling off of the P_{HCl} between DOE's of 50-60%. Further increases in the partial pressure of HCl will occur if the solution concentration (or H_2O evaporation) rate exceeds the $MeCl_x$ precipitation rate. This phenomena was observed as the degree of evaporation approached and exceeded 70%. While the onset of $MeCl_x$ precipitation could not be based on visual observations due to the rather opaque (nearly black) nature of the saturated solution, it is worth mentioning that yellow crystals were first observed on the kettle walls and on the impeller shaft at a degree of evaporation of approximately 50%.

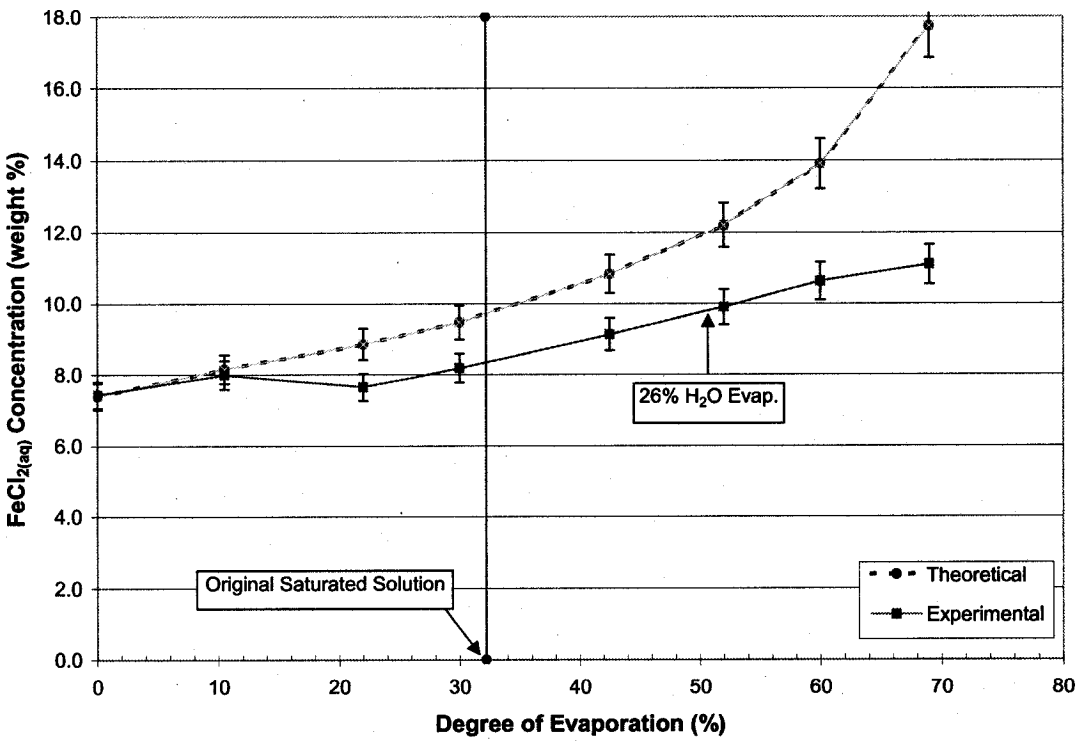

Figure 40: $FeCl_{2(aq)}$ concentration as a function of the degree of evaporation.

Ferrous and magnesium chloride crystallization take place when approximately 26% and 41% of the solvent water has evolved, respectively (Figures 40 and 41). As shown in Figure 42, ferric chloride remains in solution even after 54% of the solvent water has been driven from the saturated liquor (i.e. DOE = 69%). This is no surprise since ferric is extremely soluble in high temperature HCl systems. The solids density at this point was calculated to be 31.5wt%. As mentioned in Section 3.2.2.1, while it was possible to evaporate as much as 74% of the water in the starting solution, no meaningful liquor or crystal samples were recovered for analysis due to instantaneous crystallization during liquor manipulation at this DOE.

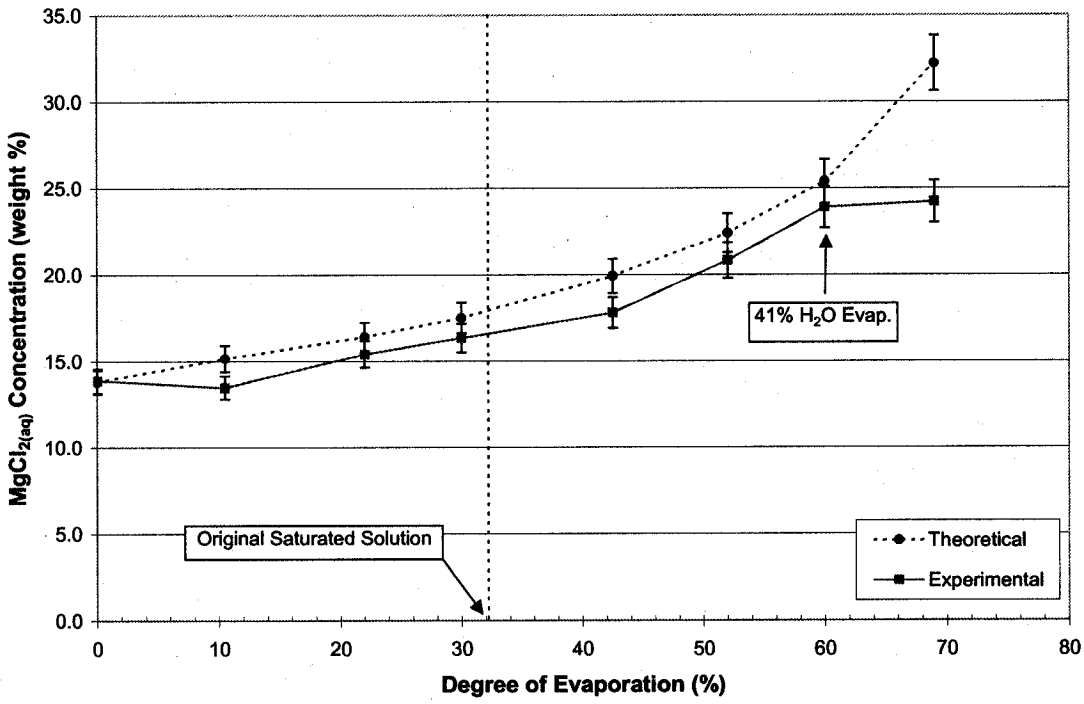

Figure 41: $MgCl_{2(aq)}$ concentration as a function of the degree of evaporation.

The above-mentioned crystallization sequence is generally supported by the XRD analyses of the crystal samples taken at DOE's of 53%, 60%, and 69% (which correspond to the evaporation of 30.7, 41.0, and 54.3% of the solvent water in the original saturated liquor, respectively). As shown in Figures 43 through 45, the line

complexity in the crystal sample spectra increases with solution concentration, which suggests the presence of several different types of $MeCl_x$ salts.

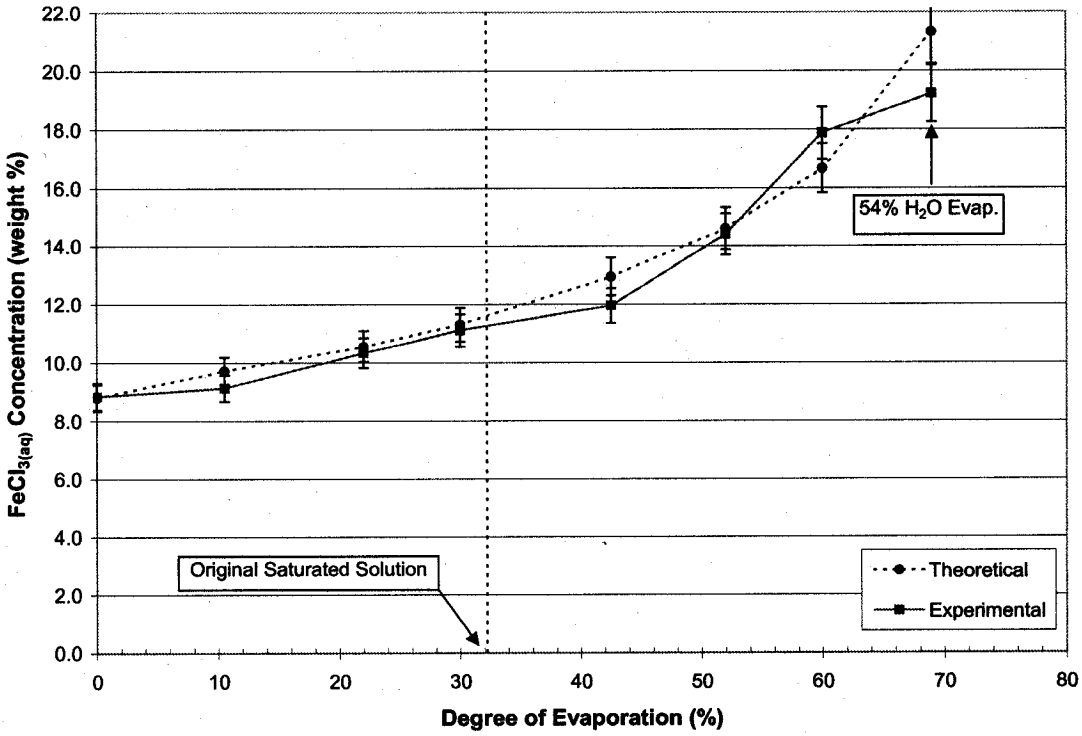

Figure 42: $FeCl_{3(aq)}$ concentration as a function of the degree of evaporation

Based on the XRD pattern shown in Figure 43, $AlCl_3 \cdot 6H_2O$ is clearly the dominant phase present in the crystals recovered after 30.7% of the water in the typical pyrohydrolyzer feed solution is eliminated. The presence of reasonable quantities of $FeCl_2 \cdot xH_2O$ (where x = 2 or 4) confirms the onset of ferrous chloride precipitation. The faint $MgCl_2 \cdot 2H_2O$ signals would suggest that the presence of this chloride is due to entrained liquor between and on the surface of the crystals. This argument is further supported by ICP analyses of the crystals that indicate the presence of ferric in this sample (which is known not to precipitate). Despite dedicated efforts to thoroughly wash the crystals with diethyl ether, liquor entrainment between the crystals could not be eliminated without damaging the chloride particles.

The crystals retrieved from the solution at a DOE of 60% (Figure 44) were composed of $AlCl_3 \cdot 6H_2O$, $FeCl_2 \cdot 2H_2O$, and $MgCl_2 \cdot xH_2O$ (where x = 2 or 4) with the tetrahydrate being most prominent. Based on the XRD data of the samples recovered at a DOE of 53 and 60%, as well as the analytical results presented in Figures 39 to 41, the crystallization sequence may be summarized as follows: $AlCl_3 \cdot 6H_2O$ precipitates first, followed by $FeCl_2 \cdot xH_2O$ (where x = 2 or 4), and then $MgCl_2 \cdot 4H_2O$.

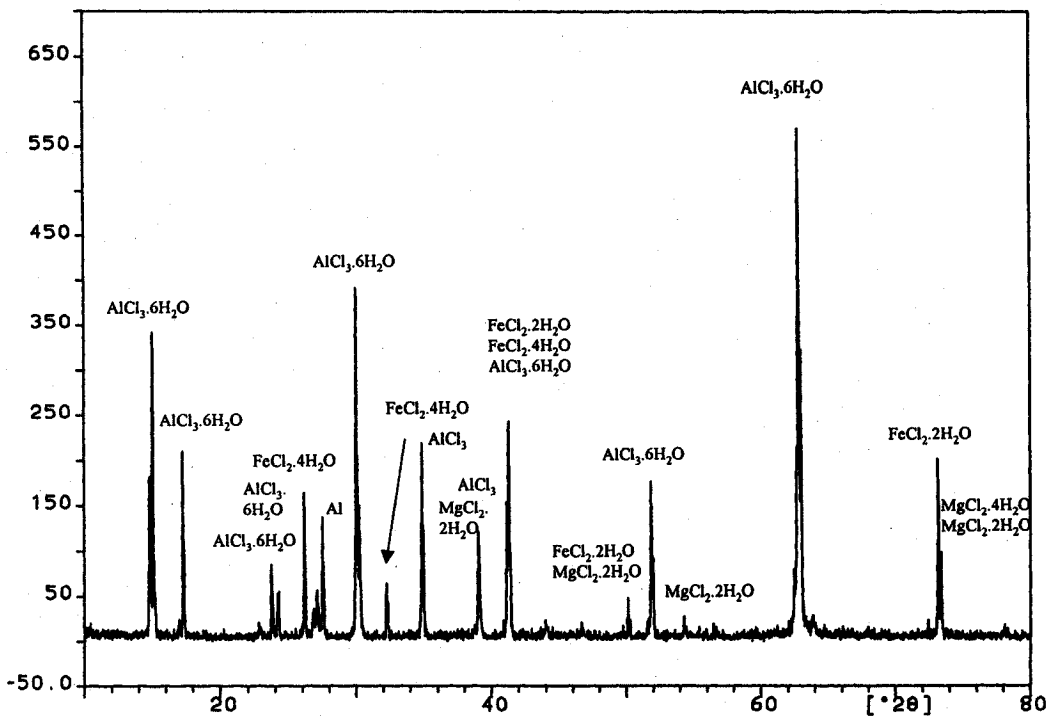

Figure 43: XRD spectra of crystal sample recovered from the solution at a DOE of 52,9%.

Interestingly enough the crystals recovered at a DOE of 69% are composed primarily of $AlCl_3 \cdot 6H_2O$, with small quantities of $FeCl_2 \cdot 2H_2O$, $MgCl_2 \cdot xH_2O$ (where x = 2 or 4) and even anhydrous $FeCl_2$ (see Figure 45). Further ICP and EDS analyses (see Sections 4.2.2.1 & 4.2.2.2) suggest that the XRD results for this particular sample are misleading. A thorough review of the analytical data and experimental procedures suggest that the apparent decrease in ferrous and magnesium chloride salt content is actually due to the washing of the crystals. As

mentioned previously, increasing amounts of the rather hygroscopic diethyl ether were used to rinse the crystals recovered at the higher DOE's. Therefore, it is reasonable to suggest that waters of hydration were stripped away from any $FeCl_2 \cdot xH_2O$ (where x = 2 or 4) during washing. This would explain the presence of the anhydrous $FeCl_2$ in the concerned sample, as well as the absence of any $FeCl_2 \cdot 4H_2O$ in the crystals collected at a DOE of 60%. In fact, based on all of the aforementioned XRD results, the degree of ferrous chloride hydration appears to decrease with increased level of washing. While technically possible, the organic washing agent is not believed to have stripped any significant amounts of crystallization waters from the $MgCl_2 \cdot xH_2O$, as it is also quite hygroscopic. On the other hand, it is possible that the ferrous and magnesium salts are somewhat soluble in the diethyl ether and that the crystal structure was being damaged during sample rinsing. In such a case, the presence of the corresponding salts would not be detected by XRD.

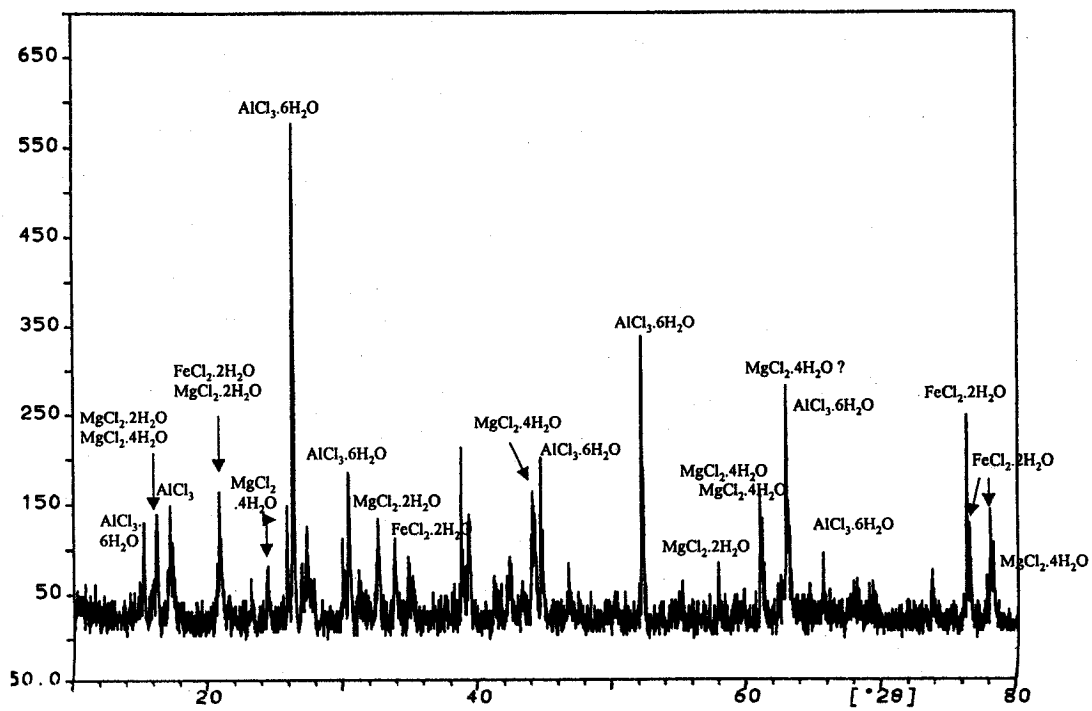

Figure 44: XRD spectra of crystal sample recovered from the solution at a DOE of 60%.

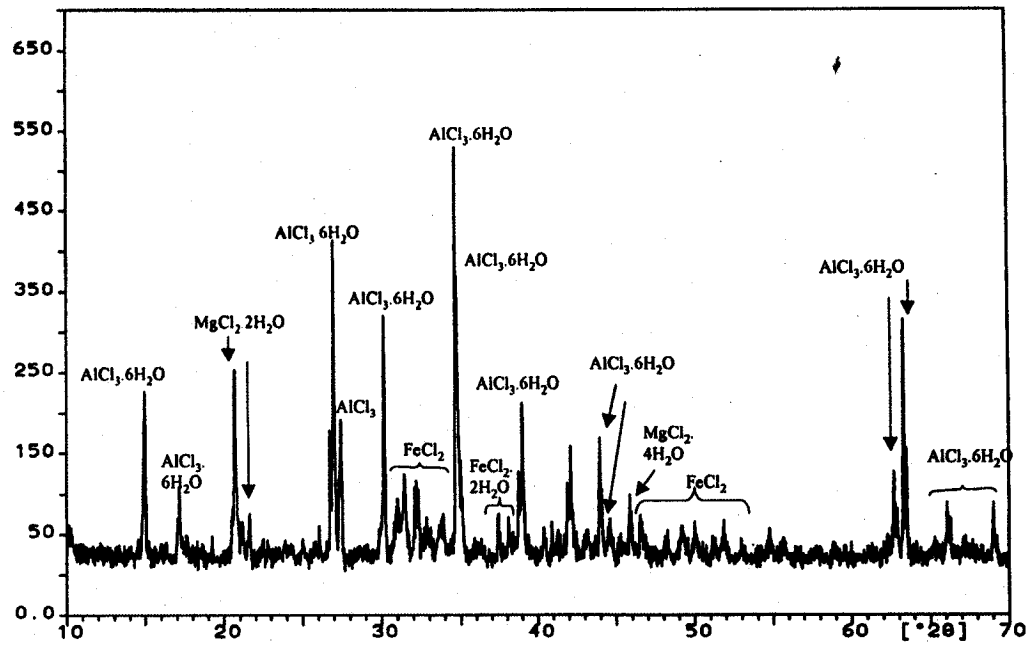

Figure 45: XRD spectra of crystal sample recovered from the solution at a DOE of 69%.

While the XRD data tends to support the solution concentration profiles shown in Figures 39-42 for the most part, it is worth recalling that this analytical technique is qualitative and the results must be interpreted with care. Analytical error arises from the fact that the spectral lines of different $MeCl_x$'s may actually overlap and the presence of several species in one sample may cause certain peaks of the resulting XRD pattern to shift. Moreover, standard spectra for complex multi-component chlorides may not even be available in the database. Therefore, certain unexplainable observations, such as the presence of anhydrous $FeCl_2$, may actually be due to the inaccuracies of this analytical technique.

4.2.2.1 Crystal Analyses by ICP:

In an effort to validate the XRD data, the crystal samples recovered at the various DOE's were dissolved and submitted for analysis by ICP. The results are reported as wt% of the salts in their expected hydrated form in Table 5.

Table 5: Chemical composition of the crystal samples collected during the experiments.

% DOE	Chemical Composition (wt%)			
	$FeCl_2 \cdot 2H_2O$	$FeCl_3$	$AlCl_3 \cdot 6H_2O$	$MgCl_2 \cdot 6H_2O$
53	0.0	1.8	94.8	2.9
60	3.3	2.6	87.9	6.1
69	9.1	3.5	66.5	20.6

The presence of any ferric in the crystal samples may be explained by liquor entrainment (i.e. insufficient washing) and was arbitrarily assumed to be in anhydrous form. While the XRD analyses suggest that magnesium chloride precipitated as a di- or tetra-hydrate, it was assumed to be present as $MgCl_2 \cdot 6H_2O$ in the crystals submitted for analysis. This may be explained by the fact that magnesium chloride is extremely hygroscopic. As a result, despite every effort to avoid moisture pickup prior to analysis, previous experience suggested that a certain degree of $MgCl_2 \cdot xH_2O$ (where x = 2 or 4) hydration would occur. Based on the XRD data, the iron was assumed to be in the form of a dihydrate. It should be mentioned that these were the very first assumptions made by the author, and interestingly enough, the resulting chemical composition of the crystals added up to $99\%^+$ in all three cases.

Surprizingly, unlike the previously reported results (i.e. Figures 39 and 42), the crystal sample taken at a DOE of 53% appeared to contain negligible quantities of $FeCl_2 \cdot 2H_2O$. This observation may be related to the fact that a very small amount of crystals (i.e. 1g) was used for analysis; therefore, the sample may not have been representative of the bulk. In fact, the composition suggests that the concerned crystals were literally pure $AlCl_3 \cdot 6H_2O$. The presence of ferric and magnesium chloride are clearly due to liquor entrainment between the crystals. The absence of any $FeCl_2$ (which should have been entrained as well) indicates that sampling or

analytical error may have occurred, or that the diethyl ether may have dissolved the small amount of ferrous present in the bulk sample.

If one were to assume that the $MgCl_2$ and $FeCl_3$ were entrained in the same proportion as in the first sample recovered and that ferric concentration is the most reliable indicator of the amount of liquor entrained, mass balance calculations indicate that the crystals collected at a DOE of 60% are actually composed of 94.4% $AlCl_3 \cdot 6H_2O$, 3.5% $FeCl_2 \cdot 2H_2O$, and 2% $MgCl_2 \cdot 4H_2O$. This coincides with the previously reported results which suggest that once 60% of the water in the starting solution has evolved, ferrous and magnesium chloride will have precipitated from the liquor as well. The rather high $AlCl_3 \cdot 6H_2O$ concentration may be explained by the fact that the crystals submitted for analysis are essentially composed of a bulk sample of all the salts present within the slurry at any given time. Therefore, given that the aluminium chloride starts to precipitate well before the others, and that its concentration in solution also drops much more dramatically (Figure 39), the relative amount of $AlCl_3 \cdot 6H_2O$ in the bulk crystal sample taken at a DOE of 60%, will obviously remain very high. While the solution concentration curves suggest that ferrous chloride starts precipitating at considerably lower DOE's than magnesium, one might have expected a much higher $FeCl_2 \cdot 2H_2O$ concentration relative to $MgCl_2 \cdot 6H_2O$. The observed deviation may, once again, be explained by the fact that a fraction of the ferrous chloride salt was dissolved by the diethyl ether during sample washing.

Using the same methodology described above, the crystal sample recovered at a DOE of 69% consists of 73.4% $AlCl_3 \cdot 6H_2O$, 10% $FeCl_2 \cdot 2H_2O$, and 16.6% $MgCl_2 \cdot 4H_2O$. These results suggest that either magnesium chloride crystallization is more favourable (for thermodynamic reasons, perhaps) at the given conditions, the nucleation and growth kinetics are faster than those of $FeCl_2 \cdot 2H_2O$, or that the concentration of the latter was negatively affected by sample washing. Moreover, these ICP results further support the claim that the XRD data for the same sample is

not as representative of the chemical composition, especially from a quantitative point of view.

4.2.2.2 SEM and EDS Analysis of the Crystals:

Scanning Electron Micrographs of the aforementioned crystal samples are shown in Figures 46, 47, and 48.

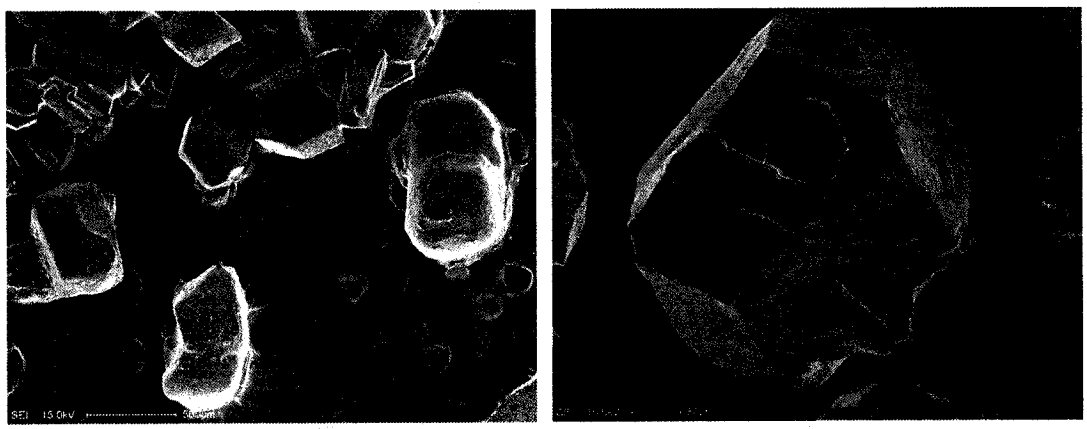

A B

Figure 46: SEM micrograph of crystals recovered at a DOE of 53%. A) Mag. x40, B) Mag. x200.

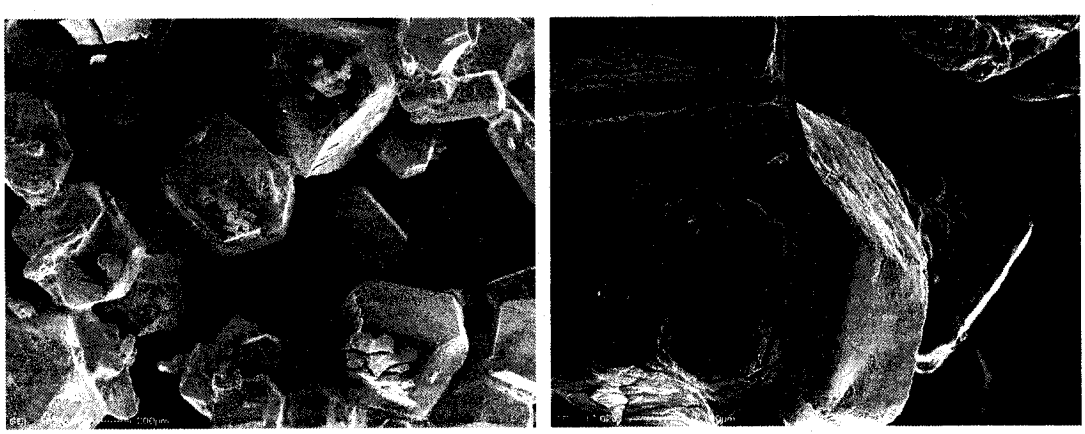

A B

Figure 47: SEM micrograph of crystals recovered at a DOE of 60%. A) Mag. x40, B) Mag. x200.

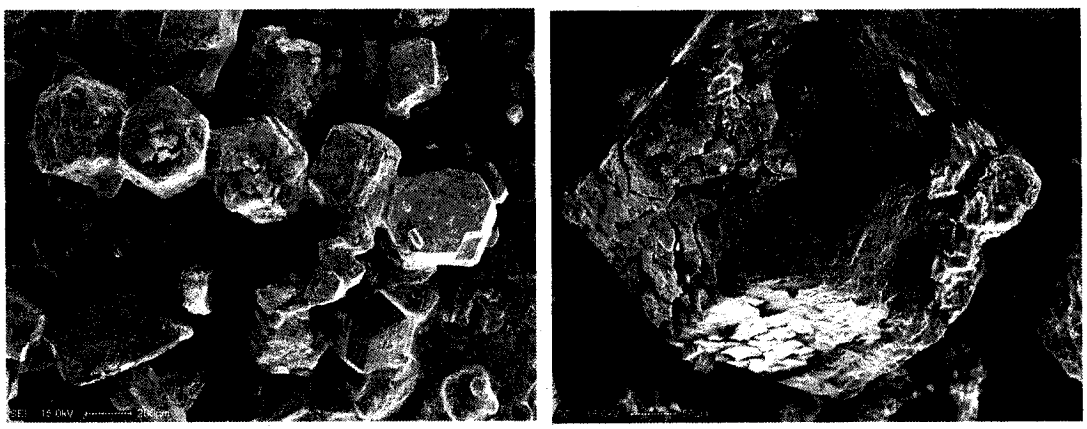

A B

Figure 48: SEM micrograph of crystals recovered at a DOE of 69%. A) Mag. x40, B) Mag. x200.

Generally speaking, the images illustrate that the evaporative crystallization procedure resulted in the production of relatively clean, well-formed individual $MeCl_x$ crystals of polygonal shape with remarkably sharp edges. The texture of the crystals recovered at the lower degrees of evaporation (i.e. 53 and 60%) is rather uniform, and close examination does not reveal any significant signs of pores or cracks. As the solution becomes more concentrated, the surface of the corresponding crystals is rougher (see Figure 47B) and started showing signs of cracking. This is most likely due to attrition that results from collisions between the soft crystals (which are present in much more numerous quantities at higher DOE's), and with the impeller blades or reactor walls. A significant fraction of the crystals recovered at a DOE of 69%, were obviously present in the slurry for a much longer period of time than those sampled from the less concentrated slurry. Furthermore, the figures reveal the appearance of an increasingly noticeable crust layer on the surface of the crystals with rising DOE. This may be explained by the fact that as the liquor density and degree of supersaturation increases, the probability that a fraction of the solution remains trapped between crystals and that the corresponding $MeCl_x$'s precipitate there also rises. This observation

supports the ICP results that revealed increasing ferric chloride concentration in the crystals recovered at higher DOE's.

Based on the micrographs, it appears as though all of the crystals in any one sample examined by SEM are essentially the same. On the other hand, the XRD and ICP analyses have clearly revealed that each of the concerned samples is composed of more than one type of salt. As a result, EDS was used to perform spot analyses on various crystals within a given sample to determine whether any significant differences in composition would be observed. The resulting spectra were relatively constant. Furthermore, EDS analyses revealed that while the Fe and Mg concentrations of the individual crystals increase with the DOE, the aluminium content drops. These observations would suggest either the formation of complex chlorides, or that the ferrous and magnesium are simply precipitating on the surface of the previously formed $AlCl_3 \cdot 6H_2O$ crystals. In fact, once the DOE surpasses 60%, the $AlCl_3$, $FeCl_2$, and $MgCl_2$ are competing for surfaces to precipitate on; therefore; the formation of crystals with various and perhaps alternating layers of $AlCl_3 \cdot 6H_2O$, $FeCl_2 \cdot 2H_2O$, and $MgCl_2 \cdot 4H_2O$ is quite probable. Moreover, in light of the fact that aluminium chloride starts precipitating well before the others, the core of most crystals will most likely be composed of that hydrated salt.

Given that EDS analyses can vary by as much as +/-20% and are therefore rather subjective, it would be very difficult to define the true form of the crystals (i.e. complex or layered) or to provide an undisputable description of the mechanisms of formation. It is generally accepted that for reliable EDS analyses, a polished, flat, homogeneous sample is required. This is physically impossible to achieve with a single crystal. The previously mentioned results were base on performing EDS analyses on the flattest possible surfaces available within a crystal sample.

On the other hand, as far as pyrohydrolysis is concerned, the important thing to retain from the EDS results is that the chlorides will most likely salt out as

intimately mixed crystals during the vigorous boiling phase. This conclusion is further supported by the fact that the duration of the crystallization process that occurs in the fluidized bed reactor, is order of magnitudes shorter than that of the aforementioned experiments; therefore, co-precipitation and the formation of mixed crystals is inevitable.

4.2.3 General Comments:

As mentioned previously, the evaporative crystallization experiments were performed in an effort to define the $MeCl_x \cdot yH_2O$ precipitation sequence that occurs as the Al-Fe-Mg-Cl liquor of interest is exposed to typical pyrohydrolyzer operating conditions. Given that the gradually increasing temperature profile or the dynamics observed during the Phase I study were not reproduced, the corresponding test results serve as a first approximation of the manner in which $MeCl_x$'s crystallize during the vigorous boiling phase

Despite some of the discrepancies observed in the results, the XRD data for the samples recovered at DOE's of 53 and 60% together with the analytical results presented in Figures 39 to 41, suggest that $AlCl_3 \cdot 6H_2O$ precipitates first, followed by $FeCl_2 \cdot xH_2O$, and then ultimately by $MgCl_2 \cdot xH_2O$ (where x=2 or 4). While it is difficult to conclude whether the chlorides precipitate independently or as complex compounds, the SEM and EDS data indicate that once 41% of the solvent water in the saturated liquor has evolved, the formation of crystals with various and perhaps alternating layers of $AlCl_3 \cdot 6H_2O$, $FeCl_2 \cdot xH_2O$, and $MgCl_2 \cdot xH_2O$ is quite probable. It also appears as though the core of most crystals will very likely be composed of the former most. This may complicate the overall transformation process, as aluminium chloride is also the first salt to hydrolyse. With regards to $FeCl_3$, it is expected to remain in solution to very high DOE's, since it did not precipitate even after 54% of the solvent water had evaporated at 105°C, and its solubility actually increases with temperature. As mentioned in Section 4.1.1, the liquor temperature actually rose to 250°C during the densification (i.e. $MeCl_x$ precipitation) stage.

It is worth mentioning that based on the results of a few additional evaporative crystallization experiments overseen by the author, the total amount of HCl that evolves from the solution at a DOE of approximately 70% increases with temperature (i.e. 60% for 105°C vs. 70% for 130°C). Therefore, the assumption that all of the HCl has evolved from the feed liquor at 225°C (see Section 4.1.2) is valid.

4.3 Phase III: Characterizing Solution Transformation as a Function of Temperature

4.3.1 Summary of Results:

The saturated Al-Fe-Mg-Cl liquor transformation profile, obtained by allowing the solution to react in the presence of a simulated pyrohydrolyzer atmosphere at a series of temperatures for close to an hour, is expressed as a percentage of chlorine loss versus temperature in Figure 49. Given that a little over 95% of the chlorine within the feed solution is consumed as the system temperature approaches 600°C, it is reasonable to conclude that excluding diffusion or kinetic effects, the overall conversion process occurs primarily over the 300 to 600°C temperature range.

The XRD analyses of the reaction product samples retrieved from the furnace at 300, 400, 500, 600, 700, and 800°C (see Figures 50-55), confirms that the transformation of the multi-component metal chloride solution proceeds in step-wise fashion.

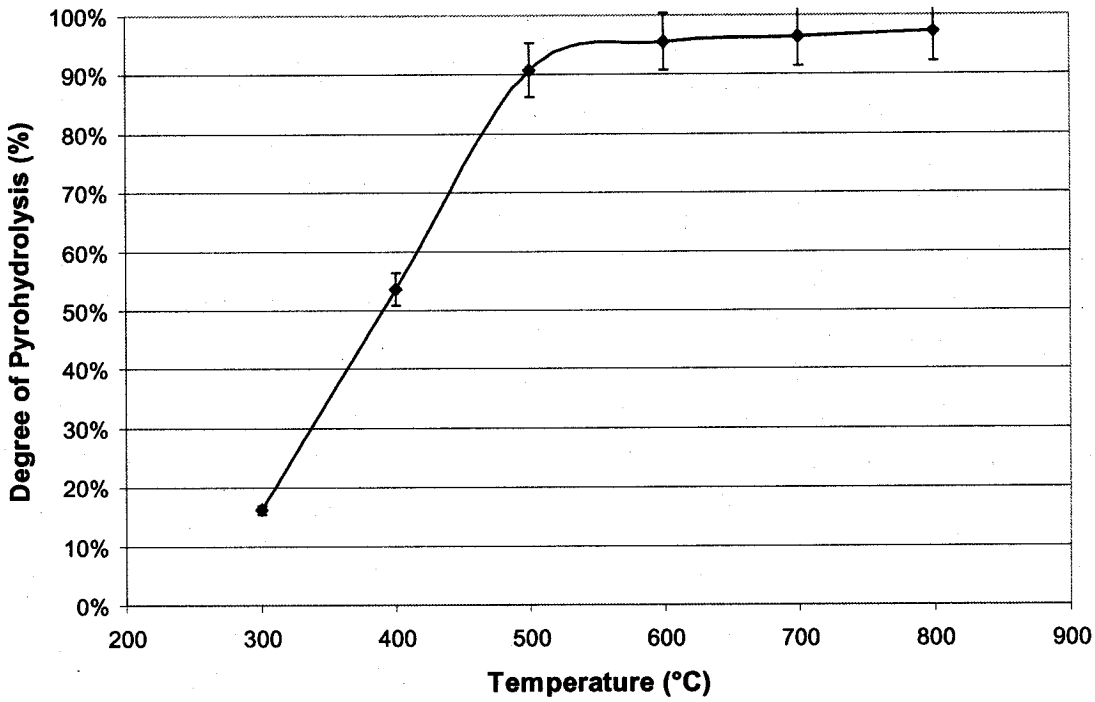

Figure 49: Degree of pyrohydrolysis versus temperature.

As suggested by the simplified pyrohydrolysis experiments, the XRD data (Figure 50) along with the results shown in Figure 49 lend further support to claims that the dissolved $MeCl_x$'s are primarily precipitating and undergoing dehydration as the reactor feed solution temperature increases to 300°C. XRD analysis of the sample that was allowed to react at this temperature shows the presence of bischofite (25-0515), magnesium hydroxy-chloride (03-0100), and hematite (33-0664). The unidentified peak at 5.36Å is believed to be low-symmetry iron hydroxy-chloride. Based on thermodynamics and other experimental observations[54], the $AlCl_3 \cdot 6H_2O$ should have pyrohydrolyzed; therefore, the absence of any alumina is most likely due to the fact that this phase is primarily amorphous in nature.[86] The presence of hematite may be explained by the partial thermal decomposition of $FeCl_3$. Given that 29,8% of the chlorine within the starting solution was consumed (see Figure 49), fundamental considerations and the starting solution composition would suggest that at 300°C, the residual HCl has completely

evaporated, and that most of the $AlCl_3$ as well as some $FeCl_3$ have pyrohydrolyzed. Assuming that 90% of the $AlCl_3$ in the feed liquor has decomposed and that only the ferric has also undergone conversion, mass balance calculations would suggest that close to 30% of the ferric chloride has also reacted once the solution reaches 300°C.

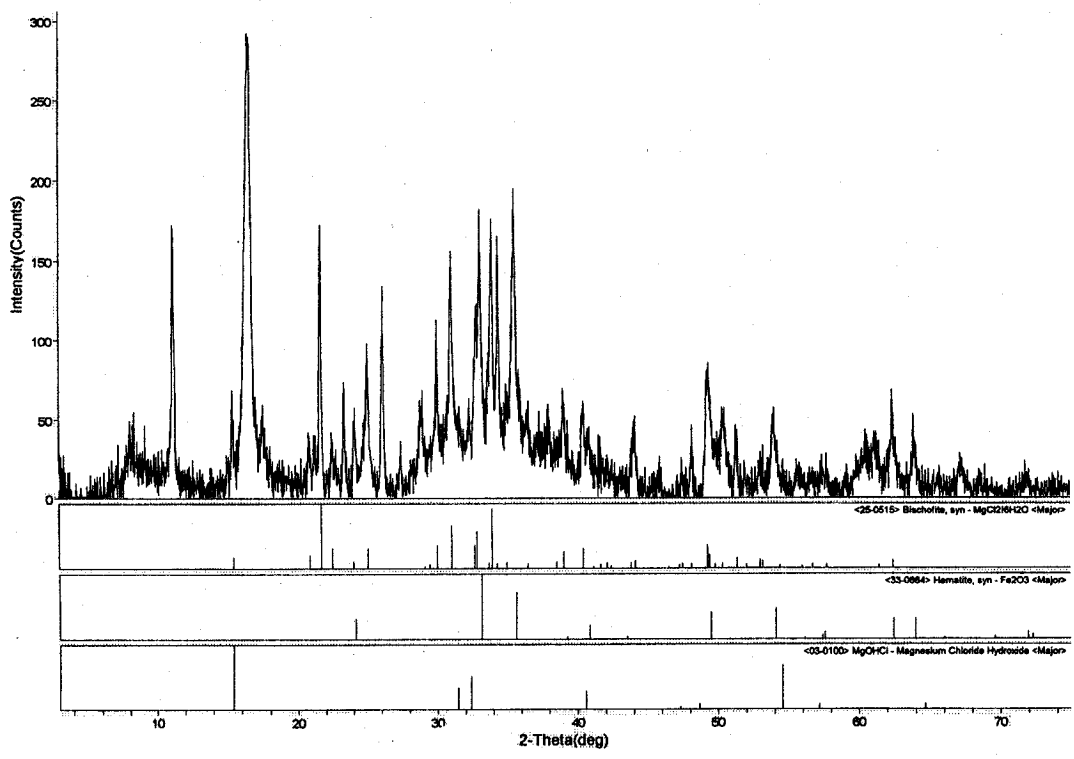

Figure 50: XRD spectra for the feed liquor sample that was allowed to react at 300°C for 1hr.

Clearly, a fair degree of background noise was observed within the aforementioned XRD pattern. This suggests that the crystal structures of a few of the compounds present within the concerned sample were not well formed.

While the magnesium is present primarily as hydroxy-chloride at 400°C, the chlorine assay and XRD spectra (Figure 51) for the corresponding sample, along with mass balance calculations indicate that the majority of the iron has transformed into hematite. Assuming that the majority of the $AlCl_3$ and $FeCl_3$ in

the starting solution have decomposed, the degree of pyrohydrolysis calculation suggests that up to 52% of the ferrous has also pyrohydrolyzed.

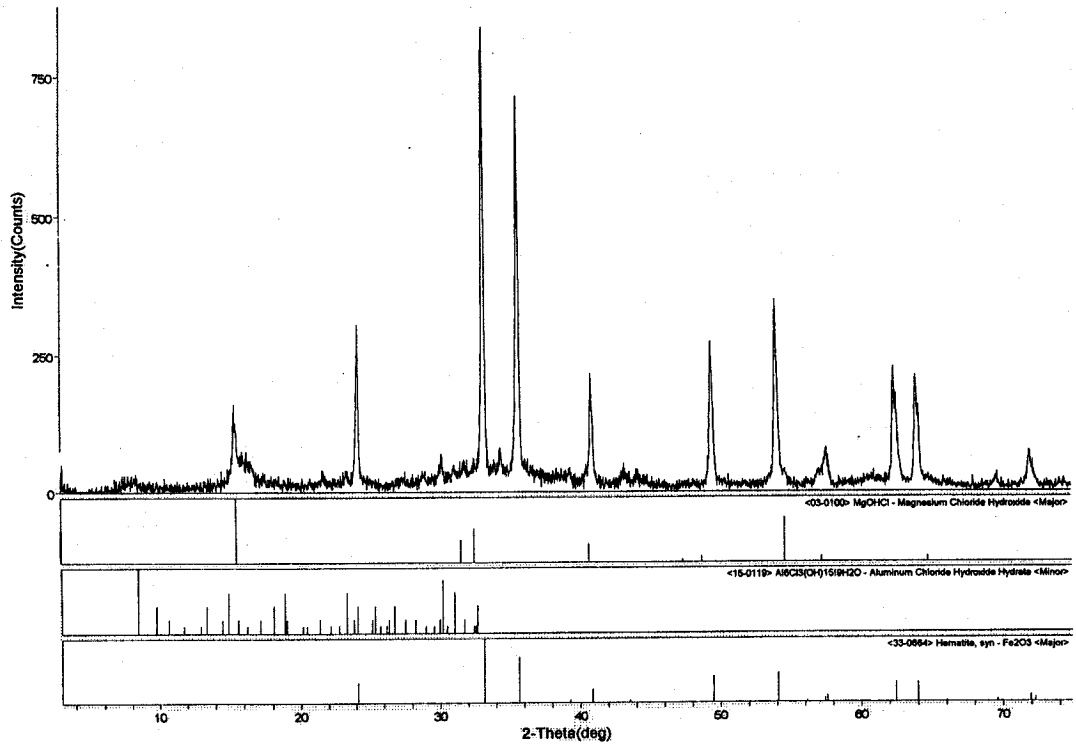

Figure 51: XRD pattern for the starting solution sample that was allowed to react at 400°C for 1hr.

As the system temperature reaches 500°C (see Figure 52), a significant fraction of the MgOHCl has pyrohydrolyzed and a portion of the hematite reacts with the magnesium compounds to form magnesioferrite, $MgFe_2O_4$. Based on the chlorine assay of the sample, it is estimated that approximately 76% of the $MgCl_2$ in the feed liquor has pyrohydrolyzed, provided that all of the other salts have decomposed.

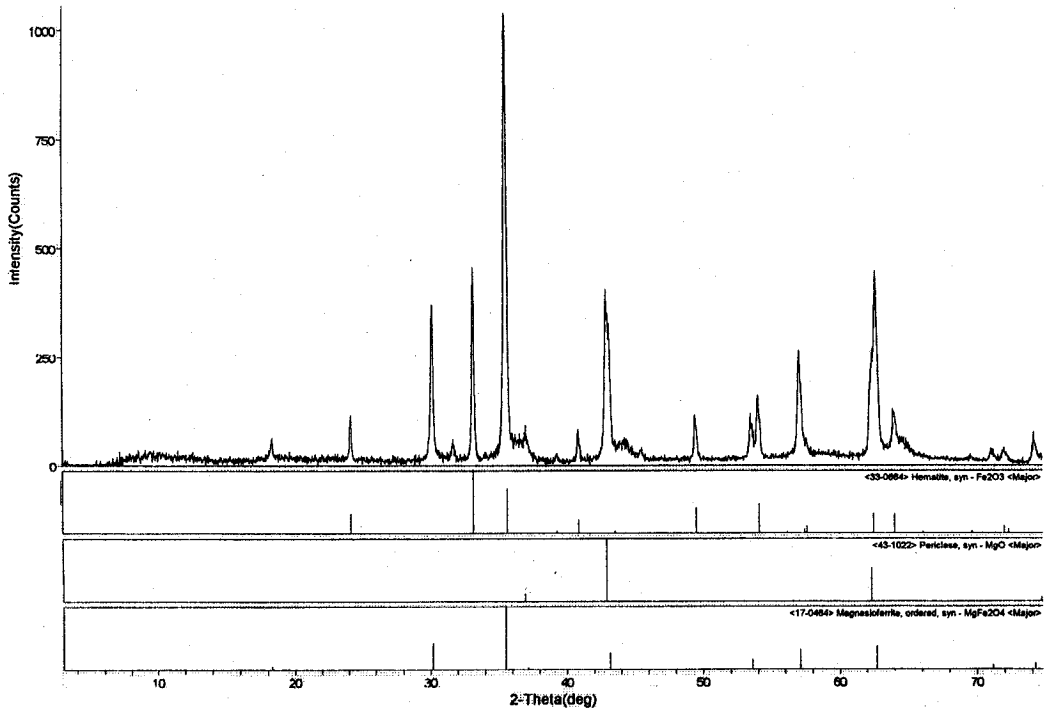

Figure 52: XRD spectra for the feed liquor sample that was allowed to react at 500°C for 1hr.

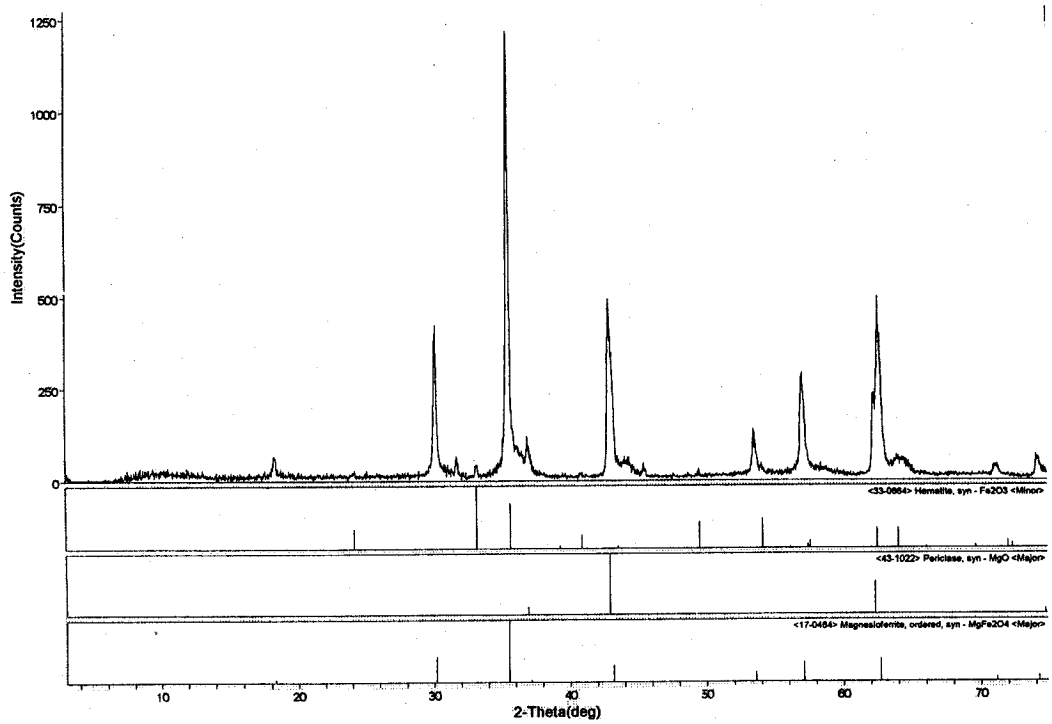

Figure 53: XRD pattern for the starting solution sample that was allowed to react at 600°C for 1hr.

Given that the hematite digressed from a major to a minor phase (Figure 53), it is reasonable to suggest that the iron oxide continues to combine with magnesium compounds as the temperature rises from 500 to 600°C. Despite what the results in Figure 49 may infer, no chloride-based compounds were observed in the XRD pattern.

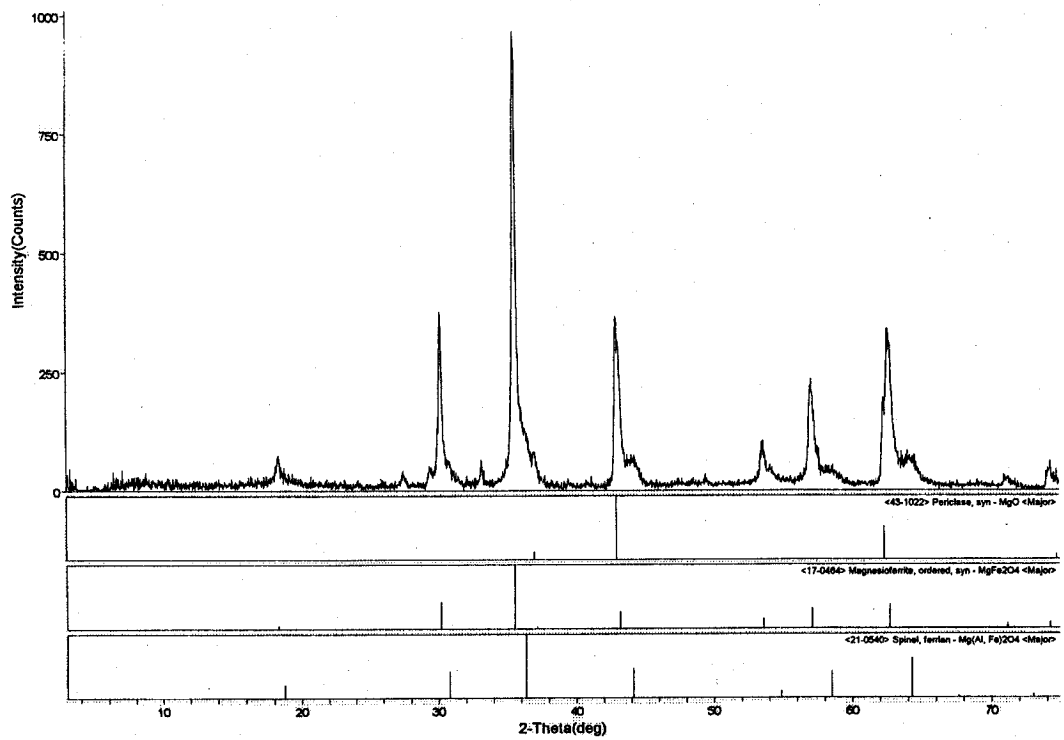

Figure 54: XRD spectra for the feed liquor sample that was allowed to react at 700°C for 1hr.

At 700°C (Figure 54), the presence of aluminium reappears as it combines with the magnesioferrite to form ferrian spinel or $Mg(Al, Fe)_2O_4$. The absence of any hematite in the XRD pattern suggests that it is primarily tied up with the magnesium and aluminium. Based on the stoichiometry, there is an excess of magnesium in the starting solution, relative to iron and aluminium, for the formation of $MgFe_2O_4$ and the ferrian spinel. This explains why MgO is present as a major phase in the concerned sample. The XRD spectra of the sample that was allowed to react at 800°C is literally identical to that shown in Figure 54. And with a degree of

pyrohydrolysis of 97.2%, a small amount of MgOHCl must still be present within the concerned product sample and therefore suggests that higher temperature or longer reaction times are required for it to fully decompose.

4.3.2. Phase I vs. III Results:

A comparison of the relevant data reveals that the degree of pyrohydrolysis as a function of reaction temperature obtained during the Phase I and III experiments are significantly different. During the simplified pyrohydrolysis tests, a little over 50% of the chlorine in the starting solution had evolved as the temperature reached 300°C. The degree of pyrohydrolysis was calculated to be 29.8% at the same temperature during the Phase III trials. This difference is most likely due to the fact that the atmosphere was much more oxidizing during the former series of experiments and this favoured iron chloride hydrolysis.

At higher reaction temperatures (i.e. 500 and 700°C), the percentage of chlorine loss was much more pronounced during the Phase III trials. This is most likely explained by the longer reaction times maintained during the latter series of experiments.

Clearly, given that a typical reactor atmosphere was maintained during the secondary pyrohydrolysis trials, it is reasonable to conclude that the corresponding results serve as a much more reliable account of the transformation process. Despite this it was decided that thermodynamic modelling be performed to validate the resulting conclusions and to elaborate further on the series of reactions that take place throughout the conversion of the multi-component chloride liquor.

4.4. Thermochemical Modelling:

4.4.1. Introduction:

In an effort to assist with the interpretation of the aforementioned experimental results, thermochemical modelling was performed to predict the equilibrium phase assemblages that could occur during the transformation of the saturated Al-Fe-Mg-Cl solution, at reaction temperatures of 200°C and above. The FactSage System, plus thermodynamic data generated by the FACT Consortium Project, was employed to model the equilibrium phase changes that occur as the feed liquor is hydrolysed in a high-temperature, natural gas-fired fluidised-bed reactor.

A fluidised bed reactor is usually considered to be very well mixed, that is, limited temperature and composition ranges occur within the overall bed. Consequently, there will be steep temperature gradients within very localized zones in the reactor. The highest temperature will exist where the natural gas fuel and air combust but on mixing the combustion gases should quickly cool to the bed temperature. The lowest temperature will be that of the injected aqueous liquor, but on mixing this should rapidly heat to the reactor temperature.

Similarly, there will be sharp composition gradients within very localized regions of the reactor. One composition gradient will be between the combustion gases and the bulk exit gas. Another will be around the drops of evaporating liquor and the reaction products derived from that liquor and the bulk reactor gases.

The relative rates at which fuel, air and liquor are fed to the reactor may vary in time. This produces a range of oxygen potentials over time, from oxidizing to reducing conditions.

When a quantity of liquid is injected into the fluidised bed it is exposed to the bulk gas atmosphere within the reactor. A drop of liquid may either be in contact with reactor solids of varying particle size or may be freely suspended in the gas.

Water will evaporate and the liquid temperature will increase from that at injection to that of the bed in a manner depending on the heat transfer mechanisms that supply the heat of evaporation of water. Only the overall thermal energy changes involved in a particular transformation could be predicted by thermochemical calculations.

It is very likely that heat transfer rates and kinetics, rather than equilibrium thermochemistry, would play the major role in determining the phase assemblage at low temperatures. As a result, it was decided to only consider general aqueous chemistry and to restrict detailed thermochemical modelling to temperatures of 200°C and above and to non-aqueous, that is, oxide and chloride non-aqueous condensed phase plus gas equilibria.

4.4.2. Equilibrium Modelling:

Thermochemical modelling requires a characteristic reaction temperature, pressure and input chemical composition in order to calculate an equilibrium phase assemblage. Equilibrium thermochemical modelling assumes infinite chemical reaction rates. As described above, a range of temperature and composition conditions can occur at various locations within a fluid bed reactor and over time, making it unsuitable to be completely described in total by a single, simple equilibrium model. A compromise was sought and, after some exploratory calculations, it was decided to calculate the stable phase assemblage that would result from simple mixing of the feed fuel, air and liquor over the temperature range 200 to 1000°C. The lower temperature limit was chosen so that only species for which reasonable thermodynamic data exists are likely to be stable and where significant chemical reaction rates might be expected. The upper temperature limit is believed to be significantly above that occurring during normal reactor operation.

It is known from experimental observation that aluminium chloride precipitates from saturated liquor as the hexahydrate[70] and that it undergoes reactive hydrolysis to yield aluminium oxide plus hydrogen chloride at relatively low temperatures.[54,55] The aluminium oxide formed is either amorphous or is in the form of gamma alumina, which has a defect spinel structure.[86]

$$2\ AlCl_3.6H_2O = Al_2O_3 + 6\ HCl_{(g)} + 9\ H_2O_{(g)} \qquad (42)$$

Solid magnesium chloride monohydrate ($MgCl_2.H_2O$) is predicted to be stable at a temperature of 200°C in the reactor atmosphere by the exploratory FACT calculations.

Iron is the only metal in the feed liquor that can undergo oxidation and reduction chemistry under reactor conditions. Preliminary equilibrium calculations indicated that under oxidizing conditions at a temperature of 200°C, ferrous chloride is predicted to convert to ferric chloride plus ferric oxide.

$$6\ FeCl_2 + 1.5\ O_2 = 4\ FeCl_3 + Fe_2O_3 \qquad (43)$$

Under reducing conditions at 200°C, ferric chloride is predicted to convert to ferrous chloride.

$$FeCl_3 + 0.5\ H_2 = FeCl_2 + HCl_{(g)} \qquad (44)$$

The kinetics of the iron chloride oxidation and reduction reactions are unknown. Therefore, the quantities of $FeCl_2$ and $FeCl_3$ present within the feed liquor were chosen as direct inputs to the model.

The equilibrium modelling of this system is considered only at atmospheric pressure. From Le Chatlier's Principle, as hydrolysis of a metal chloride produces more gaseous molecules in the products than existed in the reactants, an increase

in reactor pressure would be expected to stabilize metal chlorides relative to the metal oxides.

$$MCl_2 + H_2O_{(g)} = MO + 2\ HCl_{(g)} \qquad (45)$$

In reality, an exhaust fan is used to evacuate excess gas from within the reactor and maintain a constant pressure, which is slightly negative (i.e. ~95kPa, absolute), to avoid any corrosive $HCl_{(g)}$ emissions into the atmosphere immediately surrounding the vessel.

The metals are initially intimately mixed on an atomic scale because they enter the reactor in the form of an aqueous solution. As a result, unless significant demixing occurs as the individual chlorides crystallize, only short solid-state diffusion paths would be required to form mixed metal phases and this process should be fast. Given that heating in the reactor is likely to be rapid, significant demixing should not occur. Aqueous solutions are often used commercially as the starting phase from which to prepare solid mixed metal oxides.[86]

In the model, the possible phases covered included gas, a molten chloride solution, a chloride solid solution, spinel solid solutions, a monoxide solid solution and pure solids. The anhydrous $MgCl_2$-$FeCl_2$, spinel and the MgO-FeO solid phases were modelled by solid-solution models using optimized FACT data. The corundum phase of alumina, Al_2O_3, and hydrated aluminium oxides, such as diaspore, AlOOH, were excluded from the model because published experimental observations[55] indicated that they would not form for kinetic reasons, despite being found to be thermodynamically stable during preliminary equilibrium calculations.

4.4.3. Model Feed Composition:

Based on a review of the literature[1,53] and some of the author's personal experience, the most oxidizing conditions that appear to be maintained in fluidized bed pyrohydrolyzers are generated by air/fuel ratios of close to 10, where the fuel is assumed to be natural gas. An air-to-fuel ratio as low as 9.2 was also reported to have been used, which constitutes reducing conditions. The feed liquor composition was assumed to be constant at 49.5 wt% H_2O, 8.5 wt% $AlCl_3$, 18.5 wt% $MgCl_2$, 12.0 wt% $FeCl_3$, 10.0 wt% $FeCl_2$ and 1.5 wt% HCl.

Typically, natural gas is composed of methane (approximately 97.2 mole percent), about 1.4 mole percent ethane and limited quantities of propane, nitrogen and carbon dioxide. In an effort to simplify the calculations, the natural gas feed to the reactor was assumed to be pure methane. The effect of this hypothesis is not likely to be significant. The air was assumed to be dry and to be composed only of oxygen and nitrogen. The "dry air" assumption will have a negligible effect on the results given the large quantities of water introduced by the liquor. All gas was assumed to behave as a perfect mixture.

Linear interpolation was used between oxidizing and reducing flow rates to calculate intermediary input conditions. Hence the most oxidizing condition is represented as zero (A=0) and the most reducing condition is represented as unity (A=1) on the oxidizing – reducing scale. The constant for the nitrogen input equation into the reactor was reported as "B", and feed rate equations for all the other species or compounds use fractions of B as their constant. Given that the sources of information from which the data was obtained are considered confidential, the actual value for B could not be provided. The inputs to the thermochemical model are summarized in Table 6.

Table 6: Inputs to the thermochemical model

Input Species/ Compounds	**Flowrate** (mole/hour)
$N_{2\,(g)}$	30955.3A + B
$O_{2\,(g)}$	8179.1A + 0.264B
$CH_{4\,(g)}$	14279.4A + 0.127B
$H_2O_{\,(l)}$	69269.7A + 0.495B
$FeCl_{2\,(aq)}$	1989.0A + 0.0142B
$FeCl_{3\,(aq)}$	1865.0A + 0.0133B
$MgCl_{2\,(aq)}$	4898.4A + 0.0350B
$AlCl_{3\,(aq)}$	1607.1A + 0.0115B
$HCl_{\,(aq)}$	1037.2A + 0.0074B

4.4.4 Model Results:

The results calculated using the FactSage program EQUILIB are summarized in the following. The predicted variation of gas composition in terms of major components, for conditions ranging from oxidizing to reducing, is shown in Figure 55. The minor component and oxygen concentration profiles are shown in Figures 56 and 57, respectively. On the oxidizing-reducing scale, zero corresponds to the most oxidizing feed flow-rate considered, unity corresponds to the most reducing feed flow-rate and the intermediate values to linear interpolation between the these two limiting flow-rates. The kilo mole per hour scale is provided to allow insight into the chemical changes predicted to occur during the process and also reflects relative volumetric concentrations in the gas phase. This information would not be so obvious in a mass flow rate scale.

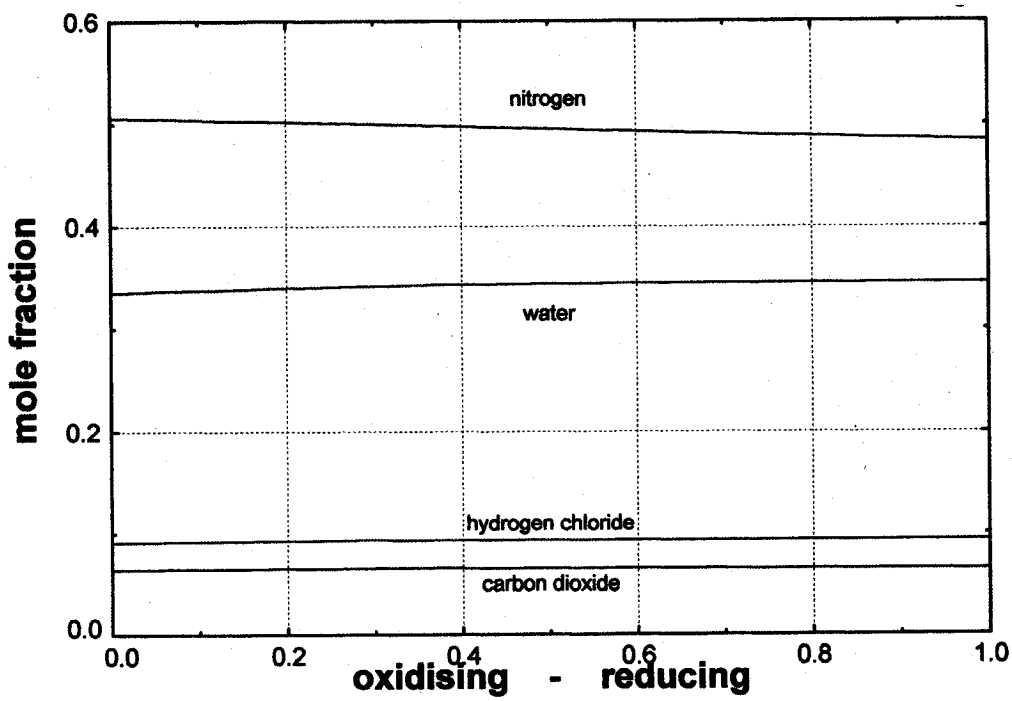

Figure 55: Predicted variation in product gas composition (major components) over the range of oxidizing/reducing conditions considered at 900°C.

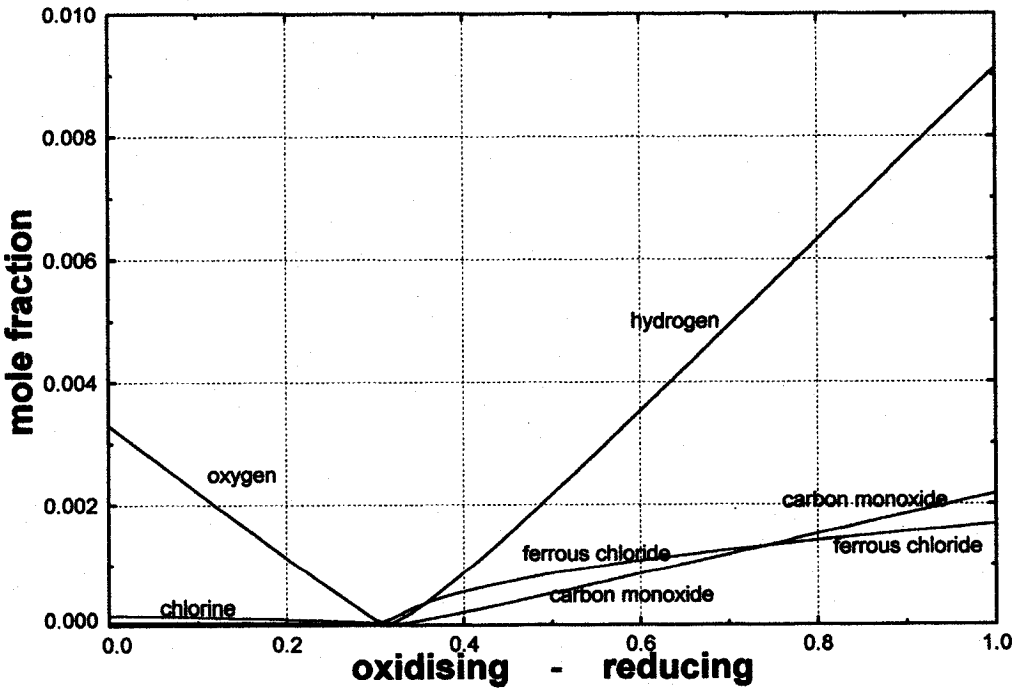

Figure 56: Calculated variation in product gas composition (minor components) over the range of oxidizing/reducing conditions considered at 900°C.

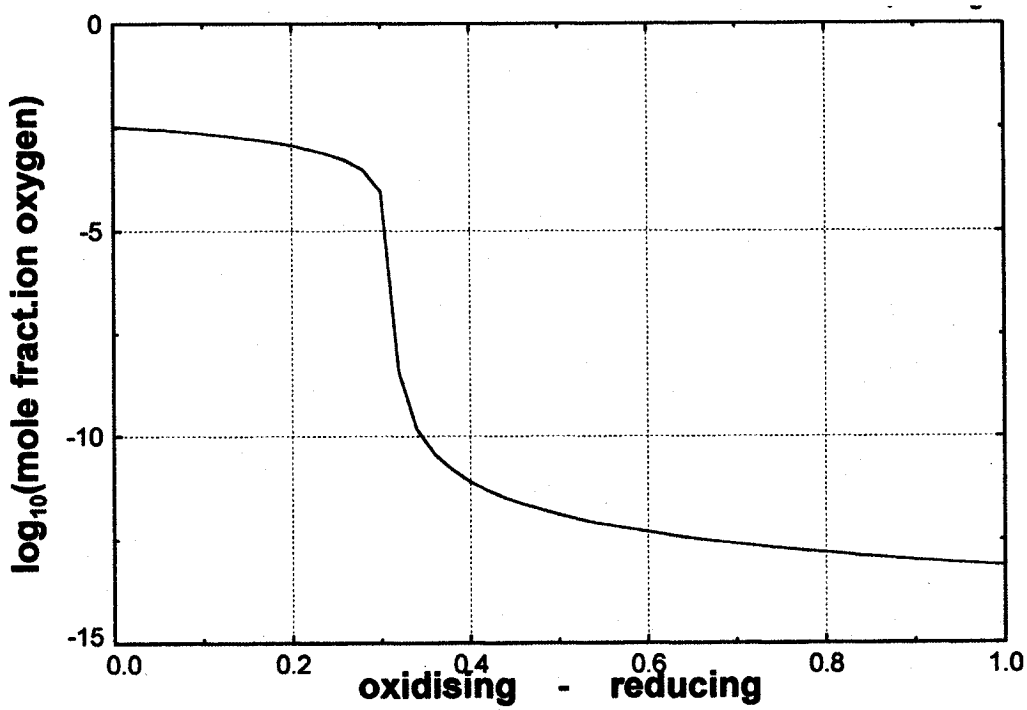

Figure 57: Predicted variation in oxygen potential over the range of oxidizing/ reducing conditions considered at 900°C.

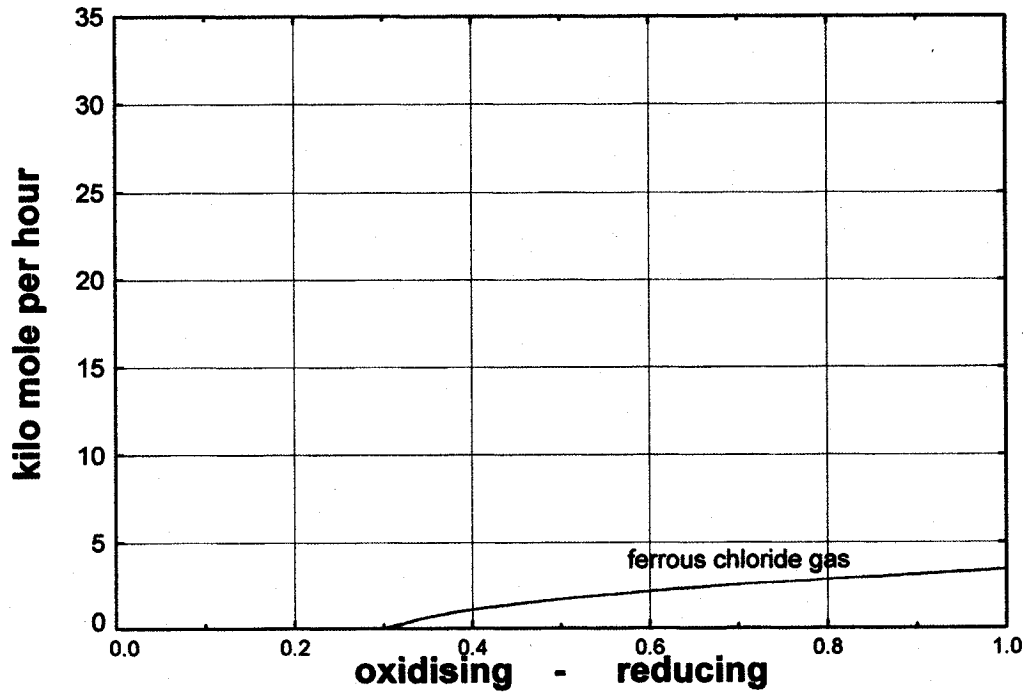

Figure 58: $FeCl_{2(g)}$ flowrate observed in gas phase at 900°C over range of oxidizing/ reducing conditions considered.

The molar flowrates of ferrous chloride observed in the gas phase at 900°C over the range of oxidizing/reducing conditions considered is graphically illustrated in Figure 58. $FeCl_{2(g)}$ flowrates observed with increasing temperatures under reducing and neutral conditions are provided in Figures 59 and 60, respectively.

The variation of solid phase production rates for oxidizing to reducing conditions on the above scale and for varying temperatures are shown in Figures 61 to 67. The composition of the product solid phases and the production rate of the components of those phases at a temperature of 900°C are provided in Figures 68 to 77.

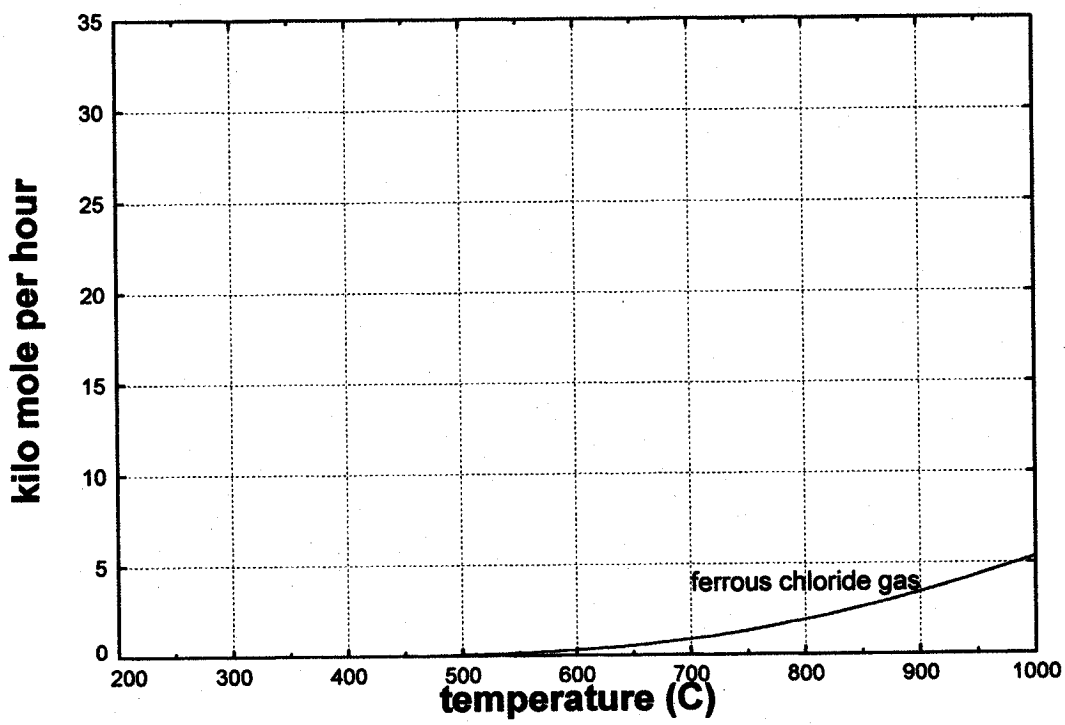

Figure 59: $FeCl_{2(g)}$ flowrate observed in gas phase, under reducing conditions, as a function of temperature.

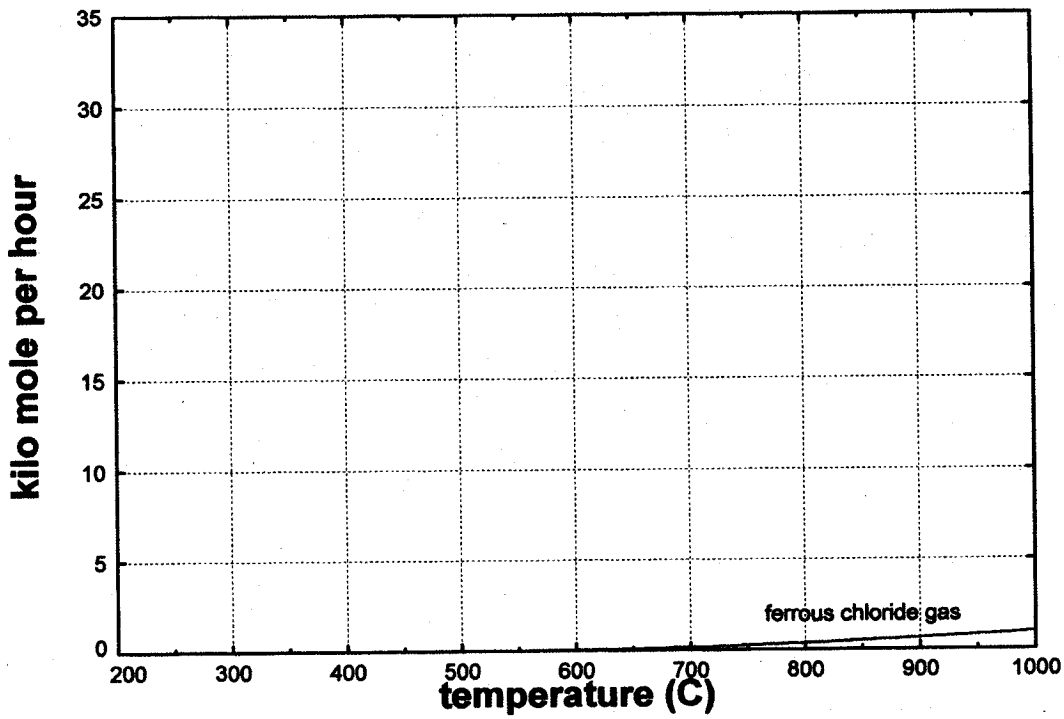

Figure 60: $FeCl_{2(g)}$ flowrate observed in gas phase, under neutral conditions, as a function of temperature.

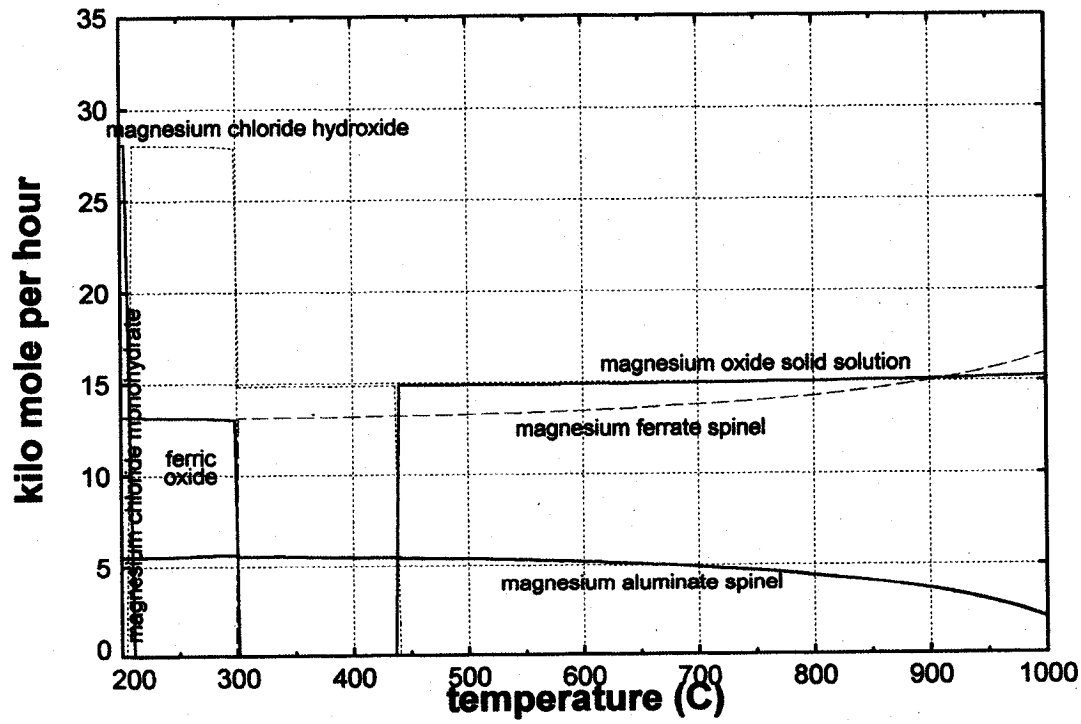

Figure 61: Molar phase production rates, under oxidizing conditions (i.e. A=0), as a function of temperature.

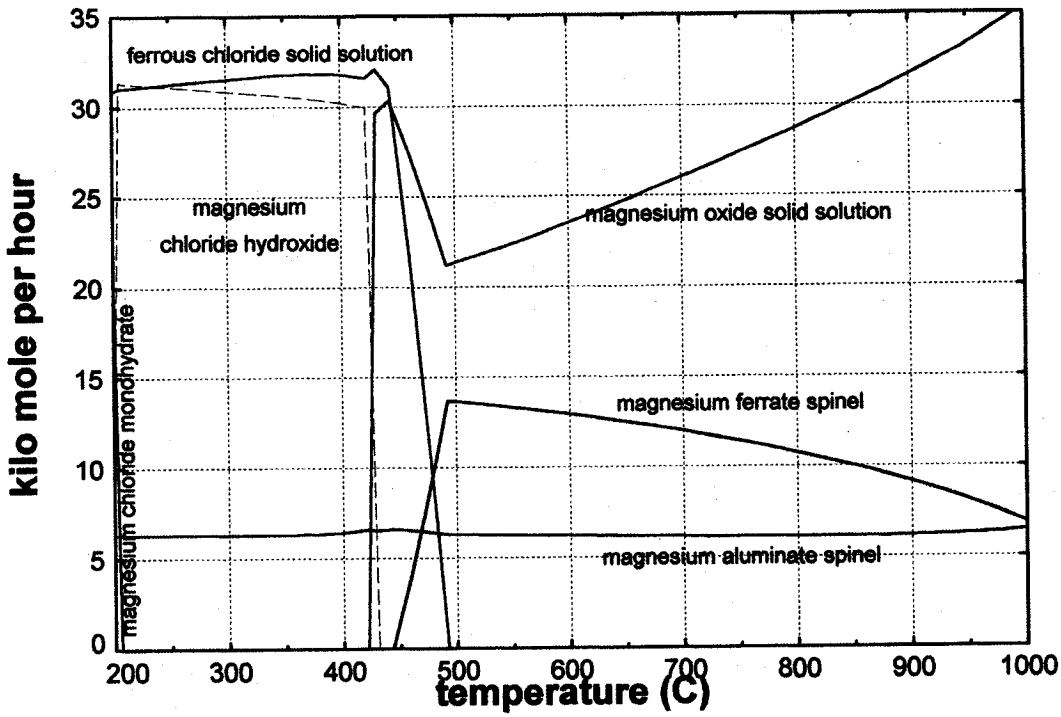

Figure 62: Molar phase production rates, under reducing conditions (i.e. A=1), as a function of temperature.

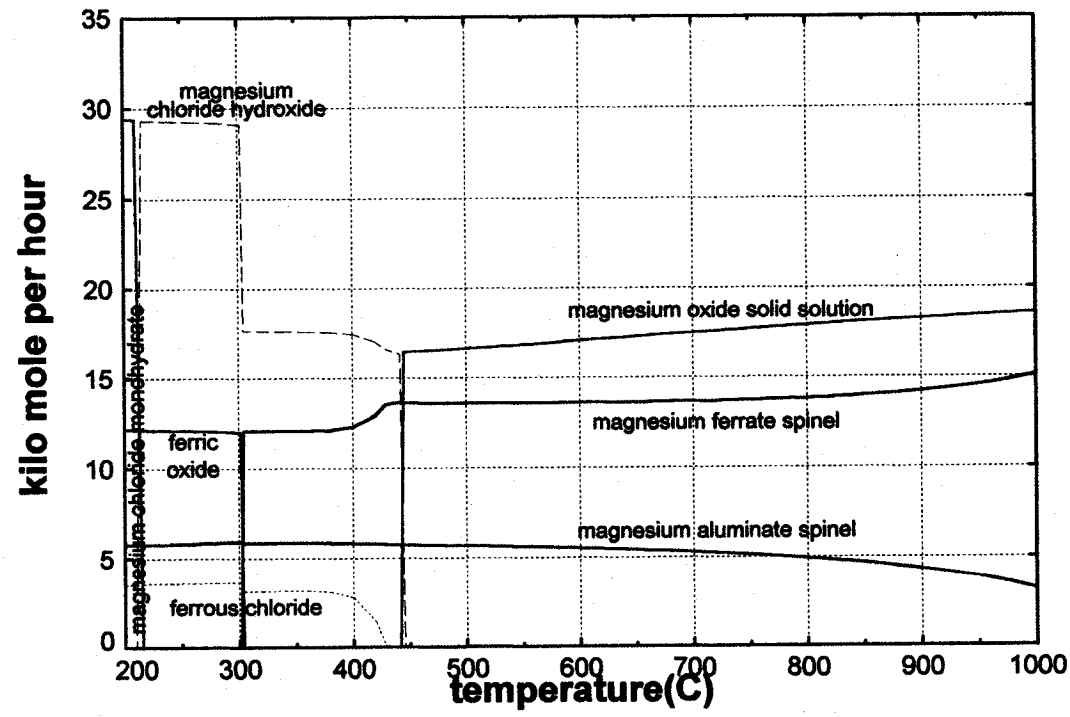

Figure 63: Molar phase production rates, under neutral conditions (i.e. A=0.35), as a function of temperature.

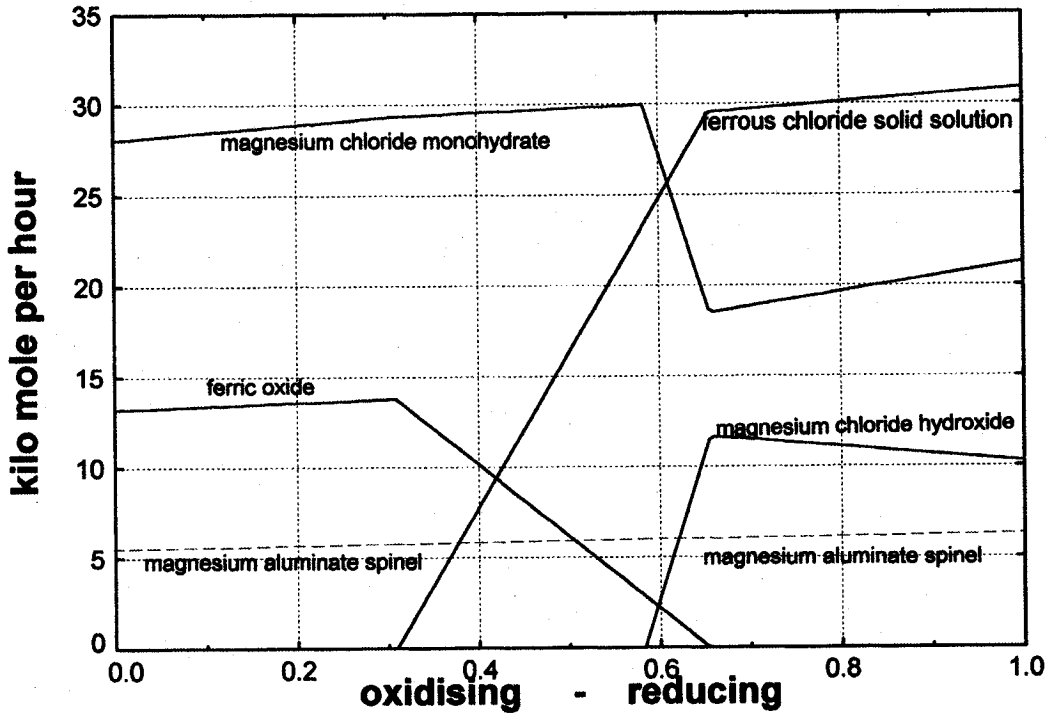

Figure 64: Molar phase production rates, over the range of oxidizing/reducing conditions considered, at 200°C.

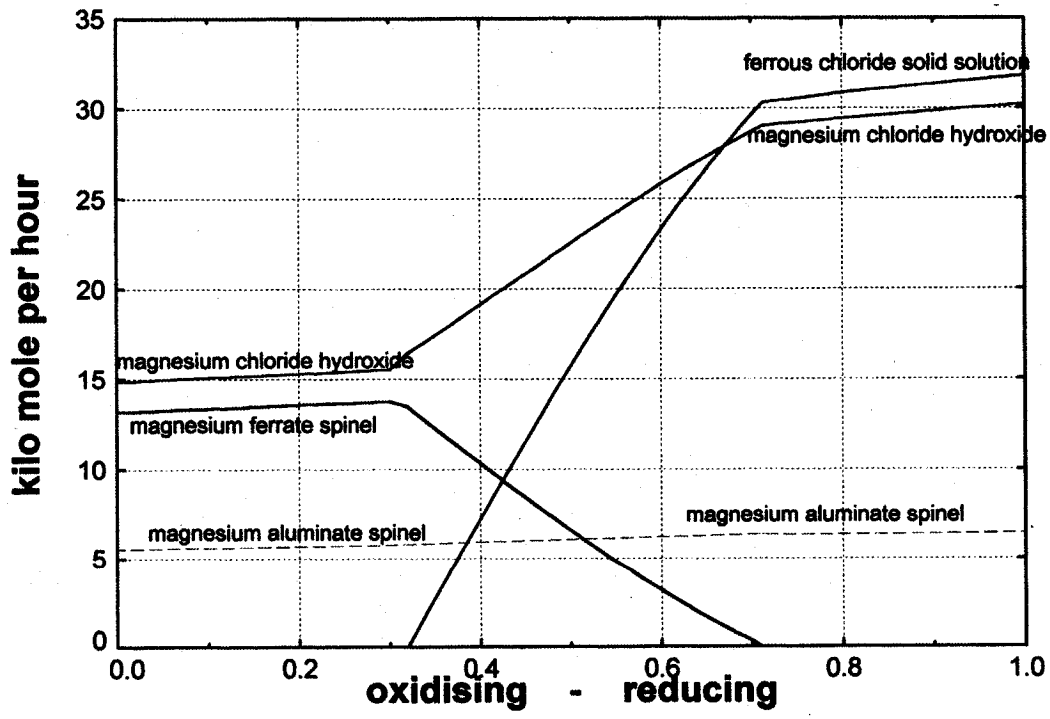

Figure 65: Molar phase production rates, over the range of oxidizing/reducing conditions considered, at 400°C.

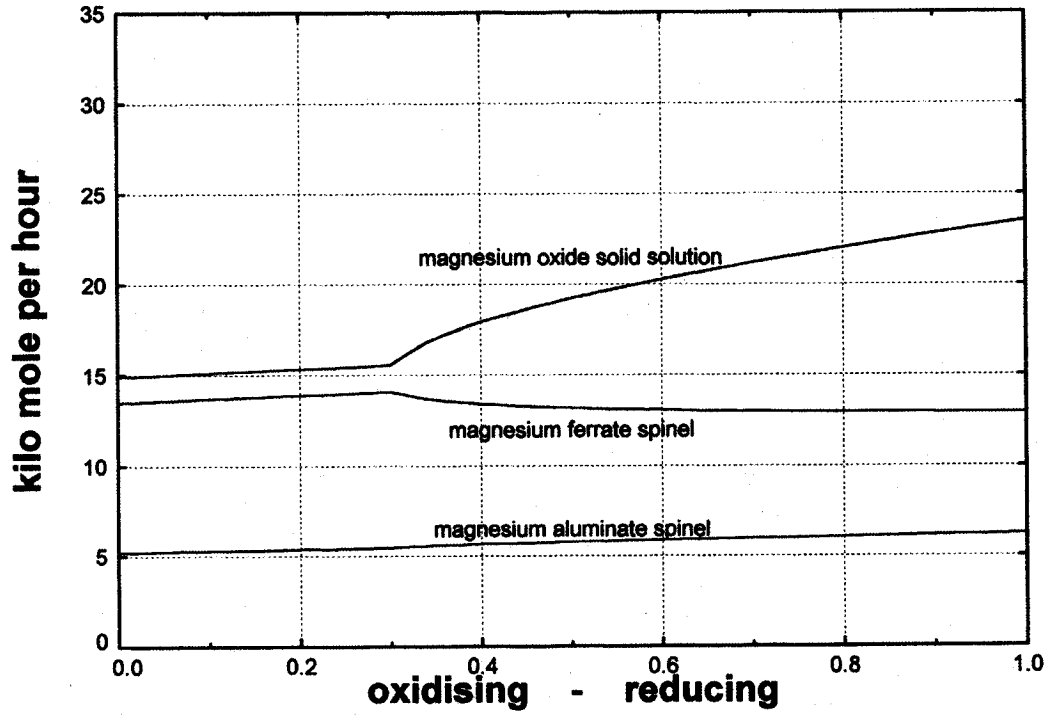

Figure 66: Molar phase production rates, over the range of oxidizing/reducing conditions considered, at 600°C.

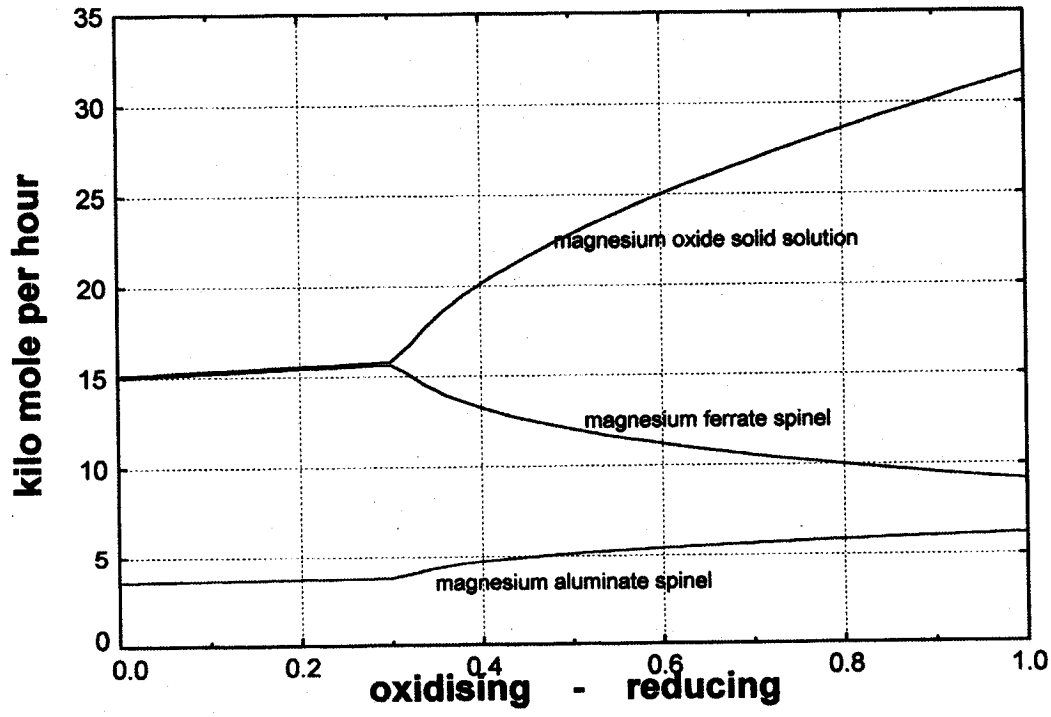

Figure 67: Molar phase production rates, over the range of oxidizing/reducing conditions considered, at 900°C.

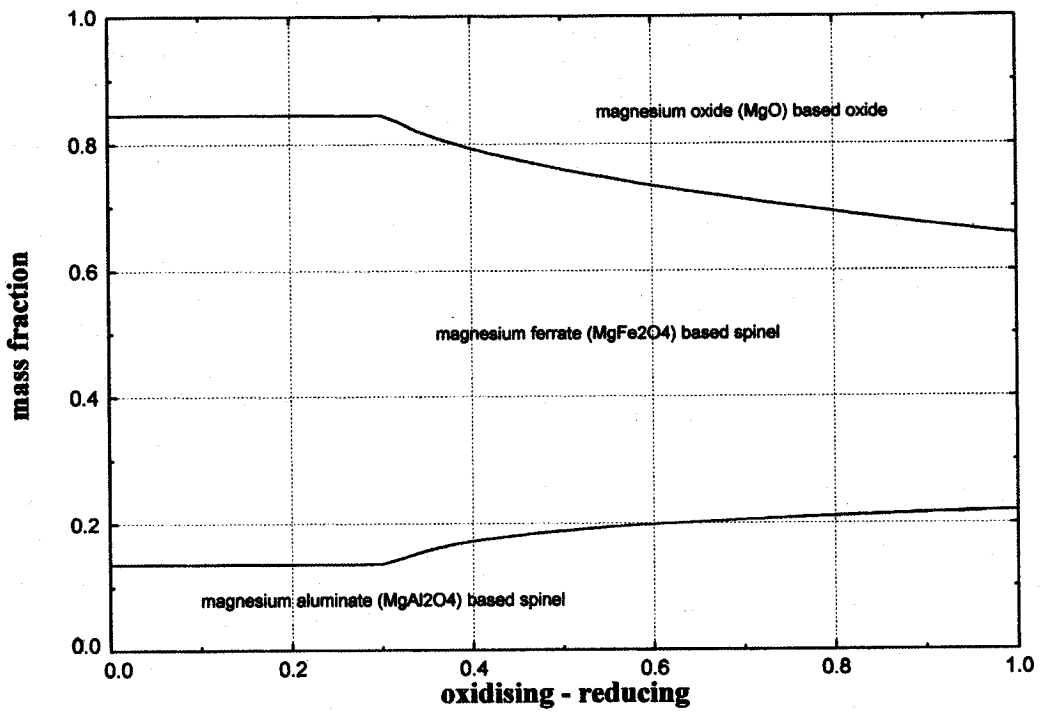

Figure 68: Solids component phase distribution over range of oxidizing/ educing conditions considered, at 900°C.

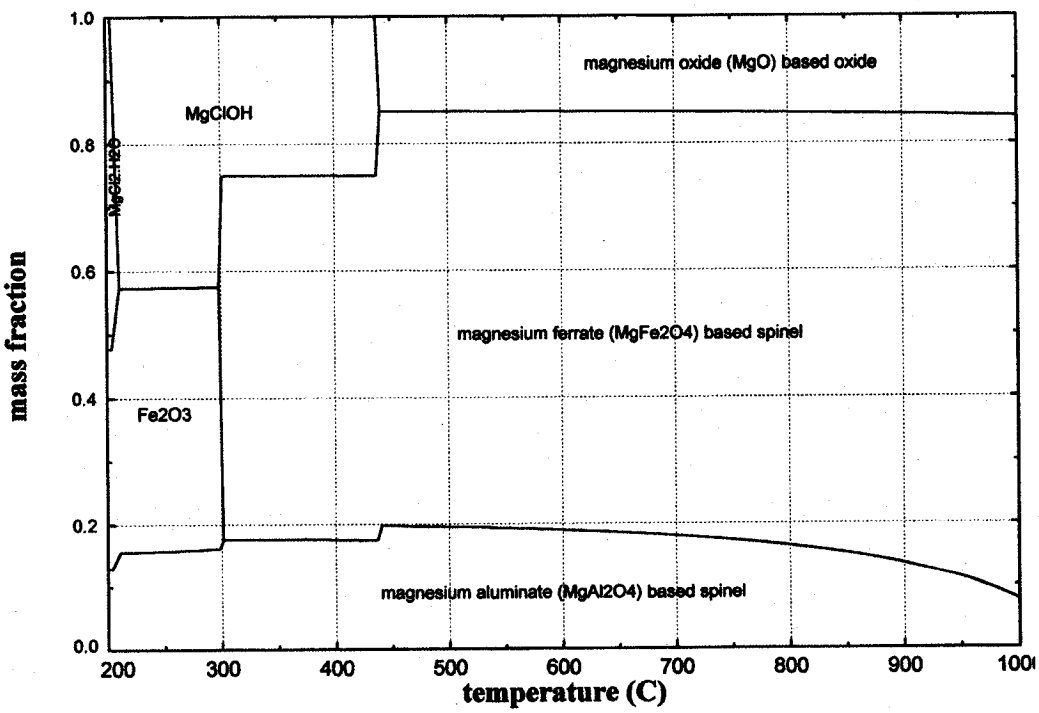

Figure 69: Solids component phase distribution, under oxidizing conditions (i.e. A=0), as a function of temperature.

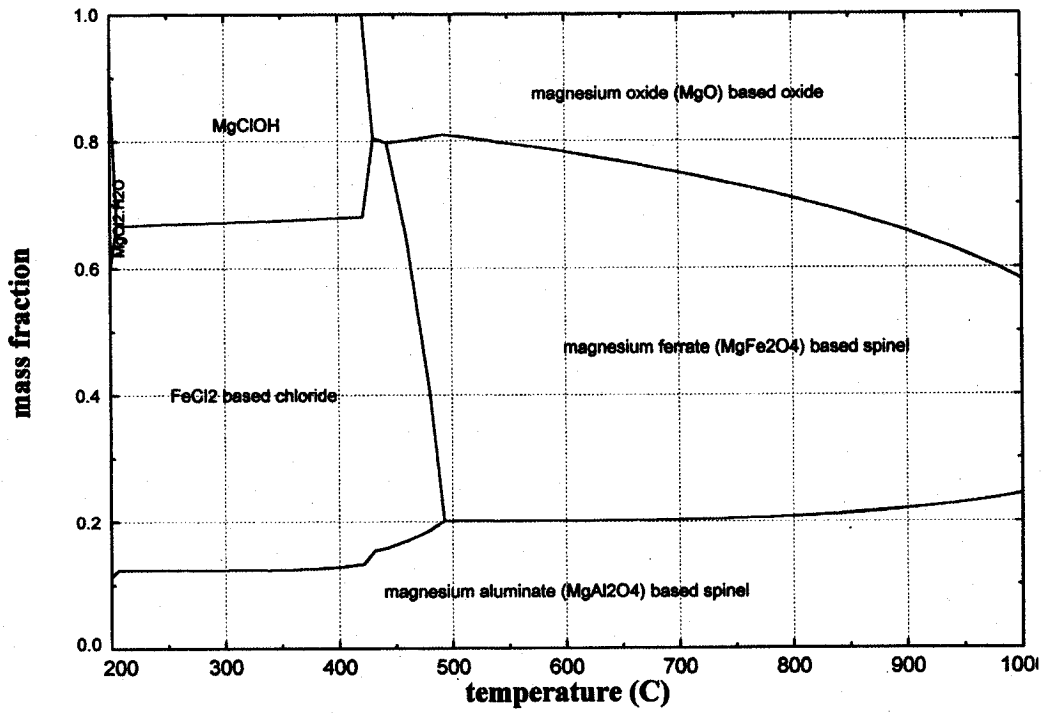

Figure 70: Solids component phase distribution, under reducing conditions (i.e. A=1), as a function of temperature.

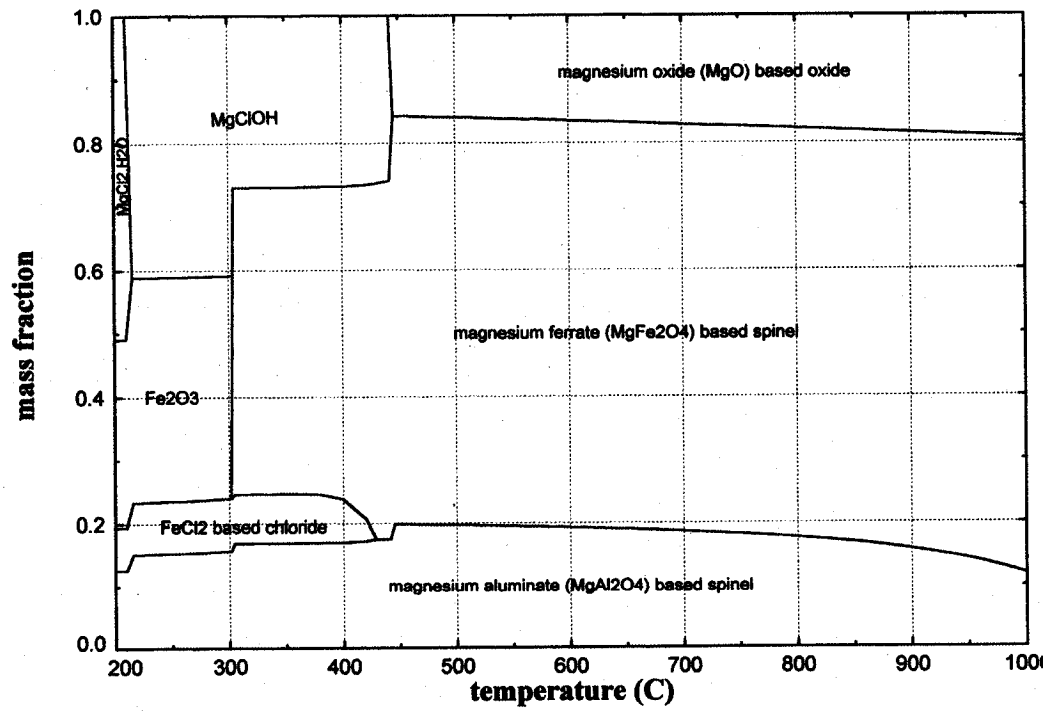

Figure 71: Solids component phase distribution, under neutral conditions (i.e. A=0.35), as a function of temperature.

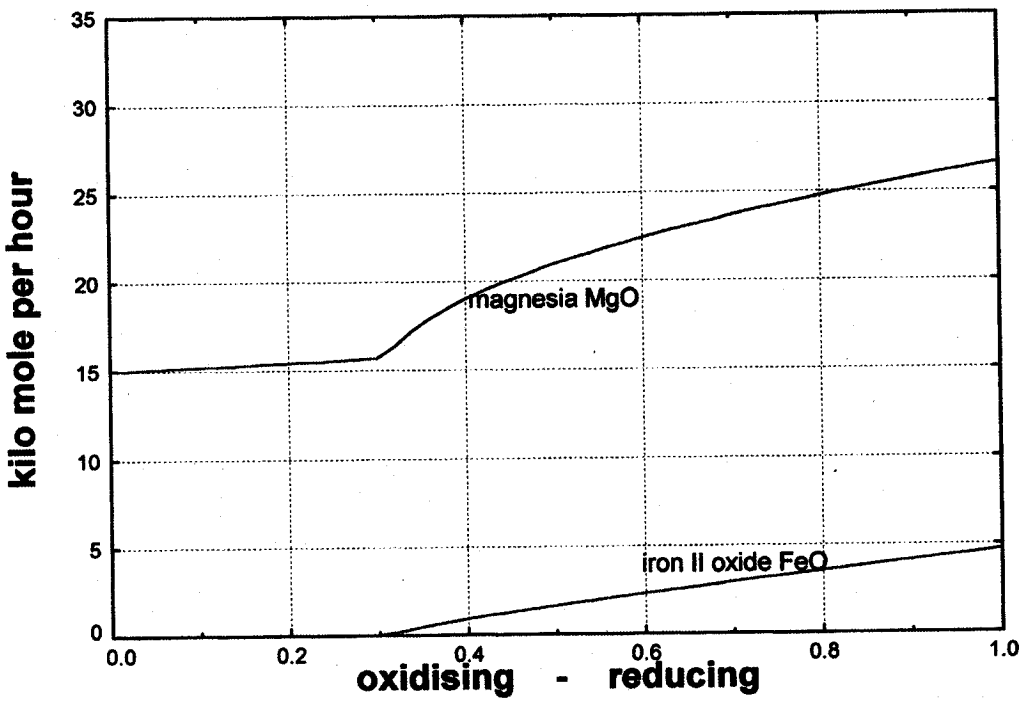

Figure 72: Molar production rates of MgO based solid-solution components, over range of oxidizing/reducing conditions considered, at 900°C.

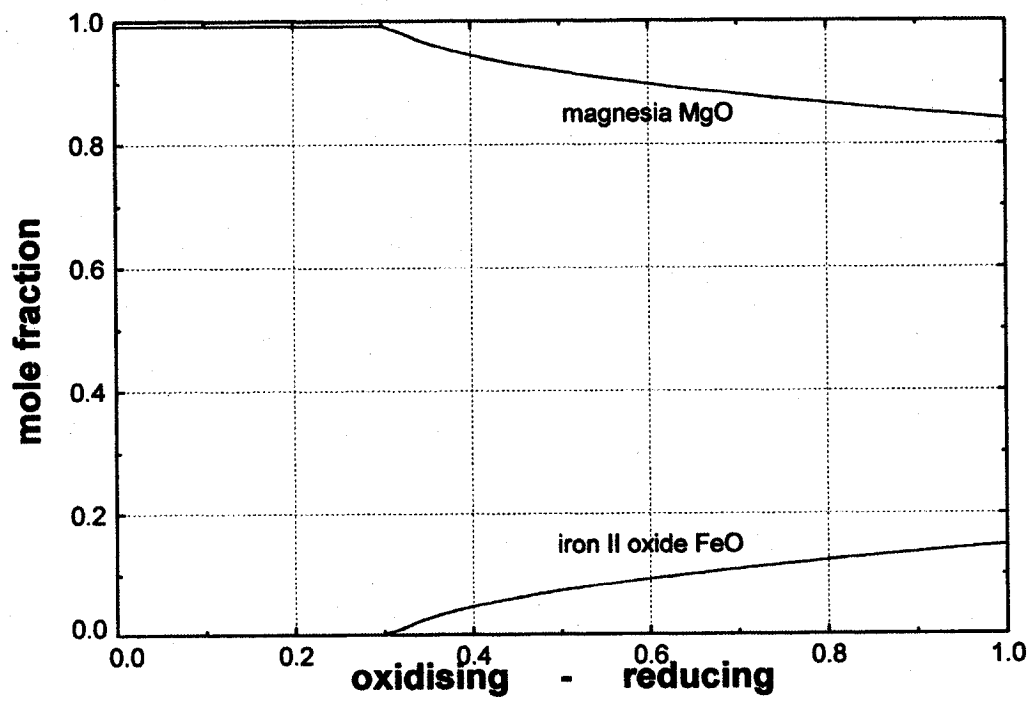

Figure 73: Composition of MgO based solid-solution, over range of oxidizing/ reducing conditions considered, at 900°C.

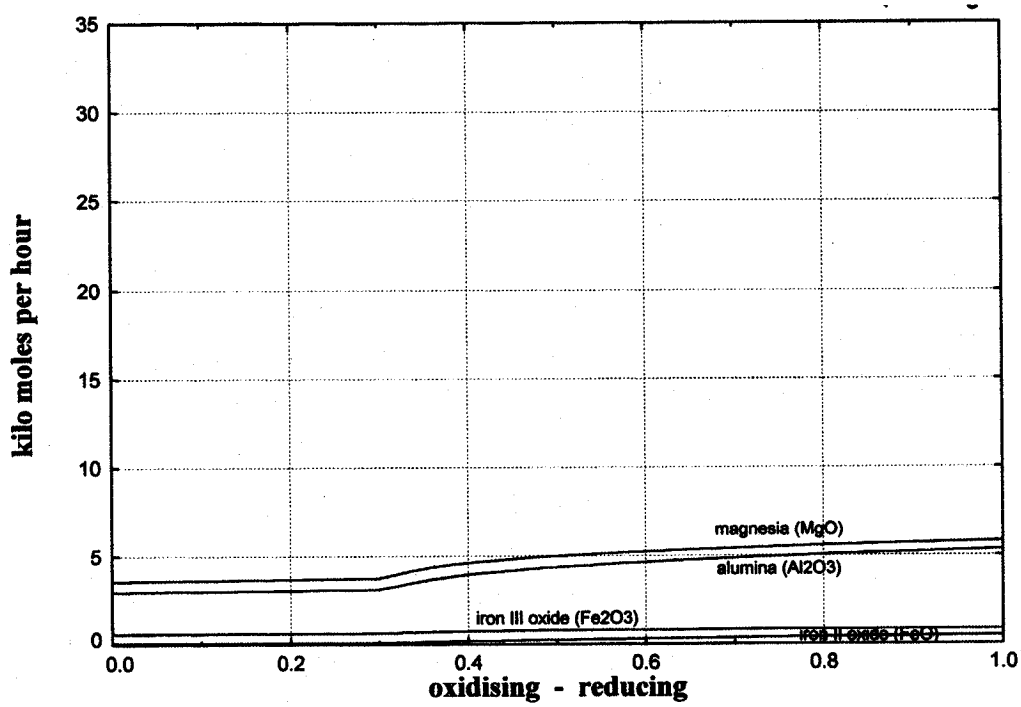

Figure 74: Molar production rates of $MgAl_2O_4$ based spinel solid-solution components, over range of oxidizing/reducing conditions considered, at 900°C.

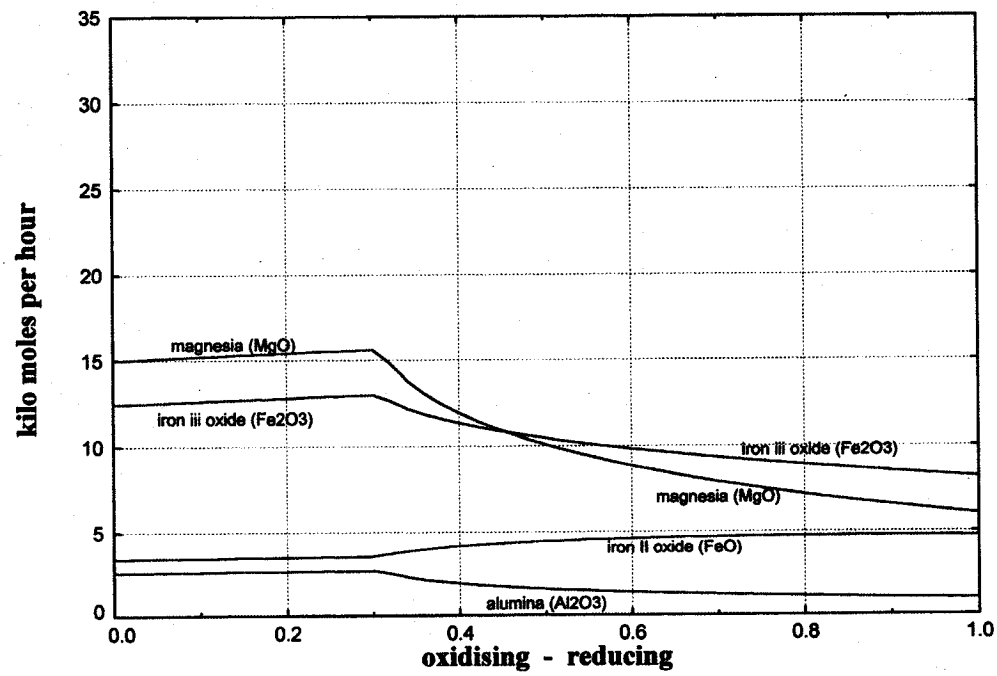

Figure 75: Molar production rates of $MgFe_2O_4$ based spinel solid-solution components, over range of oxidizing/reducing conditions considered, at 900°C.

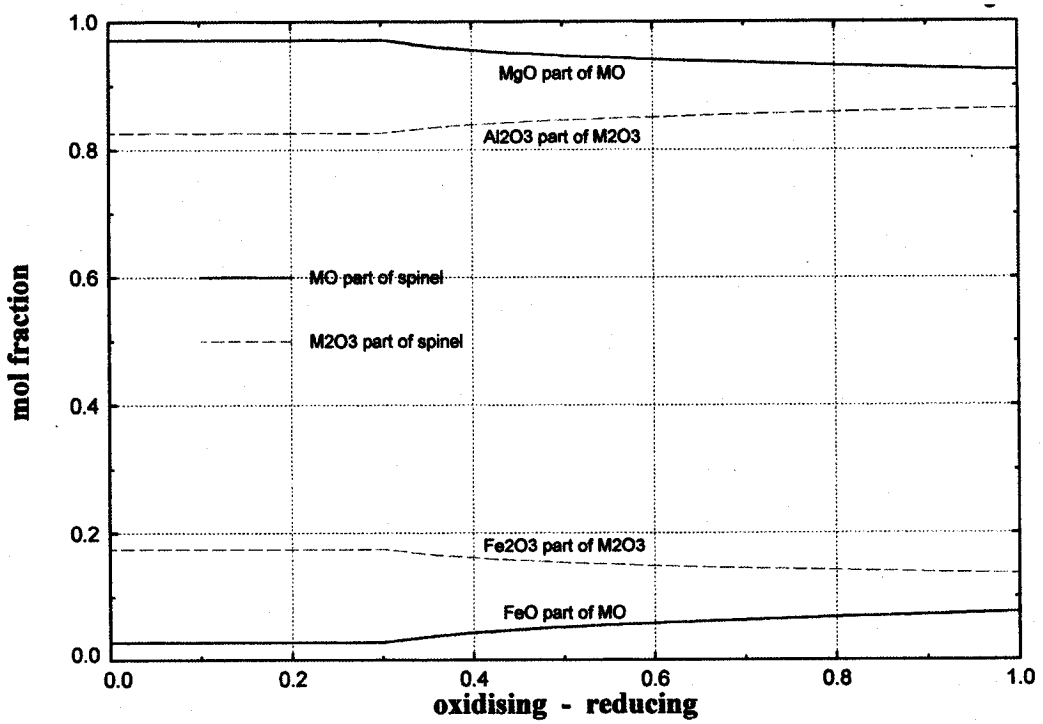

Figure 76: Composition of $(Mg,Fe)O{\cdot}(Al,Fe)_2O_3$ based solid-solution, over range of oxidizing/reducing conditions considered, at 900°C.

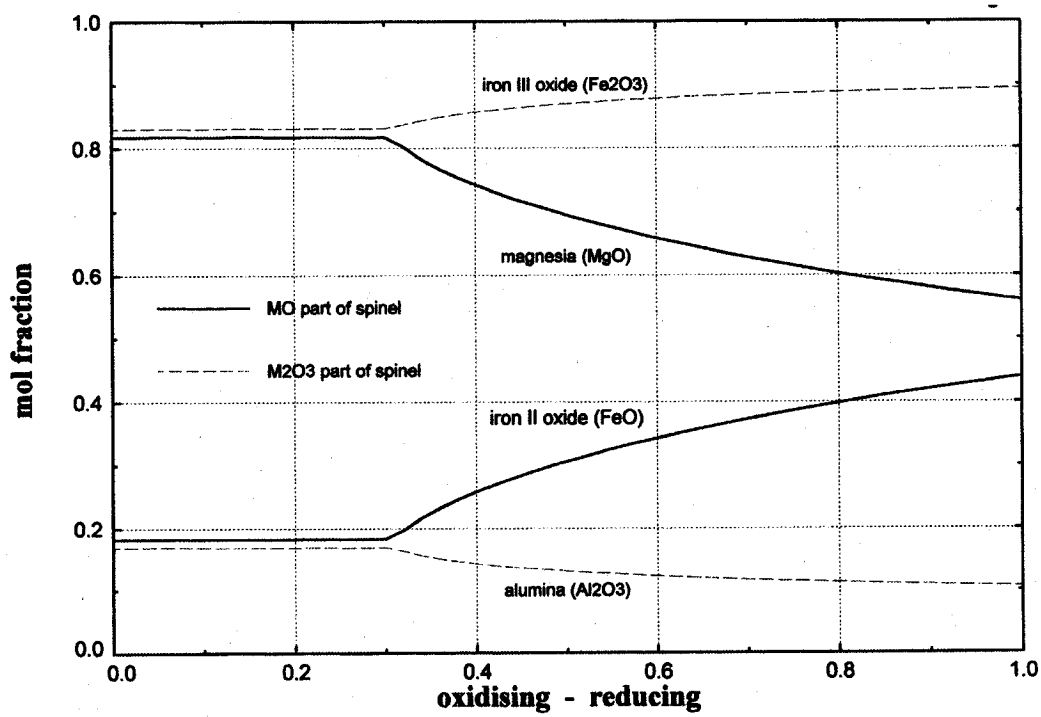

Figure 77: Composition of $(Mg,Fe)O{\cdot}(Fe,Al)_2O_3$ based solid-solution, over range of oxidizing/reducing conditions considered, at 900°C.

4.4.5. Predicted Effect of Temperature:

The decomposition mechanism for magnesium chloride is predicted to be similar under both oxidizing and reducing conditions, with magnesium monohydrate converting to magnesium chloride hydroxide at temperatures between 200 and 250°C and magnesium chloride hydroxide converting to magnesium oxide at temperatures between 440 and 460°C (Figures 61 to 63). The relative quantity of magnesium in the spinel and monoxide phases is predicted to depend on both oxygen potential and temperature.

The decomposition mechanism for aluminium chloride is predicted to be similar under both oxidizing and reducing conditions, with aluminium chloride hexahydrate converting to oxide, probably as a defect spinel phase, at temperatures below 200°C then appearing in spinel phases at temperatures at and above 200°C (Figures 61 to 63). The relative quantity of aluminium in the spinel phases is predicted to be almost independent of both temperature and oxygen potential, as a $MgAl_2O_4$-rich spinel phase is predicted to be the major product containing aluminium under all conditions investigated.

Iron is the chemical element that is predicted to display the most diverse chemistry with respect to both oxygen potential and temperature. Under oxidizing conditions, iron is predicted to convert to the trivalent state and to hydrolyse to ferric oxide at temperatures below 200°C (Figure 61). At temperatures around 300 to 330°C, the ferric oxide is predicted to convert to a $MgFe_2O_4$-rich spinel phase. Under reducing conditions, iron is expected to convert to the divalent state but to persist as a ferrous chloride-rich phase to temperatures around 480 to 520°C at which time it converts to a $MgFe_2O_4$-rich spinel phase (Figure 62). Under reducing conditions, as the temperature increases, this spinel phase is predicted to contain increasing concentrations of iron II oxide (FeO) and magnesium oxide (MgO) is expelled from the spinel phase to the monoxide $(Mg_{1-x},Fe_x)O$ phase.

The monoxide phase is also predicted to contain increasing concentrations of FeO with increasing temperature under reducing conditions. It is important to note that under reducing conditions, the gas phase is predicted to contain significant concentrations of $FeCl_2$ as well as hydrogen and carbon monoxide (see Figures 56 and 59). The gaseous ferrous chloride is predicted to result from the reversible reaction of hydrogen (or carbon monoxide) and hydrogen chloride with the magnesium ferrate spinel.

$$MgFe_2O_4 + H_{2\,(g)} + 4\,HCl_{(g)} = MgO + 2\,FeCl_{2\,(g)} + 3\,H_2O_{(g)} \qquad (46)$$

$$MgFe_2O_4 + CO_{(g)} + 4\,HCl_{(g)} = MgO + 2\,FeCl_{2\,(g)} + 2\,H_2O_{(g)} + CO_{2\,(g)} \qquad (47)$$

The relative concentrations of the major gas phase constituents, N_2, H_2O, HCl and CO_2 are predicted to not significantly change under the range of oxidation potentials considered.

Under neutral conditions, a ferrous chloride solid solution is predicted to exist to approximately 420°C, and the Fe_2O_3 tends to disappear as the temperature exceeds 300°C (Figure 63).

The $MgAl_2O_4$-rich spinel phase and the $MgFe_2O_4$-rich spinel phase are not completely miscible so two phases, each with the spinel structure, are predicted to co-exist over the wide range of the conditions observed in regeneration reactors and in the solid product (Figures 61 – 63, and 65 - 67). These phases would be difficult to differentiate by X-ray diffraction unless operational care was taken in noting peak positions and intensities.

Spinel phases may be considered in a number of ways. One example is the crystallographic approach. There are two distinct crystallographic sites for metals in oxide spinels in which the metals have either tetragonal or octahedral

coordination with oxygen atoms. These sites may be either occupied or vacant. Hence a spinel phase may be described by listing the metals together with their oxidation state at each of the sites in the crystal structure. The FACT spinel model generates enough information to use the crystallographic approach if so desired. Alternatively, in a chemical approach, a spinel may be simply regarded as a mixture of divalent ($M^{II}O$) and trivalent ($M^{III}_2O_3$) oxides. The chemical approach is adopted for describing spinels in this work because the oxidation-reduction chemistry of iron is considered to be important to the process analysis. Hence magnesium oxide (MgO) and ferrous oxide (FeO) are considered to be the divalent oxides ($M^{II}O$) and aluminium oxide (Al_2O_3) and hematite (Fe_2O_3) are considered to be the trivalent oxides ($M^{III}_2O_3$). Magnesium aluminate spinel is considered to have the following chemical formula: $(Mg_{(1-x)},Fe_x)O.(Al_{(1-y)}Fe_y)_2O_3$ where the x and y values lie between 0 and 0.5. The magnesium ferrate spinel may be represented by $(Mg_{(1-x)},Fe_x)O.(Fe_{(1-y)}Al_y)_2O_3$ where x and y have values between 0 and 0.5. Corresponding spinel compositions are reported in Figures 76 and 77, according to this model.

It should be noted that the calculations performed here predict phase assemblages under equilibrium conditions. In the actual reactor, some of the predicted phases may not form until higher temperatures are attained or may not form at all, because of kinetic considerations.

4.4.6 Predicted Effect of Oxygen Concentration:

At a temperature of 900°C under oxidizing conditions, thermochemical modelling suggests that the solid reaction product is composed primarily of magnesium ferrate ($MgFe_2O_4$) spinel, magnesium aluminate ($MgAl_2O_4$), and MgO as a monoxide phase (see Figures 74 to 77). Small amounts of Al_2O_3 and FeO would be expected to exist in the $MgFe_2O_4$, while the magnesium aluminate would contain some Fe_2O_3 and FeO. Under reducing conditions, ferric oxide, Fe_2O_3 is predicted to be partially reduced to ferrous oxide FeO. The composition of the

$MgAl_2O_4$ spinel is predicted to change by only a small amount relative to oxidizing conditions. However, the composition of the magnesium ferrate spinel is presumed to change significantly, with FeO displacing MgO from the structure and increasing the quantity of monoxide phase, which is now predicted to contain a significant concentration of FeO, that is, a composition with the general formula $(Mg_{(1-z)},Fe_z)O$ (Figures 72 – 73).

At a temperature of 900 °C under oxidizing conditions, the product gas phase is predicted to contain a small concentration of free chlorine in addition to the normal combustion gases plus hydrogen chloride (Figures 55 – 57). Under reducing conditions, the gas phase is foreseen to contain noteworthy amounts of ferrous chloride ($FeCl_{2(g)}$) as well as hydrogen (H_2) and carbon monoxide (CO). The formation of ferrous chloride is considered to be significant as it indicates that the targeted iron hydrolysis reaction is effectively reversible. The ferrous chloride gas could condense as liquid or solid in the gas train causing build-up of deposits. The ferrous chloride could also react with oxygen from air that is infiltrated into the gas train, producing ferric chloride ($FeCl_3$) and ferric oxide (Fe_2O_3). The ferric chloride could oxidize or hydrolyse to ferric oxide, most likely as very fine particles, in the offgas stream.

$$6\ FeCl_{2\,(g)} + 1.5\ O_2 = 4\ FeCl_{3\,(g)} + Fe_2O_{3\,(s)} \qquad (48)$$

$$2\ FeCl_{3\,(g)} + 1.5\ O_2 = Fe_2O_{3\,(s)} + 3\ Cl_2 \qquad (49)$$

$$2\ FeCl_{3\,(g)} + 3\ H_2O = Fe_2O_{3\,(s)} + 6\ HCl_{(g)} \qquad (50)$$

When the reducing reactor product gas makes contact with incoming liquor during pre-concentration, any residual gaseous ferrous chloride (and any secondary ferric chloride) would dissolve into the concentrated liquor and be returned to the reactor, creating a recirculating load. This situation would result in lower process efficiencies.

The model's predictions imply that, with respect to iron chloride hydrolysis, the reactor yield is likely to be under kinetic control under oxidizing conditions but under either kinetic control or thermodynamic equilibrium control under reducing conditions. This conclusion is based on the fact that the iron chloride hydrolysis reaction is predicted to be reversible or equilibrium controlled under reducing conditions in that some iron chloride is believed, by thermochemistry, to be present in the reaction products. It is irreversible or strongly favoured under oxidizing conditions because iron chloride is not among the predicted reaction products and hence thermodynamic considerations are not likely to influence the process yield. For aluminium chloride, the hydrolysis reaction is predicted to be irreversible because aluminium reports only to oxide phases and therefore the yields are likely to be controlled by kinetic considerations under all the conditions examined. For magnesium chloride, the hydrolysis reaction is predicted to be reversible at lower temperatures where its chlorides are stable and irreversible at higher temperatures where magnesium reports only to oxide phases.

For a reversible process the Gibbs energy of reaction has a relatively small magnitude and changes in conditions can affect the yield. For an irreversible reaction, the Gibbs energy of reaction has a large negative value and the yield is largely unaffected by changes in conditions. The thermodynamic properties of reaction for the hydrolysis of $AlCl_3$, $MgCl_2$, $FeCl_2$ (reducing) and $FeCl_3$ (oxidizing), as calculated by the FactSage System, are provided in Appendix 1.

The predicted compositions of the gas, mixed solids, spinel phase and monoxide phase under varying oxidizing and reducing conditions were reported in Figures 55-60, 64–68, and 72-77.

It is worth highlighting that when operating under reducing conditions at 900°C, the equilibrium product offgas is expected to contain more hydrogen on a volume basis than CO.

As mentioned in Section 2.5.3.3, metal chloride hydrolysis and the reverse hydrochlorination reaction have been studied by Kasaoka et al.[80] Their experimental observations appear to be consistent with the predictions made in this work, particularly with respect to the reversibility of the chloride hydrolysis reaction under certain conditions.

4.4.7 Predicted Liquid Phase Formation:

The modelling exercise indicated that a molten chloride salt phase would not form at any temperature under either oxidizing or reducing conditions. Based on the author's experience and that of other researchers in this area[86], small amounts of alkali metals (that are resistant to hydrolysis under some conditions) may favour a molten chloride salt phase during pyrohydrolysis. Additional thermochemical calculations revealed that the presence of even a small amount of sodium chloride would stabilize the formation of a liquid chloride phase over a wide temperature range (i.e. up to 900°C). The presence of a sticky liquid phase could have significant implications on the operation of a fluidised bed pyrohydrolyzer (i.e. build-up on reactor and offgas handling system walls, bed particle agglomeration and defluidization, etc...). Furthermore, any residual chlorides in the reactor oxide product are likely to be water-soluble and could therefore be leached by rainwater. Clearly, the effect of minor impurities on the pyrohydrolysis of the concerned Al-Fe-Mg-Cl system is certainly worth investigating.

4.4.8 Thermochemical Modelling Conclusions

The FactSage System, and thermodynamic data generated by the FACT Consortium Project, has made it possible to predict the equilibrium phase assemblages that could form during the pyrohydrolysis of the Al-Fe-Mg-Cl liquor of interest. The resulting phase assemblage is predicted to vary significantly with temperature and with the oxygen potential in the reactor.

The presence of gaseous ferrous chloride in significant quantities at higher temperatures (under reducing conditions) is likely to limit reactor performance and yields in these circumstances. Because of this, it is believed that, with respect to iron chloride hydrolysis, the reactor yield is likely to be under kinetic control when oxidizing conditions prevail, but under either kinetic or thermodynamic equilibrium control when the conditions are reducing.

A solid solution chloride phase, consisting mainly of iron II (ferrous) chloride together with some magnesium chloride, was predicted to persist to intermediate temperatures under reducing conditions. This phase was not predicted to be present under oxidizing conditions.

Thermochemical modelling indicated that a liquid chloride phase, other than the feed liquor, would not form at any temperature (i.e. 200°C or above) under the range of oxidizing or reducing conditions considered. A solid chloride phase was predicted to persist to intermediate temperatures under reducing conditions. A molten salt phase was determined to be nearly stable under reducing conditions. In other words, the predicted thermodynamic activity of a molten salt phase was less than, but close to, unity.

Through additional calculations, the model predicted that small amounts of salt forming impurities (such as NaCl) in the liquor might be enough to stabilize a chloride phase to higher temperatures. The effect of minor impurities could be the subject of further work.

Aqueous solution phase behaviour was not modelled in this work, in part because of inadequate thermochemical data for both the liquor phase and the solid compounds that are likely to be in equilibrium with the solution. Modelling in this area could be the subject of further work. This work would require optimization of the appropriate phase model parameters.

The solid solubility of iron II in magnesium chloride dihydrate, chloride monohydrate and chloride hydroxide has apparently not been measured and would require an experimental investigation. The development of thermochemical models of solid solutions involving iron II and magnesium chloride hydrates and chloride hydroxides could be the subject of further work.

More information regarding the non-thermodynamic properties of the different solid phases, such as their individual fluidising behaviour, would be required to predict their influence on reactor performance under the different conditions.

5.0 CONCLUSIONS:

Unlike what experts in the field have suggested[1,15,53], the research study at hand has shown that when the saturated Al-Fe-Mg-Cl solution at 105°C is exposed to fluidized bed pyrohydrolyzer operation conditions at 850°C, the following sequence of events take place:

- rapid H_2O evaporation (i.e. vigorous boiling) and onset of metal chloride precipitation.
- slurry densification due to a gradual increase in crystal content (i.e. $AlCl \cdot 6H_2O$, $FeCl_2 \cdot xH_2O$, and $MgCl_2 \cdot xH_2O$, where x = 2 or 4).
- hydrated crystal drying and onset of pyrohydrolysis (i.e. thermal decomposition of $MeCl_x \cdot yH_2O$).

The same holds true for the high temperature hydrolysis of typical waste pickle liquors (i.e. primarily $FeCl_2$ solution). The simplified pyrohydrolysis experiments (i.e. Phase I) have shown that the transformation of the Al-Fe-Mg-Cl reactor feed, which is obviously composed of numerous species with differing solubilities and stabilities, can take 30% longer than that of a $FeCl_2$ solution under similar conditions. Given that fluidized bed pyrohydrolyzer performance is dependent on the need for the majority of the injected liquor to coat and react on existing bed particles, the impact of the aforementioned observations on the process are rather straightforward. The longer it takes for all of the salt to precipitate from solution, adhere to the bed particles and eventually transform, the higher the probability that some of the incoming liquor will be carried off by the fluidizing gas. This, in turn, favours an inefficient recirculating loop and negatively impacts on process performance.

It is generally accepted that solid metal chlorides are rather "sticky" at elevated temperature. Furthermore, the presence of a gaseous boundary layer around the

surface of vigorously boiling droplets will impede any noteworthy adhesion of the feed liquor to the fluidized bed particles and most likely favour repulsion between the two.

The crystallization studies (i.e. Phase II) revealed that when the Al-Fe-Mg-Cl solution is allowed to gradually evaporate at 105°C, $AlCl_3 \cdot 6H_2O$ precipitates when at least 15% of the solvent water has evolved from the saturated liquor. $FeCl_2 \cdot xH_2O$ and $MgCl_2 \cdot xH_2O$ crystallization (where x = 2 or 4) takes place when approximately 26% and 41% of the solvent water has evaporated, respectively. Ferric chloride remains in solution even after 54% of the water has been driven from the liquor. While it is difficult to conclude whether the chlorides precipitated independently or as complex compounds, related SEM and EDS data indicate that once 41% of the solvent water in the saturated liquor has evolved, the formation of crystals with various and perhaps alternating layers of $AlCl_3 \cdot 6H_2O$, $FeCl_2 \cdot xH_2O$, and $MgCl_2 \cdot xH_2O$ is quite probable. This is even more likely to occur when the said liquor is actually introduced into the fluidized bed reactor, where the evaporation process is much more rapid. Additionally, the core of precipitated crystals will very likely be composed of the aluminium chloride. This will have implications on the overall transformation process, as this salt is also the first to hydrolyse when the spent solution temperature rises within the reactor. Furthermore, the crystallization results have revealed that $FeCl_3$ will remain in solution to very high degrees of evaporation, especially since its solubility actually increases with temperature. Therefore, the proportion of liquor that remains in aqueous form during the slurry densification phase increases with the ferric concentration in the starting solution. In light of this and for the same reasons cited above, higher ferric concentrations in the reactor feed are more than likely to favour an increase in the quantity of liquor entrainment by the fluidizing gases and therefore lead to lower process efficiencies. This coincides with observations made in industrial practice.[13,14]

The sequence and manner in which the precipitated chlorides pyrohydrolyze as the system temperature exceeds 300°C was elaborated upon during a dedicated series of experiments (i.e. Phase III), with a simulated reactor atmosphere (gaseous, not dynamic). These studies have shown that excluding kinetic effects, the transformation of the Al-Fe-Mg-Cl solution occurs primarily over the 300 to 600°C temperature range. When allowed to react for one hour at temperature, iron chloride begins hydrolysing at 300°C and is fully transformed at approximately 500°C. The kinetics of $MgCl_2 \cdot xH_2O$ conversion are much slower as temperatures in excess of 800°C or longer reaction times are required for this salt to fully hydrolyse. The first signs of magnesioferrite were observed when the liquor was allowed to react to 500°C, and $Mg(Al, Fe)_2O_4$ appeared at a reaction temperature of 700°C.

When compared to the results of the Phase III experiments, thermochemical modelling revealed that with the exception of $AlCl_3 \cdot 6H_2O$ hydrolysis, the majority of the reactions taking place as the saturated Al-Fe-Mg-Cl liquor is introduced into and eventually reaches 850°C are governed by either reaction kinetics or diffusion. Furthermore, the resulting phase assemblage at any given temperature was predicted to vary significantly with oxygen potential. Under the reducing conditions considered, gaseous ferrous chloride was determined to be present in significant quantities at temperatures in excess of 700°C, and a solid solution chloride phase (i.e. $FeCl_2$-$MgCl_2$), was predicted to persist to nearly 500°C. A liquid chloride phase (including molten salt), other than the feed liquor, was not predicted to form at any temperature (i.e. 200°C or above) under the range of oxidizing or reducing conditions considered. It was shown that the presence of small amounts of salt forming impurities (such as NaCl) in the liquor would stabilize a liquid chloride phase over a rather wide temperature range.

All of the aforementioned findings have helped to provide a much clearer understanding of the mechanisms behind the transformation of a saturated Al-Fe-Mg-Cl liquor (at 105°C), as it is exposed to typical reactor operating temperatures

(i.e. 850°C). The effects of oxygen potential and other impurities have also been shown. Clearly, some of the theories advanced in this thesis in regards to how the sequence of reactions influence the high temperature fluidized bed hydrolysis process can be extended to other saturated multi-component metal chloride systems. While bound by a confidentiality agreement, the author can comfortably confirm that the findings of this research were quite useful in identifying the means for improving the performance of a commercial fluidized bed pyrohydrolyzer for a spent chloride liquor containing numerous species.

6.0 CONTRIBUTIONS TO ORIGINAL KNOWLEDGE:

The research has shown that the high temperature hydrolysis of a saturated metal chloride solution in fluidized bed reactors is not necessarily a vapour deposition process[1,15,53], but depending on the spent liquor composition, actually consists of the following:

- rapid $H_2O/HCl_{(aq)}$ evaporation which triggers the precipitation of the dissolved salts,
- followed by dehydration of the resulting crystals, which eventually transform into oxides.

The aforementioned transformation process has never been used to describe the mechanisms behind the fluidized bed pyrohydrolysis of a saturated ferrous or multi-component metal chloride solution. Furthermore, the manner in which metal chloride solubility in the reactor feed impacts on fines generation and ultimately influences process efficiency, was either not well understood or simply not published by Keramchimie (i.e. supplier of technology). While it is generally accepted that an increase in the ferric concentration of waste pickle liquors results in poorer process efficiencies, no one has proposed that the relatively high solubility of $FeCl_{3(aq)}$ in the reactor feed solution is to blame for the corresponding generation of fines.

The thesis goals are unique since this is the first time that the pyrohydrolysis of a saturated Al-Fe-Mg-Cl liquor has been studied in such detail. The theory, experimental techniques, and modifications to existing industrial practices and equipment that have emerged are new to this area of metallurgy. Moreover, the bench scale studies and modelling performed to define the series of reactions that take place as the said liquor is introduced into and reaches the reactor operating temperature have never been attempted in the literature.

The experimental procedure and sampling/analytical techniques developed to define the sequence and manner in which the metal chloride chlorides precipitate from the saturated Al-Fe-Mg-Cl solution, as the solvent H_2O and HCl evaporate at 105°C, was quite novel. The concerned test methods were elaborated upon in collaboration with industry experts, such as Professor G.P. Demopoulos et al. (McGill University), R. Farrel & J. Sendra (Swenson Process Equipment, MI, USA), and D. Le Flammec (GEA Kestner S.A.S, St. Quentin-Yv., France).

The approach taken to model the Al-Fe-Mg-Cl solution transformation process during pyrohydrolysis required careful consideration and was developed in collaboration with specialists in the area of thermodynamics and thermochemistry, such as M. Wadsley and A. Pelton of L'École Polytechnique. Such a technique has never been used to fundamentally describe the series of steps that take place during the conversion of a saturated multi-component metal chloride solution in a fluidized bed pyrohydrolyzer. Once again, the results were instrumental in helping to interpret the findings of the three phase experimental approach. Furthermore, the thermochemical modelling exercise also helped explain the impact of certain parameters that were not considered during the bench scale studies, such as the effect of reactor atmosphere (oxidizing and reducing) or impurities in the feed. Based on an extensive review of the literature, the use of the given approach to study the effects of these variables on the fluidized bed pyrohydrolysis of a saturated Al-Fe-Mg-Cl solution is clearly original.

Given that the results of the concerned research has proved useful in defining the means to significantly improve the efficiency of an industrial fluidized bed pyrohydrolyzer, the combined three-phase experimental/modelling approach turned out to be quite practical, and rather novel in this particular field. The results have provided for a much clearer understanding of metal chloride pyrohydrolysis in such reactors and have also shown that the chemical reactions that are often used to describe the process (see reactions 3 through 9) are over-

simplified. Therefore, unlike what Keramchimie may suggest[1,15,53], these reactions cannot be used in combination with basic Gibbs Free Energy data alone to identify the parameters for efficient fluidized bed pyrohydrolyzer performance.

7.0 REFERENCES:

1. Peek E.M.L, ***CHLORIDE PYROHYDROLYSIS: Lixiviant Regeneration and Metal Separation***, PhD Thesis - Delft University of Technology, Netherlands, 1995.

2. Moklebust O. and Mead B., ***Regenerating HCl from Iron Chloride Solutions***, P: US Patent 3,529,931; Int'l. Cl. C01b 7/08; C01g 23/04; Patented Sept. 22, 1970.

3. Conners A., ***Hydrochloric Acid Regeneration as Applied to the Steel and Mineral Processing Industries***, CIM Bull., Vol. 68, No. 754, 1975, p. 75-81.

4. Iammartino N. R., ***Beneficiated-Ilmenite Process Recycles HCl Leach Liquor***, Chem. Eng., Vol. 83, No. 11, 1976, p. 100-101.

5. Heinz E., Beckmann M. and Diffmar H., ***Treating Iron Chloride - Hydrochloric Acid Aqueous Solutions***, P: Australian Appl. No. 58727/86, 18 Dec. 1986.

6. Walpole E. A., ***Acid Regeneration***, P: Pat. W093/16000, Int'l Cl. C01B7/03; C23G1/36; C01G23/053, 49/06; Patented Aug. 19, 1993.

7. Harris L.J.F., ***Introduction to Spray Roasting Process for Hydrochloric Acid Regeneration and its Application to Mineral Processing***, Proc. – Hydrometallurgy '94 (Int'l Symp.), Chapman and Hall, London, UK, 1994, p. 923-937.

8. Marnell P., ***Spent Hydrochloric Acid Pickling Liquor Regenerated in Fluid Bed***, Chem. Eng. (N.Y.), Vol. 79, No. 25, 1972, p. 102-103.

9. Taylor J. C., ***Continuous Regeneration of Hydrochloric Acid Pickle Liquors***, Proc. Nat.'l Chem. Eng. Conf. 3rd - Treat, Recycle and Disposal of Wastes, Mildura, Victoria, Aust., 1975, Paper T10-T12.

10. Rupay G. H. and Jewell C. J., ***The Regeneration of Hydrochloric Acid from Waste Pickle Liquor Using Keramchemie/Lurgi Fluidized Bed Reactor System***, CIM Bull., Vol. 68, No. 754, 1975, p. 89-93.

11. Jewell C. J. and Marcotte B. A., ***Regeneration of Hydrochloric Acid Waste Pickle Liquor Using a Fluidized Bed Reactor System***, Proc. CIM - Iron Control in Hydrometallurgy, (Int'l Symp.), Ed. Dutrizac J. and Monhemins A.J., 1986, p. 507-519.

12. Rituper R., ***High-Performance Effluent-Free Pickling Plants with Fluid Bed Hydrochloric Acid Regeneration***, Iron and Steel Eng., Vol. 72, No. 11, 1995, p. 50-54.

13. Coscia. C. and Kozinski J.A., ***Pyrohydrolysis of an Al-Fe-Mg-Cl Solution – Characterization of the Transformation Process,*** CIM Procs. – Chloride Metallurgy 2002 (Int'l Conf.), Vol. II, Ed. Peek E.M.L and Van Weert G., 2002, p. 683-698.

14. Patoine M-C., De Mori A., Coscia C. and Borowiec K., ***Pyrohydrolysis of a Calcium and Magnesium Bearing $FeCl_2$ Leach Liquor***, CIM Procs. – Chloride Metallurgy 2002 (Int'l Conf.), Vol. II, Ed. Peek E.M.L and Van Weert G., 2002, p. 699-712.

15. Kogler C., Barhold F. and Englehardt W., ***State of the Art, Potentials and Limits to the Fluid Bed Pyrohydrolysis Technology with Special Emphasis on Nickel Chloride***, Proc. CIM - Nickel-Cobalt '97 (Int'l Symp.), Ed. Cooper W.C. and Mihaylov I., 1997, p. 505-521.

16. Ruthner M. and Ruthner O., ***25 Years of Process Development in HCl Pickling and Acid Regeneration***, Iron and Steel Eng., Vol. 56, No. 11, 1979, p. 36-39.

17. Schuldt A. A., ***Regeneration of Hydrochloric Acid Pickle Liquor at Stelco's Hilton Works***, CIM Bull., Vol. 68, No. 754, 1975, p. 82-88.

18. Jedlicka H., ***Spray Roasting Regeneration of Spent Hydrochloric Acid as Applied to the Small Pickling Plants***, Iron and Steel Eng., Vol. 55, No. 9, 1978, p. 73-75.

19. Husken H. G. and Stawowy H., ***Up-to-date Strip Pickling Lines and Regeneration Installations***, Sthal n Eisen, Vol. 99, No. 25-26, 17 Dec. 1979, p. 1475-1481.

20. Villegas E.A., ***Regeneration of HCl and Production of Fe_2O_3 from Waste Pickling Solutions***, Proc. - 35th Annual Congress of Assoc. Brasileira de Metais, Sao Paolo, Brazil, 6-11 July 1980, p. 213-228.

21. Pavinato A.P., Pazdej R. and Nicolle R., ***Process for Separating Silica from Spent Hydrochloric Acid Bath in Pickling of Steel Sheets***, P: EP0491640A1, Int.'l Cl. C23G1/36; Patented June 24, 1992.

22. Peek E.M.L., Goedhart O.F. and Van Weert G., ***Process Evaluation of Steel Pickle Liquor Pyrohydrolysis in a Commercial Keramchemie Fluid***

Bed Reactor, Proc. CIM - Iron Control in Hydrometallurgy (2nd Int.'l Symp.), Ed. Dutrizac J. and Harris G.B., 1996, p. 483-503.

23. Karner W., ***New Developments in the Spray Roasting Process for Pickle Liquor Regeneration***, Iron Oxides '91, California, USA, Sept. 1991.

24. Jewel C. J., ***Operating Experience with a Fluid Bed Reactor***, Iron Oxides '91, California, USA, Sept. 1991.

25. Karner W. and Braun E., ***Modern Pickling and Regeneration Technology***. Proc. - 21st Century Steel Industry of Russia and CIS. (Int'l Conf.), Vol. V, Moscow, Russia, 6-10 June 1994, p. 53-56.

26. Wadhawan S. C., ***Economics of Acid Regeneration-Present and Future***, Iron and Steel Eng., Vol. 55, No. 10, 1978, p. 48-51.

27. Phelps C. W., ***Reclamation of Spent Hydrochloric Acid***, P: US Patent 3,502,432; Int.'l Cl. C01b 7/08; Patented March 24, 1970.

28. Bierbach H., Dittmar H., Heinz E., Hohmann K. and Rennhack R., ***Process for the Thermal Conversion of Metal Chlorides to Metal Oxides***, P: Patent 1,456,031; Int'l Cl2 C01b 13/14; Patented Nov. 17, 1976.

29. Hansen L. J., ***Apparatus for Treating Waste Acids***, P: US Patent 4,083,693; Int'l Cl. F27B9/14, Bo1J 6/00; Patented Apr. 11, 1978.

30. Burzynski J.P. and Torre Y., ***Method and Plant for Regenerating a Hydrochloric Solution***, P: Patent WO86/03521; Int'l Cl. C23G1/36, C01B7/03; C01G49/00; Patented June 19, 1986.

31. Hitzermann G., ***Rueckgewinnung von Beizsaenren. (Recovery of Pickling Acids)***, Blech Rohre Profile, Vol. 23, No. 10, 1976, p. 281-285.

32. Hitzermann G., ***Recovery of Pickling Acids***, Wire, Vol. 26, No. 2, 1977, p. 45-49.

33. Hitzermann G. and Heimhard H-J., ***Modern Pickling Techniques***, MPT Metall. Plant Technology, Vol. 9, No. 2, 1986, p. 67-73.

34. Bozec C., ***Effluents from Hydrochloric Acid Pickling in Jobbing Galvanizing: Problems and Possible Solutions***, Proc. Int'l Galvanizing Conf. 1979, (Publ. 1981) 12th, p. 225-229.

35. Karner W. and Gamsriegler D., ***Process for Regenerating Hydrochloric Acid from Pickling Installations***, P: EP0635586A1, Int'l Cl. C23G1/36; Patented Jan. 25, 1995.

36. Burtch J. W., ***PORI Hydrochloric Acid Regeneration Process***, Iron and Steel Eng., Vol. 50, No. 4, 1973, p. 40-42.

37. Burtch J. W., ***Hydrochloric Acid from Industrial Process Streams. The PORI Process***, CIM Bull.,Vol. 68, No. 753, 1975, p. 96-100.

38. Burtch J. W., ***The PORI Process: Regeneration of Hydrochloric Acid from Spent Pickle Liquor***, Wire Journal, Vol. 9, No. 2, 1976, p. 57-59.

39. Offinger D. and Bailey D. E., ***Acid Recycling at a Captive Finishing Shop***, Products Finishing, Vol. 59, No. 3, Dec. 1994, p. 62-66.

40. Prudon F. and Mangin P., ***Rhone-Ponlenc/Vicarb Process for the Destruction of Solid, Liquid and Gaseous Chlorinated Wastes***, Revue General de Thermique, Vol. 26, No. 303, 1987, p. 197-201.

41. Csovary M., Czegledi B., Stocker L., Erdelyi M., Egry R., Tundok S. and Horvath A., ***Regeneration of Hydrochloric Acid in Chloride Hydrometallurgy by Anion Exchange Process***, Acta Technica Academiae Scientarium Hungaricae, Vol. 101, No. 2, 1988, p. 129-141.

42. Brown C. J., ***Productivity Improvements Through Recovery of Pickle Liquors with the APU Process,*** Iron and Steel Eng., Vol. 67, No. 1, 1990, p. 55-60.

43. Vaish A. K., Prasad S. and Akerkar D. D., ***Status of Spent Pickle Liquor in Indian Steel Plants and its Regeneration by Pollution Free Methods***. Journal of Inst. of Eng. (India), Metallurgy and Materials Science Div., Vol. 69, pt 2, Mar. 1989, p. 49-53.

44. Peterson J.C., ***Waste Minimization and Recovery Techniques for Acid Pickling Solutions***, Wire Technol. Int.'l, Vol. 20, No. 1, 1992, p. 25-28.

45. Negro C., Blanco P., Dufour J., Latorre R., Formoso A. and Lopez F., ***Treatment of Hydrochloric Acid Waste Pickle Liquors***, The Périodique: Journal of Environmental Science and Health. Part A. Environmental Science and Engineering, Vol. 28, No. 8, 1983, p. 1651-1667.

46. Negro C., Cobos M., A., Dufour J., Latorre R., Formoso A. and Lopez F., ***Influence of Several Non-Ferrous Metals in the Treatment of Residual***

Liquors from Hydrochloric Acid Pickling Processes, Revista de Metalurgia, Vol. 30, No. 1, 1994, p. 11-16.

47. Hu X., ***A New Technology for Pollution Free Treatment of HCl-Pickling Waste of Cold Rolled Sheet Steel Plant***, Gangtie, Vol. 29, No. 8, 1994, p. 68-72.

48. Hantelmann H. and Sowieja D., ***Technical Hydrochloric Acid from Waste Incineration***., Sulzer, Tech. Rev., Vol. 77, No. 1, 1995, p. 22-23.

49. Van Weert G., Robertson E.C. and Christiansen J.H., ***Treatment of Ferrous Chloride Liquors in the Falconbridge Fluid Bed Hydrolyzer***, CIM Bull., Vol. 68, No. 753, 1975, p. 87-95.

50. Tang Poy R., ***Regeneration of Hydrochloric Acid from Ferrous Chloride using the Keramchemie/Lurgi Fluidized Bed Reactor System***, Proc. CIM - Iron Control in Hydrometallurgy (2nd Int.'l Symp.), Ed. Dutrizac J. and Harris G.B., 1996, p. 471-482.

51. Krivanec H. K. and Kladnig W. F., ***Manufacture of Oxide Raw Materials by Andritz-Ruthner Spray Roasting Process***, Sprechsaal, Vol. 121, No. 12, 1988, p. 1182-1189.

52. Kladnig W. and Karmer W., ***Production of Oxide Raw Materials for the Ceramic Industry***, CF1, Ceramic Forum Int.'l Cer. DKG, Vol. 67, No. 3, 1990, p. 80-84.

53. Conradi U., Kogler C., Englehardt W. Franke A. and Schwammlein K., (KCH Technical Support Staff), ***Personal Communications***, Nov. '98 - Dec. '99.

54. Hamer C., ***Acid Extraction of Alumina from Canadian Non-Bauxite Sources at CANMET***, Report 81-2E, © Minister of Supply and Services Canada, Ottawa, Canada, 1981.

55. Sato T., Ozawa F. and Ikoma S., ***Thermal Decomposition of Aluminium Salts – Hydrates of the Chloride, Nitrate and Sulfate, and of Ammonium Alum***, J. Appl. Chem. Biotechnol., Vol. 28, 1978, p. 811-822.

56. Gardner T.J. and Messing G.L., ***Magnesium Salt Decomposition and Morphological Development during Evaporative Decomposition of Solutions***, Thermochimica Acta, Vol. 78, 1984, p. 17-27.

57. Dutt P.K., Kava R.M., and Mehta D.J., ***Thermal Decomposition of Magnesium Chloride Hexahydrate***, Indian Journal of Technology, Vol. 10, January 1972, p. 41-42.

58. Vilcu R., Coseac T. and Oancea D., ***Some Kinetic Aspects of the High-Temperature Anhydrous $FeCl_2$ Hydrolysis Reaction***, Revue Roumaine de Chimie, Vol. 42, No. 2, 1997, p. 93-97.

59. Froment G.F. and Bischoff K.B., ***Chemical Reactor Analysis and Design***, John Wiley & Sons, New York, Chichester, Brisbane, Toronto, 1979, p. 239-270.

60. Dutrizac J.E. and Riveros P.A., ***The Precipitation of Hematite from Ferric Chloride Media at Atmospheric Pressure***, Metallurgical and Materials Transactions B, Vol. 30B, No. 6, 1999, p. 993-1001.

61. Dutrizac J.E. and Riveros P.A., ***The Precipitation of Hematite from Ferric Chloride Media at Atmospheric Pressure***, Hydrometallurgy, 1997, Vol. 46, No. 1-2, p. 85-104.

62. Chunpeng L., Xianwan Y. and Aiping H., ***Kinetics of Hydrolysis of the Metal Chlorides at High Temperatures***, Nonferrous Metals Society of China, Vol. 34, No. 3, 1982, p. 52-57.

63. Charlesworth D.H. and Marshall W.R. Jr., ***Evaporation from Drops Containing Dissolved Solids***, A.I.Ch.E. Journal, Vol. 6, No. 1, 1960, p. 9-23.

64. Taniguchi I., Inoue T. and Asano K., ***Evaporation of a Salt Water Drop with Crystallization***, Atomization and Sprays, Vol. 9, No. 1, 1999, p. 69-85.

65. Link K.C. and Schlünder E-U., ***Fluidized Bed Spray Granulation; Investigation of the Coating Process on a Single Sphere***, Chemical Engineering and Processing, Vol. 36, No. 6, 1997, p. 443-457.

66. deLau J.G.M., ***Preparation of Ceramic Powders From Sulfate Solutions By Spray Drying and Roasting***, American Ceramic Society Bulletin, Vol. 49, No. 6, 1970, p. 572-574.

67. Chess D.L., Chess C.A. and White W.B., ***Precursor Powders for Sulfide Ceramics Prepared by Evaporative Decomposition of Solutions***, Journal of the American Ceramic Society, Vol. 66, No. 11, 1983, p. C205-207.

68. Panda R.C., Zank J. and Martin H., ***Modeling the Droplet Deposition Behavior on a Single Particle in Fluidized Bed Spray Granulation Process***, Powder Technology, Vol. 115, No. 1, 2001, p. 51-57.

69. Kleinbach E. and Riede T., ***Coating of Solids***, Chemical Engineering and Processing, Vol. 34, 1995, p. 329-337.

70. Linke W.F. and Atherton S., ***Solubilities: Inorganic and Metal-Organic Compounds; A Compilation of Solubility Data from the Periodic Literature***, Vol. I, 4th Edition, American Chemical Society, Washington D.C., 1958.

71. Linke W.F. and Atherton S., ***Solubilities: Inorganic and Metal-Organic Compounds; A Compilation of Solubility Data from the Periodic Literature***, Vol. II, 4th Edition, American Chemical Society, Washington D.C., 1965.

72. Athir A., Marrouche A., Atif H., Boukbir L., El Hadek M. and Cohen-Adad R., ***Calcul des Diagrammes de Phases des Systems Binaires H_2O-MCl_n ($M=Mg^{2+}$, Fe^{2+}, Fe^{3+})***, J.Thermal Anal. Calorim., Vol. 61, 2000, p. 849-860.

73. Kelley K.K., ***Energy Requirements and Equilibria in the Dehydratation, Hydrolysis, and Decomposition of Magnesium Chloride***, USBM Tech. Paper 676, 1945, 22pp.

74. Wagman D.D., Evans W.H., Parker V.B., Schumm R.H., Halow I., Bailey S.M., Churney K.L. and Nuttall R.L., ***The NBS Tables of Chemical Thermodynamic Properties***, J. Phys. Chem. Ref. Data, Vol. 11, Supp.21, 1982.

75. Wang P. and Pitzer K.S., ***Thermodynamic Properties of Aqueous Magnesium Chloride Solutions from 250 to 600 K and to 100 MPa***, J. Phys. Chem. Ref. Data, Vol. 27, No. 5, 1998, p. 971-991.

76. Afonichkin O.V. and Gaidukova T.I., ***Solubility of Salts in NaCl-$FeCl_2$-H_2O and $MgCl_2$-$FeCl_2$-H_2O Systems***, Tr. Vses. N.-i. Proekt. In-t Galurgii, Vol. 74, 1976, p. 30-34.

77. Ferrari A. and Carugati M., ***$FeCl_2$-$MgCl_2$ Binary Phase Diagram***, (Phase Diagrams for Ceramists Fig. 3172), Atti. Accad. Naz. Lincei. Rend. Classe Sci. Fis. Mat. Nat., Vol. 8, 1928, p. 307.

78. Pelton A. and Wadsley M. W., ***Personal Communication***, Thermfact Ltd., Montreal, Quebec, Canada, October 2002.

79. Morozov I.S. and Zhur.Neorg.Khim., ***$AlCl_3$-$FeCl_3$-H_2O Phase Diagram***, (Phase Diagrams for Ceramists, Fig. 1436), Vol. 1, 1956, p. 2796.

80. Kasaoka Shigeaki, Sakata Yusaku and Shirata Masahisa, ***Reactions of Various Metal Oxides with Hydrogen Chloride and the Reverse Reactions***, (Japanese) Nippon Kagaku Kaishi, Vol. 11, 1977, p. 1728-1736.

81. Perry R.H. and Chilton C.H., ***Chemical Engineer's Handbook***, 5th Ed., McGraw-Hill, New York, 1973.

82. Genck W.J., ***Handbook of Separation Techniques for Chemical Engineers – Section 2.3 – Crystallization from Solutions***, 3rd ed., McGraw-Hill, New York, 1997.

83. Perkin Elmer, ***Optima 4000 Series Hardware Guide No. 0993-6373***, Version 2, July 2000.

84. Rigaku Industrial Corporation, ***Rigaku 3270 XRF Instruction Manual***, Version 2.1, Osaka, Japan.

85. Demopoulos G.P., ***Impurity Removal and Disposal by Aqueous Precipitation – The Crystallization Approach***, CIM – MetSoc (Hydrometallurgical Section) Short Course Notes, Theory and Practice of Impurity Removal in Aqueous Processing, Montreal, 1994.

86. Wadsley M.W., ***Personal Communicaton***, Thermfact Ltd., Montreal, Quebec, Canada, October 2002.

APPENDIX 1

Thermodynamic Properties of Reaction for the Hydrolysis of $AlCl_3$, $MgCl_2$, $FeCl_2$ (reducing) and $FeCl_3$ (oxidizing)

Output from FactSage Program Reaction

2 AlCl3 + 3 H2O = Al2O3 + 6 HCl
(T) (T) (T) (T)

T(C)	Delta_H(J)	Delta_G(J)	Delta_Vol(l)	Delta_S(J/K)	Delta_Cp(J/K)	Keq	T
------	AlCl3(l-FACT)	H2O(g-FACT)	Al2O3(s4-FACT)	HCl(g-FACT)	------		
200.00	-169397.5	-273389.3	1.1637E+02	219.786	-76.887	1.5162E+30	
250.00	-173162.7	-284185.0	1.2868E+02	212.219	-73.829	2.3665E+28	
300.00	-176789.6	-294626.9	1.4099E+02	205.596	-71.321	7.0867E+26	
350.00	-180301.3	-304757.0	1.5330E+02	199.720	-69.204	3.5088E+25	
400.00	-183714.8	-314609.0	1.6561E+02	194.450	-67.378	2.5834E+24	
435.90	-186112.6	-321527.2	1.7445E+02	190.980	-66.211	4.8499E+23	
------	AlCl3(g-FACT)	H2O(g-FACT)	Al2O3(s4-FACT)	HCl(g-FACT)	------		
AlCl3(1 mol):	DH = 70565.2	DG = 0	------	DS = 99.521			
435.90	-327243.0	-321527.2	5.8209E+01	-8.061	23.679	4.8500E+23	
450.00	-326907.4	-321416.8	5.9366E+01	-7.593	23.923	1.6445E+23	
500.00	-325690.5	-321078.1	6.3469E+01	-5.966	24.745	4.9176E+21	
550.00	-324434.0	-320819.4	6.7571E+01	-4.391	25.505	2.2789E+20	
600.00	-323141.1	-320638.2	7.1674E+01	-2.867	26.200	1.5175E+19	
650.00	-321815.1	-320532.0	7.5777E+01	-1.390	26.828	1.3684E+18	
700.00	-320459.4	-320498.4	7.9880E+01	0.040	27.386	1.5944E+17	
750.00	-319077.7	-320535.2	8.3983E+01	1.425	27.871	2.3110E+16	
800.00	-317673.5	-320640.1	8.8086E+01	2.764	28.281	4.0410E+15	
850.00	-316250.4	-320810.9	9.2189E+01	4.060	28.657	8.3112E+14	
900.00	-314808.4	-321045.5	9.6292E+01	5.317	29.010	1.9689E+14	
950.00	-313350.4	-321341.9	1.0039E+02	6.534	29.301	5.2792E+13	
1000.00	-311879.1	-321698.2	1.0450E+02	7.712	29.542	1.5786E+13	

MgCl2 + H2O = MgO + 2 HCl
(T) (T) (T) (T)

T(C)	Delta_H(J)	Delta_G(J)	Delta_Vol(l)	Delta_S(J/K)	Delta_Cp(J/K)	Keq	T
------	MgCl2(s-FACT)	H2O(g-FACT)	MgO(s-FACT)	HCl(g-FACT)	------		
200.00	95705.6	39920.6	3.8796E+01	117.901	-9.268	3.9171E-05	
250.00	95239.5	34049.3	4.2899E+01	116.965	-9.383	3.9845E-04	
300.00	94766.6	28222.9	4.7002E+01	116.102	-9.537	2.6788E-03	
350.00	94285.2	22438.2	5.1105E+01	115.296	-9.724	1.3158E-02	
400.00	93793.6	16692.5	5.5207E+01	114.538	-9.942	5.0668E-02	
450.00	93290.5	10983.8	5.9310E+01	113.817	-10.188	1.6093E-01	
500.00	92774.3	5310.3	6.3413E+01	113.127	-10.464	4.3776E-01	
550.00	92243.7	-329.3	6.7516E+01	112.462	-10.767	1.0493E+00	
600.00	91697.2	-5936.2	7.1619E+01	111.817	-11.098	2.2652E+00	
650.00	91133.4	-11511.3	7.5722E+01	111.190	-11.457	4.4805E+00	
700.00	90551.1	-17055.4	7.9825E+01	110.575	-11.843	8.2307E+00	
713.85	90386.2	-18585.7	8.0961E+01	110.407	-11.955	9.6289E+00	
------	MgCl2(l-FACT)	H2O(g-FACT)	MgO(s-FACT)	HCl(g-FACT)	------		
MgCl2(1 mol):	DH = 43095.0	DG = 0	------	DS = 43.662			
713.85	47291.2	-18585.7	8.0952E+01	66.745	-19.008	9.6289E+00	
750.00	46606.9	-20986.1	8.3918E+01	66.064	-18.854	1.1786E+01	
800.00	45669.0	-24266.7	8.8021E+01	65.169	-18.669	1.5175E+01	
850.00	44739.7	-27503.8	9.2124E+01	64.322	-18.501	1.9015E+01	
900.00	43818.7	-30699.7	9.6227E+01	63.520	-18.345	2.3274E+01	
950.00	42904.8	-33856.5	1.0033E+02	62.757	-18.214	2.7913E+01	
1000.00	41996.9	-36976.0	1.0443E+02	62.030	-18.103	3.2886E+01	

FeCl2 + H2O = FeO + 2 HCl

(T) (T) (T) (T)

T(C)	Delta_H(J)	Delta_G(J)	Delta_Vol(l)	Delta_S(J/K)	Delta_Cp(J/K)	Keq	T
------	FeCl2(s-FACT)	H2O(g-FACT)	FeO(s-FACT)	HCl(g-FACT)	------		
200.00	132813.8	73488.2	3.8798E+01	125.384	-3.481	7.7139E-09	
250.00	132615.8	67228.7	4.2901E+01	124.987	-4.432	1.9392E-07	
300.00	132372.2	60990.3	4.7004E+01	124.543	-5.295	2.7652E-06	
350.00	132088.4	54774.9	5.1106E+01	124.069	-6.035	2.5626E-05	
400.00	131770.9	48583.7	5.5209E+01	123.579	-6.643	1.6988E-04	
450.00	131426.3	42417.0	5.9312E+01	123.085	-7.121	8.6338E-04	
500.00	131060.7	36275.0	6.3415E+01	122.597	-7.481	3.5423E-03	
550.00	130679.9	30157.2	6.7518E+01	122.120	-7.734	1.2200E-02	
600.00	130288.9	24062.8	7.1621E+01	121.658	-7.891	3.6351E-02	
650.00	129892.2	17991.0	7.5724E+01	121.217	-7.966	9.5948E-02	
676.85	129678.1	14739.4	7.7927E+01	120.988	-7.975	1.5473E-01	
------	FeCl2(l-FACT)	H2O(g-FACT)	FeO(s-FACT)	HCl(g-FACT)	------		
FeCl2(1 mol):	DH = 43012.0	DG = 0	------	DS = 45.276			
676.85	86666.1	14739.4	7.7927E+01	75.712	-23.184	1.5473E-01	
700.00	86132.0	12993.1	7.9827E+01	75.157	-22.961	2.0072E-01	
750.00	84996.6	9264.1	8.3930E+01	74.019	-22.446	3.3655E-01	
800.00	83888.1	5589.9	8.8033E+01	72.961	-21.888	5.3447E-01	
850.00	82808.6	1966.8	9.2135E+01	71.978	-21.279	8.1009E-01	
900.00	81760.9	-1609.0	9.6238E+01	71.065	-20.621	1.1793E+00	
950.00	80747.0	-5140.9	1.0034E+02	70.219	-19.932	1.6578E+00	
1000.00	79768.3	-8631.9	1.0444E+02	69.434	-19.211	2.2602E+00	

2 FeCl3 + 3 H2O = Fe2O3 + 6 HCl

(T) (T) (T) (T)

T(C)	Delta_H(J)	Delta_G(J)	Delta_Vol(l)	Delta_S(J/K)	Delta_Cp(J/K)	Keq	T
------	FeCl3(s-FACT)	H2O(g-FACT)	Fe2O3(s1-FACT)	HCl(g-FACT)	------		
200.00	141639.8	-23817.6	1.1640E+02	349.694	-35.105	4.2592E+02	
250.00	139737.2	-41207.3	1.2870E+02	345.875	-39.945	1.3010E+04	
300.00	137760.3	-58408.7	1.4101E+02	342.265	-37.920	2.1037E+05	
303.85	137615.2	-59725.9	1.4196E+02	342.012	-37.460	2.5510E+05	
------	FeCl3(l-FACT)	H2O(g-FACT)	Fe2O3(s1-FACT)	HCl(g-FACT)	------		
FeCl3(1 mol):	DH = 43095.0	DG = 0	------	DS = 74.688			
303.85	51425.2	-59725.9	1.4196E+02	192.636	-61.718	2.5510E+05	
350.00	48647.7	-68506.9	1.5332E+02	188.004	-58.603	5.5250E+05	
400.00	45810.1	-77794.9	1.6563E+02	183.622	-54.813	1.0877E+06	
450.00	43177.1	-86879.1	1.7794E+02	179.847	-50.375	1.8849E+06	
500.00	40788.5	-95789.2	1.9025E+02	176.651	-44.976	2.9609E+06	
550.00	38703.5	-104553.9	2.0256E+02	174.036	-38.129	4.3103E+06	
600.00	37013.2	-113203.0	2.1486E+02	172.039	-29.005	5.9155E+06	
645.33	35943.1	-120971.2	2.2602E+02	170.842	-17.587	7.5784E+06	
------	FeCl3(g-FACT)	H2O(g-FACT)	Fe2O3(s1-FACT)	HCl(g-FACT)	------		
FeCl3(1 mol):	DH = 76950.9	DG = 0	------	DS = 83.781			
645.33	-117958.7	-120971.2	7.5398E+01	3.280	85.172	7.5786E+06	
650.00	-117557.3	-120987.6	7.5782E+01	3.716	86.573	7.0093E+06	
700.00	-113961.9	-121280.5	7.9885E+01	7.520	53.596	3.2335E+06	
750.00	-111448.9	-121721.3	8.3988E+01	10.040	47.549	1.6370E+06	
800.00	-109166.1	-122278.9	8.8091E+01	12.219	44.033	8.9468E+05	
850.00	-107026.1	-122939.4	9.2194E+01	14.168	41.723	5.2171E+05	
900.00	-104982.9	-123692.9	9.6296E+01	15.949	40.083	3.2159E+05	
950.00	-103011.7	-124532.0	1.0040E+02	17.594	38.816	2.0797E+05	
1000.00	-101097.3	-125450.5	1.0450E+02	19.128	37.795	1.4023E+05	

APPENDIX 2

Signed Waiver and Line of Credit for Previously Copyrighted Canadian Institute of Mining, Metallurgy and Petroleum Material, Included in Thesis.

Credit to the Canadian Institute of Mining, Metallurgy and Petroleum

The author would like to thank the Canadian Institute of Mining, Metallurgy and Petroleum (CIM) for the permission to reprint some of the information (text, graphs, figures, etc...) that was previously published in the Proceedings of the CIM Chloride Metallurgy Conference 2002 (Montreal, Canada).[13]